Diss. ETH ex.B

Diss. ETHZ No. 11280

Metabolic Studies of Mammalian Cells in a Fluidized Bed Reactor

A dissertation submitted to the

SWISS FEDERAL INSTITUTE OF TECHNOLOGY

in candidacy for the degree of Doctor of Technical Sciences

presented by

Michael Rainer Schuppenhauer

Diplom-Ingenieur, Verfahrenstechnik, TU Hamburg-Harburg

born November 16, 1966 in Hamburg, Germany

citizen of the Federal Republic of Germany

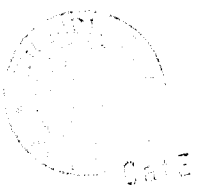

accepted on recommendation of

PD Dr. Irving J. Dunn, examiner

PD Dr. Bernhard Sonnleitner, co-examiner

Zürich, August 16, 1995

© Michael R. Schuppenhauer 1995

From 40 printed exemplars is this No. 04 **for** Hauptbibliothek ETH

LabVIEW and National Instruments are registered trademarks of National Instruments, Co. Austin, TX. All other product and company names are trademarks of their respective companies.

This dissertation has been printed on nopa-TOP acid-free paper provided by Kymmene AG for enhanced preservation according to US and European standards.

Mit Eifer hab' ich mich der Studien beflissen;
Zwar weiss ich viel, doch möcht' ich alles wissen.

J. W. von Goethe, Faust, Der Tragödie erster Teil

Acknowledgements

I am grateful to my advisor, PD Dr. Irving J. Dunn, who distinguished himself by giving me all the freedom to plan the underlying research, direct the sub-projects, and accomplish this dissertation in accordance with my convictions. It is this freedom that I have valued most during my time at ETH and that has made it possible for me to follow at the cutting-edge of international science.

This research would not have been possible were it not for the assistance and support of my fellow scientists who were so generous as to give ideas and leads, review my work and challenge my ideas, and even lend a hand when needed. It is to the spirits of those people, that I am indebted most, since without them it would have stayed what it was - a dream. I would therefore like to extent heartfelt thanks to:

Susan Sharfstein, as she provided substantial intellectual backing for the cell culture and the NMR work. Having dedicated five years of her life to the spectroscopy of animal cells, she was in the position to signal warnings prior to my commitment on severe issues and helped me afterwards when I ignored them. Throughout my entire research Susan was a vital source of scientific advice, backing, and motivation.

PD Dr. Bernhard Sonnleitner, Institute for Biotechnology, ETH Zürich, for undertaking the unexpected but hearty task of co-examiner, insisting on clarification, accuracy, consistency, compliance, and validation - striving for built-in quality.

Guido Kühne, Louis Tiefenauer, Paul-Scherrer-Institut, Würenlingen, Switzerland, who provided the magnetic resonance imaging instrument as well as crucial scientific and moral support and were always open for ideas and endeavours. Further, I am indebted to their superb HF group for constructing the RF-coil immune to EMI, departing from the initial design and parts laid down by Jürgen Link, Spectrospin, who supported us in developing the use of MRI for localized spectroscopy.

Antje Smala, TFH Berlin, for always being there with scientific and moral support, tolerating and accomplishing my many requests, initiatives and ideas.

Paul Durieux for spending endless nights discussing and explaining the faith of the Biotech industry and its characteristic hopes, expectations, margins and market shares, the motor that runs biotech, the fuel it is burning like no other industry - money.

Edwin Rock, my brother-in-arms, on thriving towards two goals in opposite directions, yet we are united by the means and the proteins. For raising my fascination in hCG to the extent that he could have been the ultimate user.

Dr. Irving Boime, Washington University, for kindly donating the cell line.

Andrea Ferrero, another brother-in-arms, for sharing his experience in the swamps of animal cell culture where results are far from a clear-cut cause-effect rationale, but also for the social experience with scenes from an Italian live-style, making live enjoyable after culture-clash impact.

Samuel Cymbalista, Gerard Mignot, and Patricio Orego, from Laboratoires Serono SA, Aubonne, for extensive material support and providing the industrial view and impact on the research.

Hans-Rudolf Tanner and Dominique Sobrinho, also from Laboratoires Serono SA, for initial backing and support of the glycosylation part of the presented research.

Dr. Steve Gorfien, Life Technologies Inc., for supporting the work by virtue of developing the right medium at the right time, crossing the Atlantic and delivery issues, for fulfilling high hopes, and giving my research an additional twist for the future.

Armin Bohmann, Peter Bösiger, John Coffman, Michael Domach, Corinne Duc, Erik Fernandez, Bruce Hammer, Bill Miller, and Ray Spier for various views and remarks during the project.

I am indebted to the Swiss Army not only for bringing such a handy tool as the Swiss Army Officers' Knife to the hands of an engineer but also for staffing their supply centers with people like Mr. Wey and Mr. Kohler heading the power unit

division at the Kloten Zeughaus who supplied us with emergency power units and serviced them whenever needed, thus vital in making the impossible possible.

There are also numerous people that helped with various bits and pieces crucial for the success of the project as a whole, some of them I would like to thank specially:

Mr. Frey for supplying and servicing the cars we used for transportation. Mr. Morf, night security guard, not only for patrolling the labs, protecting our work, fixing the negligence, but also for showing sincere interest in progress of research!

3M Corp. for providing the EMI shielded ribbon-cables. Peter Härtel, W. L. Gore GmbH, for supporting us with Gore-Tex samples and data on the diffusive sparger. Mr. Groh and Mr. Schneider, Nordland Paper and Kymmene AG for kindly providing the acid-free paper this dissertation is printed on.

Dr. Ernst Wehrli, ETH Zürich, Laboratory for Electron Microscopy I, for kindly preparing and providing the SEM pictures. Max Wohlwend for fixing the wires and my understanding of electronics, and Horst Seinecke & Co., Inc. in the machine shop.

Last but not least, I would like to thank all the people in the Bourne group who helped me in many ways while putting up with my constant hyperactivity.

While science should prevail independently from business interests, biotechnology endeavours to improve the human condition like no other science. It is a first-grade cash-burner and it is not possible to pursue without its fuel - money. I am grateful to all those who contributed to the financial bedrock on which I could build:

The Swiss Federal Government for KWF Grant 2135.1, the ETHZ, and the finest computers money can buy, my parents who both contributed significantly, Mrs. Garbers, who at the Hamburger Sparkasse always showed confidence and support, and Ernst & Young.

Credit is further due to the National Hormone and Pituitary Program, the National Institute of Diabetes and Digestive and Kidney Diseases (NIDDK) and the USDA for awarding hCG preparations used as references.

Table of Contents

Index to Figures

Index of Abbreviations

ACS	American Chemical Society	
ADP	adenosine diphosphate	
A_i	area of i	[cm^2]
AIDS	acquired immune deficiency syndrome	
Arg	argenine	
Asn	asparagine	
ATP	adenosine triphosphate	
B_0	static magnetic field	[T]
BET	Brunauer-Emmet-Teller (isotherm)	
bp	base pair(s)	
BSE	bovine spongioform encephalopathy	
Cacodylate	dimethylarsenic acid	
CFR	Code of Federal Regulation (US)	
CG	chorionic gonadotropin	
cGMP	current Good Manufacturing Practice (CFR 21)	
CHO	Chinese hamster ovary	
CHO-S-SFM-II	CHO suspended serum free medium (LTI)	
$c_{i,j}$	concentration of i in j	[$mol \cdot l^{-1}$]
ConA	concavalin A	
CSTR	continuously stirred reactor	
c_W		[-]
Cys	cystine	
D	dilution rate	[d^{-1}]
DCS	distributed control system	
d_i	diameter of i	[m]
DMEM	DULBECCO'S modified EAGLE'S medium	
DMMP	dimethylmethylphosphonate	
DMSO	dimethyl sulfoxide	
DO	dissolved oxygen	[$\mu mol \cdot l^{-1}$]
Dol-P-P	dolichyldiphosphate	
ΔE	energy difference	[J]
EDTA	ethylenediamine tetra acetic acid	
ELISA	enzyme-linked immunosorbent assay	
EMI	electromagnetic interference	
EPO	erythropoietin	
ER	endoplasmatic reticulum	
f	conversion of glucose to lactate	[-]
FADH	flavin adenine dinucleotide	
FB	fluidized bed	
FBS	foetal bovine serum (American notation)	
FCS	foetal calf serum (European notation)	

FDA		US. Food and Drug Administration, Rockville, MD
Fuc	◊	fucose
G-CSF		granular colony stimulating factor
Gal	●	galactose
GalNAc		N-acetylgalactosamine
GAMP		Good Automated Manufacturing Practice
GIBCO		Grand Island Biologicals Co., now LTI
Glc	◆	glucose
GlcNAc	■	N-acetylglucosamine
Gln		glutamine
GLP		Good Laboratory Practice
Glu		glutamate
Gluc		glucose
GMP		Good Manufacturing Practice
GUI		graphical user interface
h		hour(s)
h		PLANCK'S Number [$6.626 \cdot 10^{-34}$ J·s]
hCG		human chorionic gonadotropin
He		HENRY'S constant [µmol·mbar^{-1}]
HEPES		N-2-hydroxyl-ethylpiperazine-N'-2-ethanesulfonic acid
HF		hydrofluoric acid
HIV		human immunodeficiency virus
HPAE		high pH anion exchange
HPLC		high pressure liquid chromatography
IEF		isoelectric focusing
IL		interleukine
IMDM		ISCOVE'S modified DMEM
IQ		installation qualification
IRP		International Reference Preparation
ISPE		International Society for Pharmaceutical Engineering
IVF		*in vitro* fertilization
k		BOLTZMANN'S constant [$1.38 \cdot 10^{-23}$ J·K^{-1}]
kDa		kilo DALTON (molecular size)
k_{GLN}		decomposition constant of glutamine [h^{-1}]
k_lA		liquid phase mass transfer coefficient [h^{-1}]
KS		KAPOSI's sarcoma
Lact		lactate
LDH		lactate dehydrogenase
LH		luteinizing hormone, lutropin
LIMS		laboratory information management system
LTI		Life Technologies, Inc., Grand Island, NY, former GIBCO
LTR		long terminal repeat
M		mol·l^{-1}
$m_{recycle}$		recirculating medium flow [ml·min^{-1}]
MAb		monoclonal antibody
Man	○	mannose
MCB		master cell bank
MCR		metabolic clearance rate

MCWB	master cell working bank	
MDPA	methylenediphosphonic acid	
MEM	modified EAGLE'S medium	
m_i	mass of i	[g]
MMI	man-machine-interface	
MRI	magnetic resonance imaging	
MRP_2	manufacturing and resource planning program	
NADH	nicotinamide adenine dinucleotide	
NDP	nucleoside diphosphate	
Neu, NeuAc ❑	neuramic acid, sialic acid	
NGF	neutrophic growth factor	
N_i	number of i	[-]
NMR	nuclear magnetic resonance	
NTP	nucleoside triphosphate	
OQ	operation qualification	
OUR	oxygen uptake rate	[µmol·ml^{-1}·h^{-1}]
OxP	oxidative phosphorylation	
P	phosphor	
P/O	phosphorylation ratio; mol ATP from ADP per mol O_2	
PAb	polyclonal antibody	
PAGE	polyacrylamide gel electrophoresis	
PBS	phosphate buffered saline	
PDE	phosphodiester	
PDGF	platelet derived growth factor	
PEP	phosphoenol pyruvate	
PI	proportional-integral	
P_i	inorganic phosphor	
pI	isoelectric point	
PID	proportional-integral-differential	
PIPES	piperazine-N,N'-bis(2-ethanesulfonic acid)	
PME	phosphomonoester	
pO_2	partial pressure of oxygen (DO)	[mbar]
ppm	parts per million	
PQ	performance qualification	
PSN	penicillin-streptomycin-neomycin	
PTC	points to consider	
QA	quality assurance	
qAmm	specific ammonium production rate	[µmol·ml^{-1}·h^{-1}]
qATP	specific ATP production rate	[µmol·ml^{-1}·h^{-1}]
QC	quality control	
qDO	specific oxygen uptake rate, OUR	[µmol·ml^{-1}·h^{-1}]
qGln	specific glutamine consumption rate	[µmol·ml^{-1}·h^{-1}]
qGluc	specific glucose consumption rate	[µmol·ml^{-1}·h^{-1}]
qhCG	specific rhCG production rate	[µIU·ml^{-1}·h^{-1}]
qLact	specific lactate production rate	[µmol·ml^{-1}·h^{-1}]
RCF	relative centrifugal force	[g]
Re	REYNOLD'S number	[-]
RF	radio frequency	

rhCG		recombinant hCG	
RO		reverse osmosis	
rpm		rounds per minute	[min^{-1}]
SA	❑	sialic acid, neuramic acid	
SCADA		setpoint control and data acquisition	
SDS		sodium dodecyl sulfate	
SEM		scanning electron micro graph	
Ser		serine	
SNR		signal-to-noise ratio	
SOP		standard operating procedure	
T		temperature	[K]
t-PA		tissue plasminogen activator, Alteplase	
TBS		Tris buffered saline; Tris NaCl (pH 7.5)	
TCA		tricarbonic acid-cycle, KREBS-cycle	
TGF		transforming growth factor (?)	
TIFF		tagged image file format	
TPA		triphosphonic acid	
Tris		Tris(hydroxymethyl)amino methane	
TSH		thyroid stimulating hormone, thyrotropin	
TTBS		0.05 % Tween-20 in Tris buffered saline (NaCl)	
u_c		superficial velocity	[$cm \cdot s^{-1}$]
u_{lam}		terminal velocity, laminar case	[$cm \cdot s^{-1}$]
u_t		terminal velocity	[$cm \cdot s^{-1}$]
VI		virtual instrument (in LabVIEW)	
V_i		Volume of i	[ml]
WFI		water for injection	
WHO		World Health Organization, Geneva, Switzerland	
$Y_{i/j}$		yield i from j	[-]
γ		gyromagnetic constant	[0.1 $MHz \cdot rad \cdot T^{-1}$]
ε		porosity	[-]
η		viscosity	[mPa·s]
ν		resonance frequency	[MHz]
ρ_i		density of i	[$g \cdot ml^{-1}$]

Abstract

The present work is directed at the investigation of a fluidized bed reactor for animal cell culture, where cells adhere to macro-porous borosilicate glass carriers (SIRAN), and are suspended by recirculating upwards flowing medium.

Axial gradients for relevant metabolites in fluidized bed reactors used for industrial production of recombinant proteins in high-density cell culture systems were investigated using a new approach. A system is presented that allows non-invasive localized ^{31}P-NMR spectroscopy in a solid-liquid fluidized bed using a biomedical magnetic resonance imaging instrument. Further, stabile process control, allowing direct measurement of metabolic rates was achieved using a hardware controller (IMCS 2000) and a LabVIEW based object-oriented setpoint control and data-acquisition program with graphical user interface. This set-up allowed the non-invasive monitoring of the influence of pH and oxygen gradients on the energy state of the cells at different locations within the reactor. Application of step changes gave access to transport pattern and revealed an axial cell density gradient causing stratification.

The application of step changes and limiting conditions for the lead-nutrient glucose revealed the relationships between the calculated energy metabolism, protein synthesis and glycosylation in a CHO cell line expressing recombinant human chorionic gonadotropin (hCG). During a longterm chemostat steady-state cultivation it was shown that the cell shifted pathways to generate energy for metabolism according to availability of substrate. However, the glycosylation pattern was not influenced as determined by the 7 acid isoforms detectable using immunoblotting techniques. Change to a proprietary medium formulation (CHO-S-SFM-II) increased metabolic activity and triggered specific protein production, but did not change the relative position or amount of isoforms. However, it added two isoforms at higher pI (4.7 and 5.5).

Zusammenfassung

Die vorliegende Arbeit untersucht einen Wirbelschichtreaktor für die tierische Zellkultur, in dem Zellen adhärent auf offenporigen Borosilikat Trägern wachsen, und mit den Trägern durch eine aufwärts gerichtete Strömung rezirkulierenden Mediums suspendiert werden.

Axiale Gradienten für die relevanten Metaboliten in der Wirbelschicht, die auch für die industrielle Produktion von rekombinanten Proteinen in hochdichten Zellkulturen eingesetzt wird, wurden mittels eines neuen Ansatzes untersucht. Ein System wird vorgestellt, das nicht-invasive lokalisierte ^{31}P-NMR Spektroskopie in einer fest-flüssig Wirbelschicht mittels eines biomedizinischen Kernspintomographen erlaubt. Eine stabile Prozesskontrolle, die die direkte Bestimmung metabolischer Raten erlaubt, wurde durch einen Hardware-Controller (IMCS 2000) und ein auf LabVIEW basierendem objekt-orientierten SCADA Programm mit graphischer Benutzeroberfläche erreicht. Dieses erlaubte die nicht-invasive Bestimmung des Einflusses von pH und gelöstem Sauerstoff auf den Energie Zustand der Zelle an verschiedenen Orten im Reaktor. Die Verwendung von Stufenänderungen erlaubte Zugang zu Transportmustern und deckte einen axialen Gradienten bezüglich der Zelldichte auf, der in einer Klassierung der Wirbelschicht resultierte.

Die Anwendung von Stufenänderungen und Limitationen bezüglich des Leitsubstrates Glukose, zeigte den Zusammenhang zwischen berechnetem Energiemetabolismus, Proteinsynthese und Produktglykosylierung einer CHO Zellinie, die rekombinantes humanes Choriogonadotropin (hCG) produziert. Während einer kontinuierlichen Langzeit-Kultivierung konnte an verschiedenen Fliessgleichgewichten gezeigt werden, dass die Zelle ihre Stoffwechselpfade in Abhängigkeit vom zur Verfügung stehenden Substrat wechselt, um ausreichend Energie zu erzeugen. Eine

Veränderung des Glykosylierungsmusters, gemessen mittels Immundetektion der sieben im sauren Bereich gefundenen Isoformen, konnte nicht beobachtet werden. Mediumwechsel auf eine serum-freie Formulierung (CHO-S-SFM-II) steigerte die metabolische Aktivität und erhöhte die spezifische Proteinproduktion, veränderte jedoch nicht die Lage und relative Menge der Isoformen. Es fügte jedoch zwei Isoformen mit höherem pI (4.7 und 5.5) hinzu.

Leer - Vide - Empty

1. Introduction

The aggregated market capitalization of biotech companies was in 1994 $45 billion. This equals the size of the worlds second largest pharmaceutical firm Merck & Co. Biopharmaceuticals or bioceuticals are of significant economic importance. 1993 net sales of the top ten biotech drugs totalled $4.5 billion, and thus the biotech and associated industry became more important to California, home of the Silicon Valley, than the computer industry. This prompted Barbara Boxer, Senator of California, to intervene 1994 against the proposed health-care bill aiming at a price cap on drugs, which would make it potentially less interesting to pursue biopharmaceutical developments. Further, the number of new biotechnological drug developments, as measured by issued INDs outnumbers those for traditional pharmaceuticals [27]. The European situation is lagging behind the American dimension, with only 480 biotech companies in Europe compared to 1400 in the US, and 35 % involved in the life-sciences and health-care market, yet market volume is increasing (Figure 1-1).

Most products of biotechnology are extracellular eukaryotic proteins and thus likely to be glycosylated. Mammalian cells are used increasingly to express such recombinant proteins of significant therapeutic potential, due to their unique capability to perform complex post-translational modifications essential for full biological activity of the product. From the leading biopharmaceuticals, erythropoietin (EPOGEN by AMGEN) is the top selling drug and expressed in mammalian cells. Further, more than 95 % of the top drugs are glycosylated, and most of these are expressed in mammalian cells. Production of recombinant Factor VIII (KOGENATE, BAYER) is the first approved continuous process for the production of pharmaceuticals and it also uses mammalian cells.

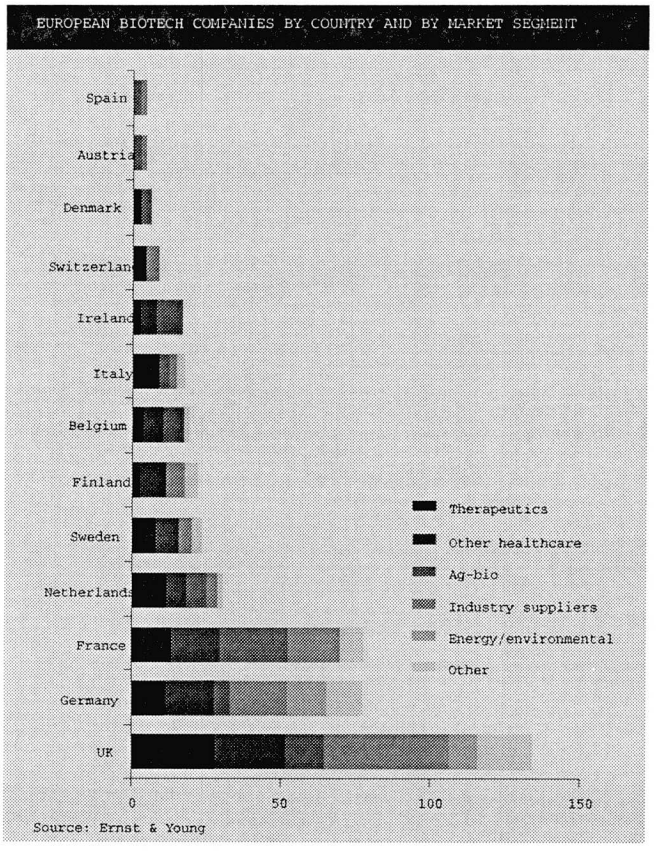

Figure 1-1. *Primary market focus of biotech companies in Europe;* [130]

To increase volumetric productivity, fluidized beds are used best for the high-density cultivation of mammalian cells in continuous industrial production of recombinant proteins. Cells are then grown on the internal and external surface of macroporous microcarriers which are suspended by recirculating medium supplying the cells with nutrients and removing the secreted product as well as metabolic waste products. Advantages are simple design, integrated cell retention, low shear stress, high cell densities ($2 \cdot 10^8$ cells/ml), and scalability. Due to metabolic activity, radial gradients can exist for nutrients and inhibitory waste products through the carrier particles and the surrounding cell layer. Yet more apparent are axial gradients from top to bottom.

Although the basic concepts of the fluidized bed reactor and of cell metabolism in general are clear, the relationship among environmental conditions, nutrients, reactor conditions, cell metabolism and productivity are not yet fully understood. This is in part due to the fact that essential variables such as cell density and intracellular concentrations of metabolites are not directly accessible without significant disturbance

to the whole system. On-line application of localized nuclear magnetic resonance spectroscopy can offer new insight into the fluidized bed reactor for animal cells. The present research attempts to elucidate the influence of oxygen and pH, as the principal biochemical parameters, and their gradients in a typical high-density reactor system, such as the fluidized bed, on cellular metabolism. Of particular interest is the energy state of cells in culture in their bioprocess environment, the bioreactor, which is in this case a fluidized bed. Step changes were applied to obtain dynamic metabolic responses.

Environmental conditions may result in micro-heterogeneity of the product with different degrees of glycosylation, due to shifts in the metabolic regulation. Information about cell performance and characterization of the reactor is therefore essential also for economic production and approval from the legal authorities (FDA). In the present research the chosen product gives possibilities for variations in the degree of complete formation of the protein backbone as well as in the carbohydrate domain. In order to achieve the highest yield of optimal, that is correctly assembled and glycosylated, product, the fermentation conditions (environment) need to be investigated and optimized, e.g. using electrophoretic and immunoblotting techniques to monitor the product. The metabolic relationships during steady-states in a chemostat and the effects of step changes in the lead nutrient glucose on the glycosylation pattern are analyzed in the present research.

Due to the nature of the project this dissertation is organized in several distinct and independent chapters representing the individual research aspects, rather than a sequential investigation and account. A possible repetition of a said aspect, such as introductionary remarks, may therefore rather accentuate the independence of the affected chapter. Specific techniques are detailed where they are reasonably related to the respective experiments and results.

The power of information lies in using it.

2. Mammalian Cell Metabolism

2.1. Energy Metabolism

An overview of the primary pathways used by mammalian cells that simultaneously catabolize glucose and glutamine is summarized in Figure 2-1. Whereas the predominant source of pyruvate is the glycolytic pathway, some may also be formed from the pentose pathway, the malate shunt (conversion of malate to pyruvate), and the pyruvate/malate shuttle associated with lipid synthesis. Pyruvate can enter the TCA cycle by two main enzymes, pyruvate dehydrogenase and pyruvate carboxylase. For energy production, pyruvate enters primarily through pyruvate dehydrogenase, whereas cells exhibiting high rates of lipid synthesis have significant fluxes through pyruvate carboxylase [163]. All reactions are enzymatically catalyzed concurrently with phosphorylation of high-energy phosphates, such as ADP to ATP, FAD to $FADH_2$, or NAD to $NADH_2$, the latter ones having a higher energy content which is released when taking the reverse reaction. Further, ATP is formed with conversion from $NADH_2$ to NAD and $FADH_2$ to FAD, yielding three and two mol ATP, respectively, per mol. Thus the energy balance can be understood with ATP as the universal currency. Specifically, the balance yields per mol glucose in the glycolysis 6 or 8 mol ATP, of which 4 are consumed within, in the oxidative decarboxylation 6 mol ATP, and in the TCA cycle 24 mol ATP [8].

Some evidence has been found that the pool size of ATP, the adenylate energy charge (AEC), or the pool size of UTP influence and / or are dependent upon the cell cycle, the stimulation of cells by serum, and growth control [187]. Comparatively high levels of ATP, for instance, are associated with the log phase of growth, indicating a greater catabolic flux than during the stationary phase of growth [174]. ATP is further utilized for the biosynthesis of proteins (88 %), e.g. recombinant proteins, and together

with other high-energy-phosphates, such as UTP, and GTP used as a precursor for glycosylation.

2.1.2. pH and Oxygen Influence

During aerobic respiration an organic compound is oxidized consuming oxygen. Specifically, in the respiratory chain the four hydrogen pairs formed during the TCA are transferred to dissolved oxygen, by enzymes located in the mitochondrial wall from hydrogen bearing $FADH_2$ or $NADH_2$, generating 2 or 3 mol ATP, respectively, per mol high-energy-phosphate, ultimately forming water. Because mammalian cells are believed to derive a large portion of their energy as ATP from oxidative phosphorylation as opposed to other energy producing pathways, the concentration of ATP should be a useful indicator of the cells' access to oxygen. Depriving cells of dissolved oxygen results in decreased ATP production, ultimately truncating the energy gaining capabilities and metabolism of the cell severely.

Electron flux through the mitochondrial membrane is by virtue of an enzymatic chain accompanied by a proton transfer resulting in a pH gradient along the mitochondrial membrane of about 1.4 pH units, with the membrane side being more alkaline than the cytosolic side. Therefore the ATP synthesis can also be written as:

$$ADP + P_i + [H^+]_{outer} \longleftrightarrow ATP + H_2O + [H^+]_{inner}$$

From this we can deduce that a membrane gradient, specifically a pH gradient, can be transformed into energy, such as ATP, or that a small gradient will result in lower ATP content [120]. Therefore, the existence of a suitable pH gradient in fact contributes to the energy state of the cells, and thus also supports the existence of pH optima for animal cells differing from their intracellular pH.

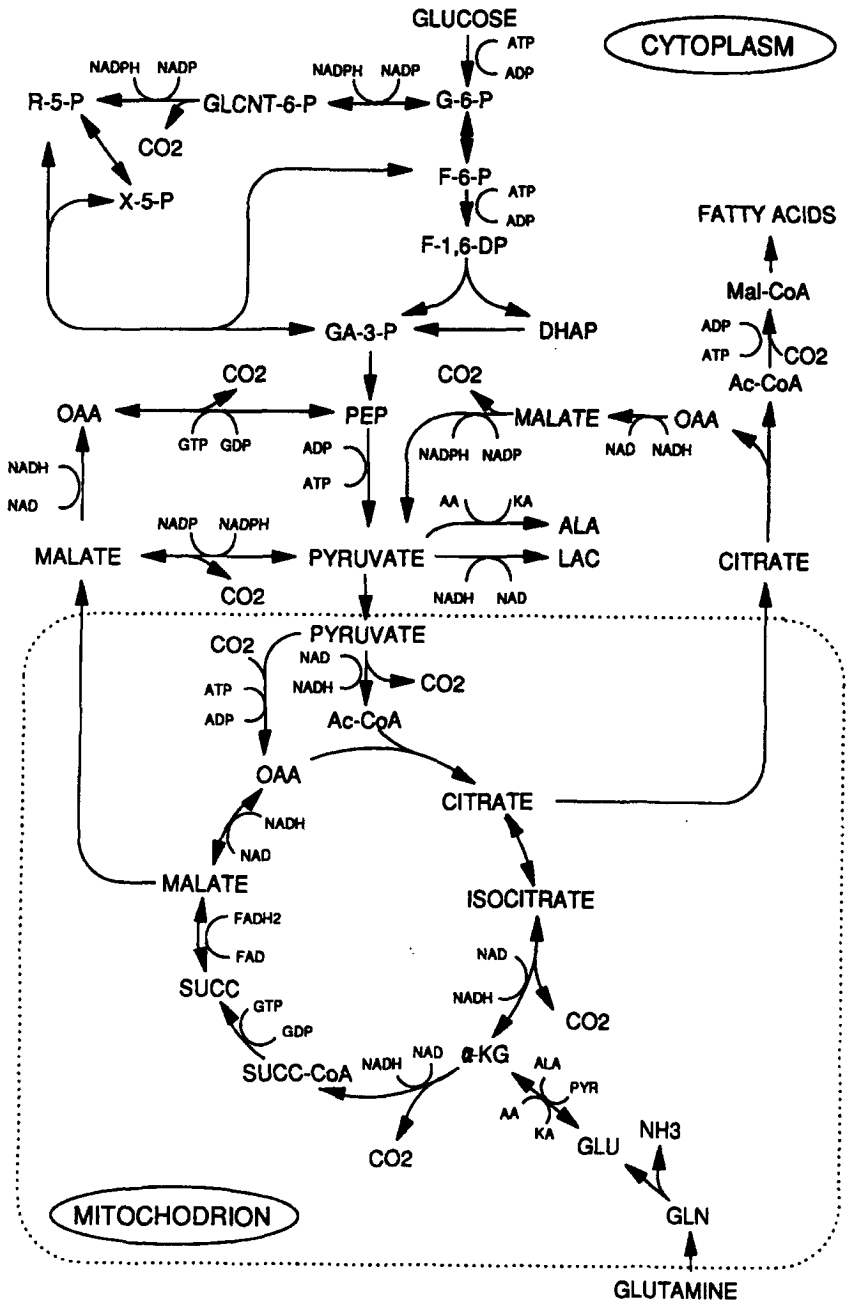

Figure 2-1. *Metabolic pathways in mammalian cells; Glycolysis and TCA* [142]*, Abbreviations used are: G-6-P glucose-6-phosphate; F-6-P fructose-6-phosphate; F-1,6-DP fructose-1,6-diphosphate, GLCNT-6-P gluconate-6-phosphate, R-5-P ribose-5-phosphate, X-5-P xylose-5-phosphate, GA-3-P glyceraldehyde-3-phosphate, PEP phosphoenolpyruvate, DHAP dihydroxy acetone phosphate, OAA oxaloacetate, Ac-CoA, acetyl-coenzyme A, Mal-CoA malonyl-coenzyme A, α-KG α-ketoglutarate, SUCC succinate, SUCC-CoA, succinyl-coenzyme A, GLU glucose, GLN glutamine, CO2 carbon dioxide, ADP adenosine 5'diphosphate, ATP adenosine 5'-triphosphate, GDP guanosine 5'diphosphate, GTP guanosine 5'triphosphate, FAD/FADH2 flavin adenine dinucleotide oxidized/reduced forms, NAD(P)/NAD(P)H nicotinamide adenine dinucleotide (phosphate) oxidized/reduced forms, AA amino acids, KA keto acid*

2.2. Protein Glycosylation

2.2.1. Glycoprotein Translation

Protein translation occurs by virtue of an mRNA template produced from cellular DNA, assuring high fidelity of the protein structure. After assembly of the protein backbone in the ribosome, post-translational modification, e.g. glycosylation, takes place in the rough endoplasmatic reticulum (ER) to which the ribosome is attached. Oligosaccharide translation follows then as a sequence of enzymatic reactions in several intracellular compartments, prone to various influences. The main carbohydrate structures that will be attached to the backbone are fucose, glucose, galactose, N-acetylglucosamine, N-acetylgalactosamine, mannose, and neuramic acid (sialic acid), as well as their sulfurylated or phosphorylated derivatives. The oligosaccharides are covalently attached through the side chain amide of asparagine (Asn) in the case of N-linked or side chain hydroxyl of threonine (Thr) or serine (Ser) in the case of O-linked carbohydrates.

Existence and character of glycosylation significantly determine the surface chemistry, i.e. surface charge. This affects solubility, which is usually enhanced by presence of carbohydrates, in the same way as resistance to protease attack and thermal inactivation are enhanced.

2.2.1.1. N-linked Carbohydrates

All N-linked oligosaccharides posses an invariant pentasaccharide core composed of three residues of mannose and two residues of GlcNAc. Further categorization is made based upon the type of residues and branches found peripheral to the invariant core: *high-mannose*, if only mannose is present, *complex* if other monosaccharides are present, *hybrid* if features of both types are present in the bi-, tri, tetra-, or penta-antennary branches [39].

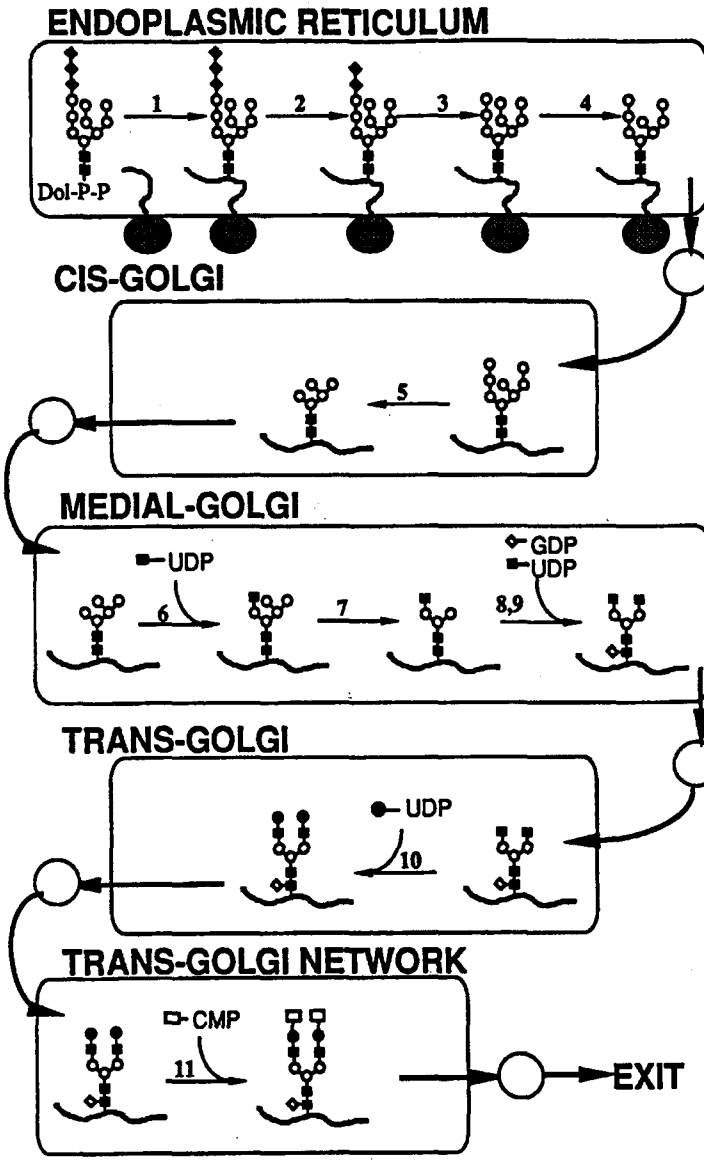

Figure 2-2. *Possible pathway for N-glycosylation;* [73] *Abbreviations used are : 1-11 enzyme catalyzed reactions,* ■ *GlucNAc,* O *mannose,* ◆ *glucose,* ◊ *fucose,* ● *galactose,* ❒ *SA.*

N-linked glycosylation (Figure 2-2) starts with the synthesis of a lipid-linked carbohydrate moiety ($Glc_3Man_9GlcNAc_2$) and its transfer to the nascent polypeptide chain in the ER during transport across the ER membrane, where it is attached to the sequence Asn-X-Ser/Thr of the backbone. Subsequent initial trimming occurs in the rough ER as a sequence of exoglucosidase catalyzed reactions. Processing of the N-linked carbohydrates follows after vesicular transport to the cis-Golgi cisternea. The glycoproteins traverse the stack of Golgi compartments from cis- through medial- to trans-cisternea by means of vesicles and undergo a sequence of site- and substrate-

specific exoglucosidase-, mannosidase-, fucosidase-, and glycosyltransferase-catalyzed reactions. This results in high-mannose, hybrid or complex-type oligosaccharide structures at the specific sites. A subset of glycoproteins undergo phosphorylation or sulfurylation depending on presence of the respective catalyzing enzyme and processing pathway. The final steps in the trans-Golgi cisternea add the outer chain galactose and sialic acid residues to the glycoprotein, which is secreted by means of a vesicular transport into the extracellular space [75, 113].

The oligosaccharide structure as such depends on the order and extent to which the distinctly localized enzymes are encountered. The efficient N-glycosylation of proteins is dependent on a sufficient pool of completely assembled and glycosylated lipid-linked oligosaccharide donors, an adequate activity of oligosaccharyltransferase, and a properly oriented and accessible Asn-X-Ser(Thr) sequence in the acceptor.

2.2.1.2. O-linked Carbohydrates

O-linked oligosaccharides can be sub-classified according to the core structure linked to the hydroxyl side chains of Ser or Thr, with the largest naturally occurring fraction linked via N-acetyl-galactosamine (GalNAc) and other linkages via fucose or glucose. Four general core structures with GalNAc have been reported [39].

The first step in O-glycosylation by mammalian cells is the enzymatic covalent attachment of, e.g. N-acetylgalactosamine, to serine or threonine. Then a series of subsequent glycosyltransferase-catalyzed reactions follow, with UDP-, GDP-, and CMP-monosaccharides as donor substrate, in the Golgi compartments similar to the N-glycosylation. However, no specific template or lipid-linked precursor has been found as for N-glycosylation. O-linked sites are usually less branched and shorter glycosylated than N-glycosylation sites.

2.2.1.3. Natural Microheterogeneity

Based upon the pathway for post-translational modification it becomes clear that the succession of enzyme-catalyzed reactions and mass transfers is susceptible to variability. The phenomenon of variability in oligosaccharide structure at a particular

site appears to be a rule of nature and is termed *site microheterogeneity*, sometimes also variations in the occupancy of specific sites, as in the case of t-PA, exists (*variable site occupancy*). A group of glycoproteins with identical protein backbone but different local oligosaccharide structures are designated *glycoforms* or *isoforms*.

Specific reasons for variability include participating enzymes being spatially dispersed along the route of synthesis, steric hinderance locally and across the molecule, site- and substrate specific processing of the glycosyltransferase, interdependency and competition of enzymes, incomplete terminal processing, and pH- and temperature-optima of the involved enzymes.

It is estimated that about 100 enzymes are necessary to explain the known oligosaccharide structures of mammalian glycoproteins. But only a small subset may be present in the host system, thus the number of possible isoforms is limited[73].

The theoretically possible number of structures, e.g. in comparison to a protein structure, depends on the number of available monomers (seven oligosaccharides and their respective sulfurylated and phosphorylated derivatives, thus a total of 21 as opposed to only four nucleic acids), the number of glycosylation sites, e.g. eight for hCG, and the possible different (glycosidic) bindings (2,144,640 for a pentasaccharide as opposed to 120 for a penta-nucleic acid).

The subtle physiological control of glycosylation appears to add another level of regulation to alter the activity and circulatory concentrations of hormones. It seems however more likely that the expression, rather than the activity of an involved enzymes is under such control [215].

Incorrectly folded proteins, e.g. due to mutagenesis at distinct residues during translation, are rapidly degraded and internally recycled. Subtle conformational differences between partially folded or misfolded β-subunits determine whether β-hCG is degraded or whether it undergoes intracellular translocation and secretion [11]. This suggests the existence of intracellular recognition receptors and correction mechanisms [64].

2.2.2. Structure-Function Relationships

Bioactivity analysis of TSH isoforms showed that the more basic and less sialylated fractions were *in vitro* more active than the more acidic fractions. However, *in vivo* the acidic and higher sialylated fractions showed longer half-lives and higher *in vivo* bioactivity [212].

Lack of terminal sialic acids has been shown to increase clearance via the hepatic galactose N-acetylgalactosamine receptor mechanism [7]. A low clearance rate, due to higher sialic acid content and thus lower pI of the molecule, has the advantage of allowing the product sufficient time to exert an effect on the human system. Treatment utilizing such proteins would allow lower dosage to maintain the therapeutic serum level. However, the hepatic caption by the ASHWELL receptor is not necessarily the main route of elimination of hCG [6], as the continuous removal of proteins smaller than 70 kDa via kidney glomerular tubules was found to be considerable. Cleavage of sialic acids to increase the *in vitro* activity does not result in enhanced *in vivo* efficiency as the clearance rate reduces the benefit.

Tetraantennary structures are more active than complex biantennary structures *in vivo* [213]. Completely deglycosylated hCG, prepared using site-directed mutagenesis was shown to be an irreversible receptor blocker with antagonistic properties, such as not stimulating cAMP accumulation [48].

Oligosacccharides have been shown to influence antigenicity by conformational change, steric hinderance or charge interactions, e.g. due to sialic acid termination. The influence on the ability to elicit an immune response, e.g. formation of antibodies in the receiving organism or immunogenicity, does not seem to be influenced in the case of EPO, t-PA, IL-2 or interferones where the recombinant forms differ slightly from the natural forms and multiple isoforms were likewise found. However, non-glycosylated forms can aggregate more easily and thus form immunogenic structures [73].

2.2.3. Bioprocess and Environmental Effects

2.2.3.1. Host System

Carbohydrate analysis of glycoproteins has demonstrated the uniqueness of the oligosaccharides in terms of increased branching, specifically when secreted by tumors as compared to natural forms [178], not only for hCG, but also for other glycoproteins.

Recombinant bovine LH glycan branches terminated in sialic acid linked to galactose, whereas the pituitary form of LH terminated in sulfated GalNAc. The latter form showed less biological activity [39].

Further, glycoprotein hormones expressed in CHO cells, yeast and insect cells contain distinctly different glycan structures characteristic to the cell type. This is due in part to the fact that yeast and mammalian cells do not have identical protein recognition sequences for the initiation of O-linked glycosylation. Insect cells seem to produce generally shorter branches with no sialic acid termination [73]. Transgenic animals have been reported to glycosylate mainly towards high-mannose or fucose type proteins with low sialic acid termination.

Slowly dividing confluent HepG2 cultures expressed transferrin with a 4.5 fold greater proportion of biantennary complex-type oligosaccharides than rapidly dividing, sub-confluent cultures mostly expressing non-glycosylated transferrin. This regulation is due to the lower activity of GalNAc-transferase V [87].

Using mutant cell lines and radio-labelling techniques it was recently demonstrated that CHO cells express many glycoproteins containing O-linked fucosyl residues [210]. Alterations in the glycosylation *site* found in these CHO glycosylation mutants raises caution when selecting specific clones after gene amplification [207] and can therefore also be affected genetically.

All these differences in oligosaccharide structure among different cell lines and species are attributable to subtle differences in the presence, relative activity and spatial localization of the involved substrate-specific glycosyltransferases in the Golgi. Still, overall the CHO cell glycosylation corresponds closest to the human (native) isoforms.

2.2.3.2. Culture Method

Variations in the cell culture method, such as substrate (glucose) and oxygen availability and presence of ammonia have also been shown to influence the glycosylation pattern. Glycoproteins from cells grown in monolayers can have a different array of carbohydrates as compared to those growing in suspension [207]. A 3 l small-scale microcarrier fed-batch process resulted in a reduced amount of sialylated oligosaccharides as compared to a 20 l large-scale continuous perfusion suspension process. Specifically, the perfusion culture resulted in a higher proportion of more complex oligosaccharides. However, it was not found, using enzymatic digestion and HPLC separation of the released carbohydrate side-chains, that a change in pattern occurred over the length of a three month period in either system, the heterogeneity was consistently stable for each system [226].

Hollow-fiber bioreactors were found to produce recombinant TSH with lower sialylation and galactose content as compared to TSH from large scale microcarrier bioreactors with the same cell line. It was found that this is due to an increase in sialidase activity due to activity derived from disrupted cells, or possibly caused by a decrease of intracellular sialyltransferase activity due to oxygen limitations [212].

The effect of the dilution rate on CHO cell physiology and recombinant interferon-γ production in glucose-limited chemostat suspension culture was recently assessed. Despite changes in the IFN-γ production rate and cell physiology, the pattern of IFN-γ glycosylation was similar at all except the lowest growth (dilution) rates, where there was increased production of non-glycosylated IFN-γ [91].

2.2.3.3. Medium

A variety of other environmental factors have been mentioned to influence the glycosylation, such as vitamins, hormones, specifically when acting on tissue they are directed towards also *in vivo*, and chemicals, such as DMSO, TPA, EDTA, HEPES, PDGF, and tunicamycin.

Cells starved for *glucose* use an alternate pathway to synthesize N-linked structures [113]. An observed increase in mRNA as result of a cell culture environment change correlates to the increase of the respective enzyme. Further the glycosylation reaction catalyzed by this enzyme results in a change of pattern. Glucose starvation led to smaller precursors being attached to the nascent glycoprotein in the initial glycosylation step taking place in the ER, as well as to an absence of oligosaccharide moieties [75]. The mechanisms involved are depletion of the cellular energy state, cell and compartment disruption, disturbance of vesicle transport, modulation of glycosidase and glycosyltransferase activities.

Ammonia has typically been identified as a harmful component in cell culture media because of its inhibitory effect on cell growth [70, 116, 149, 153]. It has been reported to affect many cellular processes including the Golgi compartment pH enzyme activity, vesicle fusion and transport, and lyosomal proteolysis, all of which may contribute to the pH-dependent effect of ammonia on glycosylation of hormonal glycoproteins, e.g. placental lactogen-1 (mPL-I) in CHO cells [20]. Specifically, high levels of ammonia (9 mM) inhibited the expression rate of mPL-I at low pH and shifted the amount of highly glycosylated isoforms from 90 % to 25 %.

Control of terminal sialylation of the oligosaccharides of glycoproteins via a multi-level *pH* control strategy was suggested to manage the effect of high level of ammonia on the glycosylation of cell products. Specifically, as it was observed that high ammonia concentrations (above 6 mM), resulting from high glutamine or alanine nutrient feed levels, inhibited the terminal sialylation [139]. It was proposed, as the culture approaches production phase, that the culture pH be shifted gradually from a higher pH, of around 7.2 optimal for growth, to a lower level (6.7 to 7.1) optimized to achieve the desired terminal sialylation.

10 mM NH_4Cl or 20 mM Tris inhibits terminal sialylation in various cell lines [74]. Further investigations revealed that ammonium ion concentrations of just a few millimol, commonly reached in mammalian cell culture, seem to reduce the degree of final O-linked

sialylation in CHO cells producing G-CSF. The reduction was not the effect of an extracellular sialidase, but rather a result of a change of the intracellular pH due to an increased intracellular ammonia concentration. This pH change reduced the activity of glycosyltransferases in the intracellular compartments (Golgi) responsible for terminal sialylation. Ammonia levels of below 6 mM were considered to be safe [3, 5].

2.2.3.4. Post-Expression modification

CHO and other mammalian cell lysates contain enzymes, such as sialidase, β-galactosidase, β-hexosaminidase, and fucosidase that can accumulate in the medium during long-term cultivation after cell rupture and can lead potentially to modification of carbohydrate side-chains. Enzymes are released either upon damage to the respective vesicle, i.e. Golgi, or secreted due to missorting of the enzymes, which in return can be enhanced by high ammonia levels. Namely, sialidase from CHO cell lysates has been shown to be stable and active at cell culture conditions (pH 7.5, 37 °C) with a half-life of 57 h. A sialidase could recently be identified in cell culture fluid from several CHO cell lines. It was purified and showed a pH-optimum at 5.9 with an activity of 25 % at common cell culture conditions [225].

2.2.4. Importance of High Energy Phosphates

The nucleotide sugars, UDP-glucose, GDP-mannose, and UDP-N-acetyl glucosamine, which are required for the initial steps in the assembly of the oligosaccharide chains, are derived from glucose-6-phosphate and fructose-6-phosphate. The availability of precursors, such as sugar-phosphates and nucleotide-phosphate sugars (NDP, NTP) may therefore limit or vary the post-translational modification. Indeed in glucose starved CHO cells, there is some evidence that the transfer of mannose to the dolichol-phosphate carrier may be limited by the supply of mannose, which may in turn be limited by a diminished supply of fructose-6-phosphate. In addition to sugar moieties, glycosylation is also depending on nucleotide and lipid precursors, and although both of these may be adversely affected by glucose limitation, they are also related to other metabolic pathways. There is evidence that the activity of some

glycosylation enzymes is regulated by phosphorylation, and that some glycosyltransferase genes may be cell-growth associated [91].

Investigations [112] showed that a markedly elevated amount of lipid-linked core oligosaccharides and the flux through the pool is responsible for increased N-glycosylation. It is upwardly regulated by the presence of cAMP. In other words, a large pool of cAMP increases the chance of N-glycosylation. cAMP, a secondary messenger substance, is in return upward regulated by the presence of glucagon and ATP as substrate and downward regulated by the presence of glucose [120].

2.2.5. Other Factors Influencing Product Heterogeneity

Besides the expression system and the overall bioprocess conditions, downstream processing and purification may also contribute to the heterogeneity of the product. Existence and character of glycosylation significantly determine surface chemistry, i.e. surface charge. This results in changes of both solubility, which is usually enhanced by presence of carbohydrates, and affinity to chromatographic resins, such as ion-exchange or hydrophobic interaction. Downstream processing protocols may be used to purify, solubilize, reduce, renature, and oxidize proteins. They may be selective for subsets of a heterogeneous product based on their underlying biochemical and physico-chemical mechanism. Therefore, their influence either by narrowing or broadening heterogeneity must be assessed and carefully validated as outlined below [194].

2.2.6. Regulatory Aspects

Based on the Food, Drug and Cosmetics Act from 1918, the current Good Manufacturing Practice (cGMP) has been established as part of the Code of Federal Regulations (21 CFR). Together with the Guides and Guidelines, published by the US. Food and Drug Administration (FDA), as well as the Points to Consider (PTC) by the Center for Biologics Evaluation and Recommendation (CBER), they represent the legal and administrative framework in which the approval for marketing of a new drug is regulated. Specifically, it is stated that documented evidence providing a high degree of assurance has to be established that a new drug is safe, efficient and consistent in

quality. Lot release specifications and tests focus therefore on purity, potency, and identity. At least two analytical methods based on unrelated molecular characteristics should be employed for such purity testing. Suggested methods are SDS-PAGE, immunoblots, size-exclusion chromatography, reversed-phase and HPAE HPLC, and peptide mapping. However, in peptide mapping and MALDI-MS chromatography many glycopeptides show as broad peaks, and only little information can be deduced about their heterogeneity. Comparison with reference material, which by itself has to be characterized and validated, is crucial in assessing the quality. It is however specific policy of the regulatory body to review the process and documentation on a case by case basis before granting approval for the product licence application (PLA). Process changes after the PLA has been approved, are normally reasons for partial re-validation with considerable associated economic implications [231, 232].

Similar requirements are set forth in the corresponding EU regulation (EC 19-22/1987). However the legal and administrative situation has not yet been finalized, despite existence of the newly established (January 1995) European Medicines Evaluation Agency in London, UK. Due to the economic importance of the affected market and the impact on the respective national economies, a competition gearing towards faster approval processes has started with impact on administration and regulatory procedure. This also includes the opportunity to approve rather a mixture of biologically active proteins as biopharmaceutical drug than an analytically defined, pure, small molecule.

2.2.6.1. Practical Implications and Actual Cases

As outlined, heterogeneity in carbohydrate structure is the rule rather than the exception, and therefore a glycosylated biological submitted for approval is most likely composed of a mixture of several distinct glycoforms (isoforms) each possibly having characteristic biological properties. Thus heterogeneity has the potential to affect a protein's biological activities. It is therefore crucial to control the heterogeneity of a protein product and to demonstrate that it can be produced consistently from batch to

batch, in order to comply with the outlined regulations. These objectives are accomplished by appropriate validation of the entire manufacturing process, use of well-designed in-process controls to monitor critical steps in manufacturing, and specifications for the purified protein that use tests designed to discriminate its different forms, e.g. lot release testing. Heterogeneity should then be demonstrated to be produced consistently between different production lots. For instance, it is possible to determine the relative immune reactivity of different peptide peaks found in an HPLC profile and show their consistency. If more than one peptide is immunoreactive, it is then necessary for the manufacturer to demonstrate that the same distribution pattern of peaks and intensity can be obtained on a routine basis, which means usually in at least three different batches.

Isoelectric focusing (IEF) capable of discriminating protein species that differ in sialic acid contents or amino acid composition was used to asses consistency of the murine monoclonal antibody OKT3 (Ortho Biologics) with respect to the number of bands and staining intensities [157].

The IEF pattern of erythropoietin (Amgen), a 40 kDa glycoprotein with 50 per cent carbohydrates in three N-linked and one O-linked site, shows four predominant bands with two minor bands. This is by no means indicative of all variations in molecular structure, but is sensitive in monitoring lot-to-lot reproducibility and has been used as the main QC/QA tool. The production process is essentially a fed-batch cultivation in roller bottles with media changes for harvest. A Radioactive-immuno-assay, bioactivity, SDS-PAGE, *N*-terminal sequencing, IEF, WESTERN blotting (Immunodetection), peptide mapping and SEC-HPLC were applied to fulfil regulatory requirements [129]. This appears less intense than the t-PA process.

Size exclusion chromatography in the presence of SDS is used to validate heterogeneity during large-scale semi-continuous production of t-PA (Alteplase, Genentech), a 70 kDa glycoprotein containing a number of sulfide bridges and four N-linked glycosylation sites, which undergoes proteolytic processing during production to

a two-chain form. In fact, process change and optimization, such as feeding strategy, revealed changes in glycopattern and potency [230, 233]. Overall an array of genetic, cellular and product traits, including peptide map, neutral sugar content, and sialic acid content, was necessary to satisfy regulatory concerns in an exceptionally comprehensive approval process.

GM-CSF, an 18 kDa glycoprotein containing two disulfide bridges and sites for both N- and O-linked glycosylation, has been shown to affect clinical efficacy due to differences in carbohydrate content. Produced from yeast, three isoforms are apparent in GM-CSF on SDS-PAGE. Yeast is known to produce high-mannose carbohydrates. Immunoblotting (WESTERN blotting) was added to assess the consistency [157].

Soluble CD4 (SmithKline-Beecham) was monitored using tryptic peptide mapping, oligosaccharide fingerprinting using ion exchange chromatography, SDS-PAGE and OKT4a binding. The process showed production inconsistencies, such as plasmid copy loss, mRNA levels, variable specific productivity, and contaminants. However the purification process was designed robust enough to provide a consistent and safe product meeting specifications [129]. This underlines the importance of downstream-processing for the actual industrial process with respect to quality.

Despite that a framework has been developed for evaluating questions regarding diversity associated with protein primary structure, such as amino acid sequence and composition, the answers to many of theses questions are less than satisfactory when addressing diversity due to carbohydrate structure. A full characterization would require determination of the proportions of each glycoform and the contribution of each to the product's biological activity. Methods are not currently available for the rapid and routine determination, and therefore assessment of proper protein structure usually relies on an appropriate biological potency assay. Products will therefore continue to be heterogeneous despite technological advances. Though not satisfactory, this is accepted by the regulatory authorities [157, 194].

2.3. Human Chorionic Gonadotropin

2.3.1. Physiology

Human chorionic gonadotropin (hCG) is secreted by the anterior lobe of the pituitary gland or adeno-hypophysis, as well as the synciotrophoblastic cells of the placenta. It is regulated by a complex interaction between the hypothalamic gonadotropin-releasing hormone (GnRH) and both positive and negative feedback effects of circulating sex hormones on the pituitary and hypothalamus. ASCHHEIM and ZONDEK are credited with discovering the presence of gonadotropic activity in the urine of pregnant women (1927). Their discovery has led to numerous tests and patents in the field of early pregnancy based upon the immunological detection of hCG.

The main feature of hCG is its capability of maintaining the corpus luteum in the ovary, and its function in the early stages of pregnancy appears to be the rescue of the corpus luteum from declining and stimulation of luteinized cells to produce progesterone which is necessary to support the endometrium and sustain the early weeks of pregnancy [30]. hCG plasma levels rise sharply up to 160-280 $IU \cdot ml^{-1}$ in the first trimester of pregnancy and fall to under 10 IU/ml during the rest of the pregnancy. Whereas hCG is found mainly as a heterodimer in the early stages of pregnancy, in the later stages both subunits are found in large quantities as separate molecules.

Patients with choriocarcinoma excrete large quantities of hCG in their urine. The amino acid composition of this hCG is in good agreement with pregnancy hCG, and they appear to be immunologically identical [30]. Their carbohydrate structure is different however, as will be outlined below.

2.3.2. Biochemistry

hCG is a heterodimeric glycoprotein (M_r 38,000) with approximately 30-35 % carbohydrate (w/w) composed of two polypeptide chains of 92 (α) and 145 (β) amino acids (Figure 2-3). The α-subunit is common to all hormonal glycoproteins, e.g. hCG, thyroid-stimulating hormone (TSH), follicle-stimulating hormone (FSH), and luteinizing hormone (LH), and it is encoded by a single gene. Among the hormones appearing in

early pregnancy, β-hCG is the most predominant. Although the heterodimer is required for receptor binding and full biological activity, it is the β-subunit that determines the specific activity of each hormone.

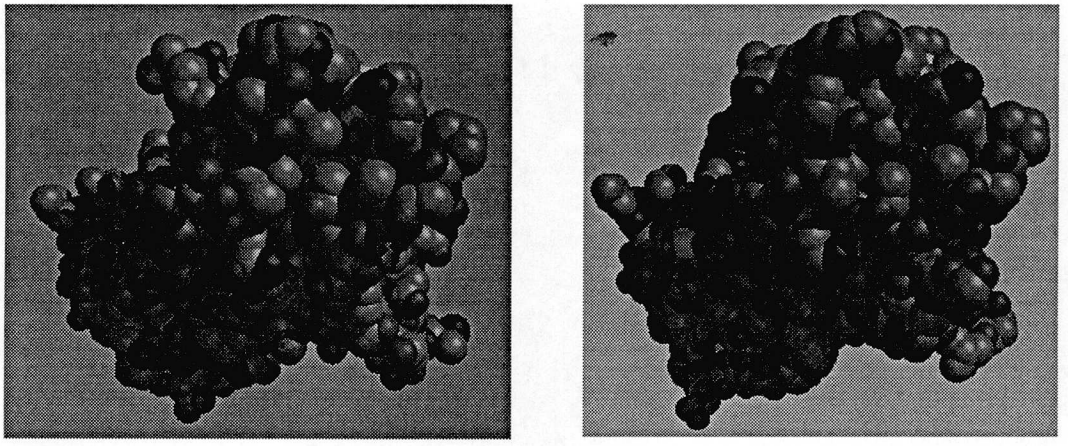

Figure 2-3. *Unglycosylated hCG as space-filling model; (PDB, GenBank)*

1 mIU hCG corresponds according to the first International Reference Preparation (IRP) 75/537 to 0.1077 ng hCG or in other words 1 mg equals 9,285 IU. The second IRP (1986) was however determined to have a bioactivity of 13,450 IU per mg highly purified hCG in rats.

2.3.2.1. α-chain

The α-chain (P01215; M_r 10206) consists originally of 116 amino acids, of which the first 24 amino acids are a signal peptide, which is cleaved from the mature protein prior to assembly of the dimer. It features two fully glycosylated N-linked oligosaccharides at Asn-52 and Asn-78, which have site-specific functions with respect to secretion and assembly, such as the connection to the β-chain. Asn-52 and its N-linked oligosaccharide play an important role in signal transduction, unlike the Asn-78 site. 10 Cys residues form five intra-molecular disulphide bridges [146]. Sulphide bonds at Cys-7, 31, 32, 59, and 87 are not essential for folding and dimerization but influence biological activity [64]. The theoretical pI of the backbone *without* carbohydrate side-chains is 8.38. The amino acid sequence as found by various authors and retrieved from GenBank is given below:

```
1234567890  1234567890  1234567890  1234567890  1234567890  1234567890
apdvqdcpec  tlqenpffsq  pgapilqcmg  ccfsrayptp  lrskktmlvq  knvtsestcc
vaksynrvtv  mggfkvenht  achcstcyyh  ks
```

Figure 2-4. *Amino acid sequence of α-hCG; (one letter code; GenBank)*

2.3.2.2. β-chain

The β-chain (P01233; M_r 15532) consists originally of 165 amino acids of which the first 20 amino acids are a signal peptide, which is cleaved from the mature protein prior to dimerization. The β-chain has 85% sequence homology with the β chain of LH and probably evolved from it. hCG and LH bind to the same receptor. It is encoded by seven genes contained in the human genome. Its difference lies mostly in the unique 37 amino acid hydrophilic carboxyl-terminal extension (115-145) containing the four mucin-like O-linked oligosaccharides at Ser-121, Ser-127, Ser-132, and Ser-138. In addition it features 2 N-linked oligosaccharides at Asn-13 and Asn-30. The Asn-13 carbohydrate group plays a more important role in steroid formation than the Asn-30 carbohydrate group. 12 Cys residues form six disulphide bridges. The theoretical pI of the protein *without* carbohydrate side-chains has been calculated to be 8.65.

```
1234567890  1234567890  1234567890  1234567890  1234567890  1234567890
skeplrprcr  pinatlavek  egcpvcitvn  tticagycpt  mtrvlqgvlp  alpqvvcnyr
dvrfesirlp  gcprgvnpvv  syavalscqc  alcrrsttdc  ggpkdhpltc  ddprfqdsss
skapppslps  psrlpgpsdt  pilpq
```

Figure 2-5. *Amino acid sequence of β-hCG; (one letter code; GenBank)*

2.3.3. Crystal Structure

Crystals have been successfully grown following hydrogen fluoride treatment that results in a roughly 50 per cent reduction of the carbohydrate content of the hormone [173]. Subsequent x-ray crystallography revealed that the folding topology (Figure 2-6) of hCG is most unusual in that it has unexpected folding motifs, interlocking subunit-subunit interactions and symmetry, as well as a surprisingly high

ratio of protein surface to hydrophobicity [118]. The heterodimer adopts an elongated shape consisting of β-sheets with the two subunits intertwined. The core structure contains a cystine knot motif, where a disulphide bridge connecting two strands penetrates into an eight residue circle, generated by a pair of disulphide bridges connecting two other strands. The global folds of the subunits are surprisingly similar when super-positioned, it is striking in the cystine knot region. Both subunits are members of a structural super family of cystine-knot growth factors, such as NGF, TGF-β2 and PDGF. The disulphide-tethered carboxyl-terminal end of the β-subunit embraces a long loop of the α-subunit. This unprecedented *seat-belt* arrangement has implications for possible *in vivo* folding pathways for hCG heterodimer formation, because this process will be governed by the precise order of disulphide bridge formation. Another striking feature of the hCG heterodimer structure is the large surface-to-volume ratio, which results in a one-layer structure with a minimal hydrophobic core at the heterodimer interface.

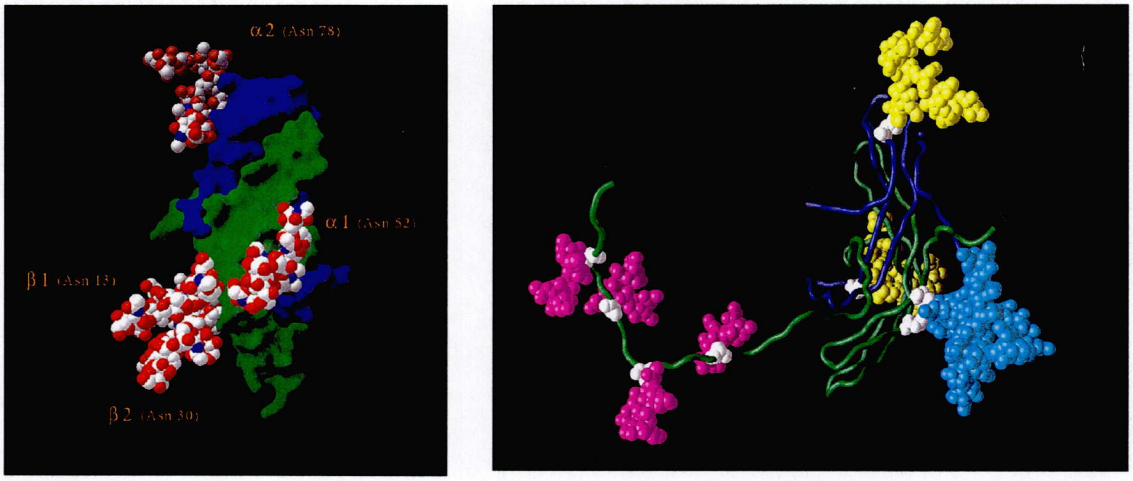

Figure 2-6. *Model carbohydrate side-chains on the hCG molecule; The protein, represented as surfaces (left; α, blue; β, green), with the carbohydrates represented as space-filling model (right) with atom coloring: N, blue; O, red; C, white, illustrates the extent of the carbohydrate structure* [117, 118].

2.3.3.1. Carbohydrate Structure

In its native form hCG is heavily glycosylated with carbohydrates making up 30 to 34 % by weight of the molecule. N-linked carbohydrates are at Asn-52 and Asn-30

on the α-subunit and at Asn-13 and Asn-30 on the β-subunit and are usually of the complex type with a minor population of mannose and hybrid types [215]. In addition the β-subunit has four O-linked carbohydrates at Ser-121, 127, 132, and 138 (Figure 2-6). The only carbohydrate that interacts at the subunit interface is apparently at α-Asn-52 and within the proposed receptor-binding domain. The positions of the β-Asn-13 and β-Asn-30 carbohydrates are very close, forming a large bulk of carbohydrate (Figure 2-6 left). Besides modifying the rate of clearance of the glycoprotein hormone from the body, some glycosylation is essential for full biological activity. The LH/hCG receptor contains, within the extracellular domain, a sequence similarity to soybean lectin, which suggests that there is a binding site for carbohydrates. HF treated hCG binds to receptors, but with loss or reduction of potency comparable to recombinant hCG lacking carbohydrate at all four N-linked sites. Using site-directed mutagenesis it was shown that (1) N-glycosylation sites are more important than the O-linked sites for receptor binding, (2) glycosylation is not necessary for receptor recognition *in vitro*, and (3) N-glycosylation at Asn-52 is critical for signal transduction, i.e. biological activity [145, 146]. However the O-linked oligosaccharides are important for maintaining circulatory half-life, extracellular stability and *in vivo* response [18, 145]. There is no evidence in the crystal structure for conformational change caused by deglycosylation.

The heterogeneity found in hCG is principally in the carbohydrate portion of the molecule. Variation in the sialic content of the terminal end of carbohydrates exhibited heterogeneity in electrical charge, and isoforms of gonadotropins showed varying biological activity [107]. The dibranched complex structure was shown to be the major form in purified urinary hCG [175], yet the extent and proportion of oligosaccharide branching in recombinant CHO cells expressing wild-type hCG is unknown. Variable branching was found to be responsible for the multiple, apparently larger forms of uncombined α-subunits derived from transfected cells and tissue explants [37]. One of the structures on the α-subunit is a complex-type monoantennnary chain, not commonly found on other glycoproteins. It was also proposed on the basis of the molar

proportions that there is site-specific glycosylation, with each site being homogenous [178]. The structures of the sugar chains in hCG produced from choriocarcinoma is quite different from those on the native hormone, due to an increase in fucosyl transferase activity and the presence of an abnormal β-N-acetylglucosomanyl transferase in the transformed cells. This results in higher receptor-binding affinity and lower biological activity. Further, it was suggested that the carbohydrates on the free α-subunit differ from those bound to the β-subunit [178].

Using site-directed mutagenesis, it was found that recombinant complete hCG has almost exclusively dibranched complex-type structures, but that the free recombinant human α-subunit has a tri-branched structure at Asn-52, and association of the β-subunit influences processing of this oligosaccharide. This study revealed also that this site is independently glycosylated from the Asn-78 site [13]. Recombinant human α-subunit expressed in C127 cells bear N-linked oligosaccharides with highly heterogeneous structure [37].

The use of mutant cell lines to create oligosaccharide variants, together with site-directed mutagenesis of the oligosaccharide acceptor sites, showed that subtle changes in oligosaccharide structure affect activity [107]. Thus, control of the post-translational processing of oligosaccharides represents a desirable level of control for bioactivity of biopharmaceuticals for the endocrine systems.

2.3.4. Therapeutic Relevance

2.3.4.1. In-vitro Fertilization (IVF)

Up to 10 kIU are given by intramuscular injection to induce ovulation following follicular stimulation with FSH or menotropin in the treatment of female infertility due to absence or low concentrations of gonadotropins (anovulation). It is also given for hypogonadotrophic hypogonadism due to pituitary deficiency, in the treatment of delayed puberty in males, and oligospermia. In fact, the first IVF ever was performed using a preparation of hCG from natural sources [182].

2.3.4.2. Contraceptive Vaccines

Two approaches are possible. Firstly, raising antibodies against hCG and injecting them posterior to insemination would capture hCG and the declining phase of the corpus luteum would be induced and the pregnancy (abortion) would cease. Secondly, blocking the hCG receptors competitively with hCG analogons prior or posterior to fertilization would mimic a pregnancy and therefore prevent the formation of a new ovum. Structure-function relationships suggest that the glycosylation is not necessary to perform this inhibitory task as deglycosylated derivatives of hCG behave as such antagonists [18]. It is therefore conceivable to use truncated forms of unglycosylated hCG expressed in prokaryotes, e.g. *E. coli,* as contraceptive vaccines. These possibilities are currently under investigation by the WHO Task Force on Fertility [82, 83].

2.3.4.3. Anti-Viral Activity

The majority of infants born to HIV-positive mothers are not infected in utero, suggesting, that the pregnancy factors produced by fetal trophoblasts may provide protection against HIV-I infection. hCG, the major glycoprotein produced by the placental trophoblast throughout the pregnancy, showed at low non-cytotoxic doses (0.01-1.0 $IU \cdot ml^{-1}$ range) inhibition of viral replication in maternal blood cells. Specifically, it inhibited the reverse transcriptase activity, necessary for viral replication, and the release of the p24 HIV gag antigen in HIV-infected lymphocytes and monocytes in a U-shaped dose response curve. This specific antiviral effect is not related to the suppression of cell proliferation [22]. Therefore, except for interferon alpha, hCG appears to be the only protein secreted by the human body that has been shown to have this antiviral activity, the mechanism and function as an immunoregulator is however not well understood at this time.

It should be noted that physiological low doses of two other main pregnancy hormones, estrogen and progesterone, have also been reported to inhibit viral production from monocytes but not from lymphocytes [22].

2.3.4.4. Anti-Tumor Activity

For unknown reasons KAPOSI's sarcoma (KS), a tumor which contains many newly-formed blood vessels and produces skin lesions, occurs much more frequently in men than women and HIV-1 associated KS has a particular high occurrence in homosexual men (over 30%). Its frequency has greatly increased with the spread of human immunodeficiency virus type 1 (HIV-1), and it also may be associated with a new herpes virus [66]. KS was noted to regress in pregnancy, two cases have been reported in which during pregnancy all observed KS lesions disappeared. An immortalized AIDS-KS cell line (KS Y-1) producing malignant metastatic tumors in nude mice was killed *in-vitro* and *in-vivo*, apparently by apoptosis, after treatment with both native and β-hCG [134]. This effect was dose dependent and untreated control cells developed metastatic tumors. Further, KS-SLK cells, as well as KS cells from clinical specimens were killed in short term culture by hCG, but normal endothelial cells were not killed [135]. A treatment based on native β-hCG is currently in pre-clinical trials, and a recombinant version is apparently under evaluation [133].

2.3.5. Economic Relevance

Conventionally hCG, like other hormones, was first isolated from the respective secreting glands, e.g. hypohysis, placenta, spleen or thymus. Later from body liquids of animal or human origin, mainly urine or plasma. The purification schemes however are unable to remove viruses from such preparations. In the case of human growth hormone somatotropin (hGH) which has been purified from human thymus, this has led to infections with diseases such as CREUTZFELD-JAKOB syndrome, a prion disease. In the case of preparations from urine, the risk of infection for the receiving patient with viral diseases such as Hepatitis and AIDS due to unsafe resources and unsatisfying virus removal is evident. When curing autoimmune diseases, using such resources would even defy the whole therapeutic aim. The presence of other contaminants with partially purified hCG, such as epidermal growth factor-like components and an hCG/LH binding inhibitor has been documented. In highly purified preparations of hCG, fragments of

hCG, e. g. β-core fragments and nicked forms of hCG which affect receptor binding and steriodogenisis, have been found. Also recently, in the widely used hCG standard reference preparation CR-127, two serine proteases that enhance cAMP production and thereby mimic biological activity, were isolated [43]. This situation led to a severe shortage in supply of pure, safe and efficient hCG in the beginning of 1995. Therefore, a process needs to be developed that is safe, consistent and efficient by means of a recombinant, biopharmaceutical approach.

The recently solved structure will in addition open up new more specific and targeted ways for structure-based approaches to the design of drugs for the treatment of cancer, autoimmune diseases, contraception, and stimulation of fertility. Based on the possible clinical indications the world-wide market can be estimated (Figure 2-7).

hCG-Indication	**Total**
Infertility / IVF	$260m
Diagnostics	$19m
Total	$279m
Total Market	
Anti-Viral	$7,200m
Anti-Cancer	$15,300m
Total	$22,500m

Figure 2-7. *Market forecast for different hCG indications; (Source: Scrip, Keynote)*

Science proceeds mostly from an abundance of materials, not understanding.

3. Materials and Methods

In general the techniques laid out previously [131] and common to the art [28, 123] were followed under special consideration of Good Laboratory Practice, mandatory in work with recombinant DNA, and if applicable Good Manufacturing Practice. Only a brief review and particularities are therefore given.

3.1. Cell Line and Characterization

3.1.1. General Properties of the CHO cell line

The Chinese hamster ovary (CHO) cell line is derived from the ovary of the Chinese hamster, *Cricetulus griseus*. The species is a favorite for cytogenetic studies because of its small chromosome number since the pioneering work of PUCK [177], who first isolated the cell line. The cell line is aneuploid with 2n = 22 chromosomes and has epithelial-like morphology. The cell line has provided model systems for the study of genetic alterations in cultured mammalian cells with more than 80 classes of mutant cell lines [77]. Two main sublines exist, CHO-S, growing well in suspension and CHO-K1, which grows anchorage dependent. Both require proline (auxotroph), some sublines glycine, adenine, hypoxanthine, alanine, glutamate, inositol, or serine for growth and serum in concentrations from 0.5 % to 10 % preferably 5 % but serum-free alternatives to the initially used medium HAM'S-F12 or α-MEM have been developed. A completely defined medium with comparable growth and production properties is not available for adherent CHO cells.

The immunological reactivity of cell membranes of CHO and human cells exhibit a high degree of species specificity. Virtually no killing occurred when they were exposed to quite high concentrations of the heterologeous antiserum. The cells have a fairly broad temperature optimum between 36 °C and 38.5 °C, but they are relatively sensitive to variations in pH growing from 7.0 to 8.2 with an optimum from 7.5 to 8.0 [77].

3.1.2. Recombinant CHO-αβhCG cell line

The recombinant CHO cell line (rCHO-αβhCG) used throughout the experiments was cloned by Martin MATZUK [146] and kindly provided by Irving BOIME (Washington University, St. Louis, MO). In brief, the cell line was constructed from wild-type CHO cells as described [146] from a pM^2 vector containing the ampicillin resistance gene, the neomycin resistance gene and the Harvey murine sarcoma virus long terminal repeat (LTR) promoter using a modification of the calcium phosphate method. Specifically, the DNA containing either β-hCG gene (3600 bp) or α-hCG fusion gene (2400 bp) were inserted into the pM^2 vector. The αβ-hCG dimer expression vector encoding both subunits was constructed by inserting the LTR-β-hCG fragment into the $pM^2CG\alpha$ vector (Figure 3-1). Selection was carried out in the presence of the neomycin analogue, G418, at 0.25 $mg \cdot ml^{-1}$.

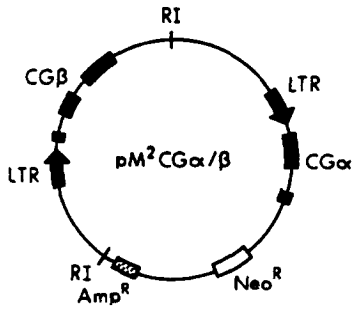

Figure 3-1. *Vector containing genes for α- and β-hCG; transfected into wild-type CHO cells* [147]. *Abbreviations used are:* Amp^R *ampicillin resistance gene,* Neo^R *neomycin resistance gene, RI EcoRI site.*

The cell line showed in low densities fibroblast-like behaviour, growing as elongated structures tending to align in parallel fashion to form colonies with rough edges. When cells grew in high cell density they exhibited rather epithelial-like behaviour forming almost regular polygons which pack tightly on glass (Figure 3-2) [177].

3.1.3. Cell Banking

A master cell bank (MCB) and a manufacturer's working cell bank (MWCB/MCWB) were prepared and maintained in 25 cm^2 T-Flasks with weekly subpassage at a dilution rate of 1:50 and one to two medium changes [78]. Methods were

as suggested by CBER using techniques common to the art [28, 123]. Regular control for contamination for mycoplasma was carried out and found to be negative.

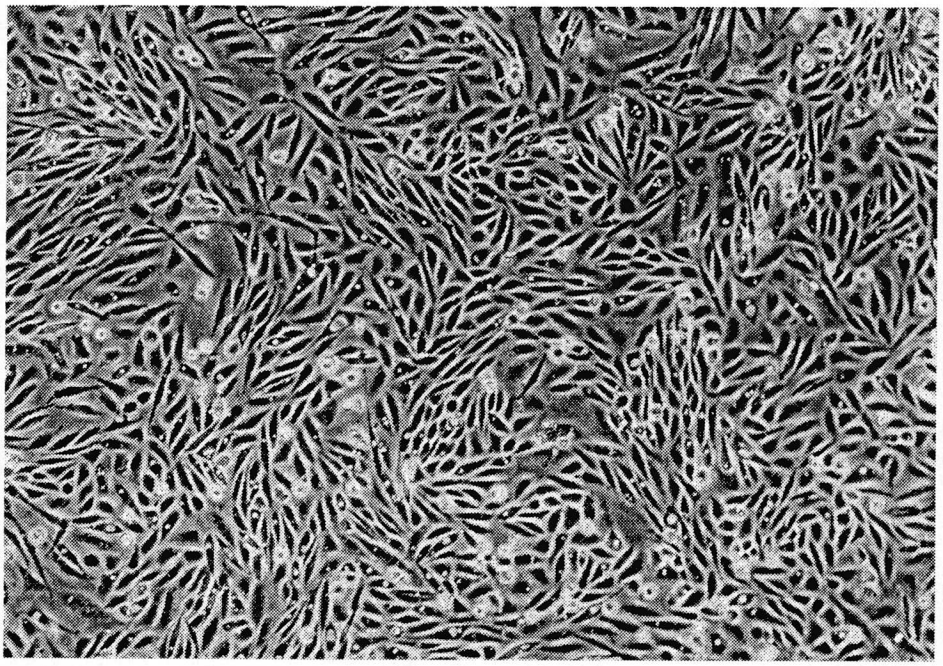

Figure 3-2. *Nearly confluent CHO-αβhCG cells in T-Flasks; cells show mainly elongated fibroblast and epithelial morphology but some cells start to form spheres.*

3.2. Water

Water as basis for the preparation of media and buffer used for the propagation of animal cells, as well as quantitative analysis is the single most important component in animal cell culture as it directly influences performance by virtue of present residual contamination [12]. Four different qualities were prepared and used:

- tap water was used as is for cooling and the preparation for higher water qualities
- deionized water (RO) was prepared using cationic and anionic exchangers or reverse osmosis units, mainly to remove ions and delivered through dedicated piping, it was used for the preparation of higher qualities and washes of equipment, including the preparation of cleaning solutions,
- distilled water was prepared from deionized water using an automatic destillation unit performing two additional destillations further reducing ion content and removing organic contamination, and was used for the preparation of buffers for analytical procedures,

- water for injection (WFI) was prepared from destilled water through additional sterilization at 123 °C for 40 minutes and kept in the glass sterilization bottles (Schott). WFI was used for the preparation of media as well as buffers for use in the propagation of cells. This quality is required by the relevant regulatory bodies for the preparation of biologics as laid down in the respective pharmacopoeias.

3.3. Equipment

The equipment used was selected and, if necessary, tested for potential toxicity when used with animal cells, and a list of approved materials was established. Specifically approved and used were polycarbonate only as Lexan (General-Electric) or Macrolon A (Hoechst), PTFE only in pure qualities, stainless steel only in 316L(N), V4A, CrNi 1810 Mo(Ti) or equal qualities, plastic ware from Nunc (T-Flasks), Costar (pipettes) and Eppendorf (cups and tips), glassware from Schott (Duran 50; bottles, microcarrier), tubing in PharMed quality (Norprene, Cole-Palmer, Watson-Marlow), Tie-Rap in black heat-stabilized nylon from Panduit and filter from Milipore (FG50, FG25) and Gelman (mini-capsule).

All equipment used in contact with cells for propagation or with solutions intended for contact with cells for propagation, if not delivered in single-use sterilized form, was washed overnight in an alkaline detergent solution (Deconex-20NS; prepared according to instructions) and washed three times in tap water, following with three washes of deionized water and subsequent triple sterilization at 125 °C for 40 minutes, as measured inside an equal liquid sample volume inside the autoclave, with one day rest intervals. This procedure was applied as single sterilization was not found to be sufficient to eliminate all fungi and spores and the security and safety of the individual experiments needed to be guaranteed. Carrier preparation is detailed in Chapter 4.2.

Stainless steel was degreased using trichlorethylene and passivated in concentrated nitric acid prior to the washing. Occasional sterilization of suitable materials with ethylenoxid was used to eliminate possible heat-resistant contaminants. All biologically contaminated waste was sterilized at 125 °C for 40 minutes prior to disposal.

3.4. Media

The cells were originally maintained in Ham's F-12 supplemented with penicillin (100 IU·ml^{-1}), streptomycin (100 µg·ml^{-1}) and glutamine (2 mM) containing 5% FCS (Medium I) at 37°C in a humidified 5 % CO_2 incubator [144, 147]. To optimize for large-scale use, the cells were grown in IMDM/F-12, a medium richer in amino acids and nutrients with HEPES buffer capacity, reducing the need for carbondioxide when aerating, at a slightly higher pH, under addition of 5% FCS and absence of antibiotics. This medium, termed Medium II and IIIa, was used for the MCB and MCWB as well as for post-production cell line maintenance (PPCB). Antibiotics were generally not used in T-Flask cultures in order not to mask low-level contamination.

Several modifications were made for production media (Media III, IV). First, FCS containing media were made with lower FCS concentrations, e.g. 1 %, to reduce foam potential and to improve the rhCG to total protein ratio and therefore to increase downstream processing properties. During batch cultures in T-flasks it was found, that IMDM/F-12 with 1 % FCS does have the same metabolic and productivity performance as medium containing 5 % FCS. This was also found in related studies [101].

Second, media for production, e.g. in the fluidized bed, were prepared with lower glutamine concentrations (4.1 mM). Glutamine was replaced equimolar with asparagine (2.64 mM). The rationale was to prevent excessive ammonia production by both metabolic conversion and decomposition [235].

Further, 1 g Pluronic F-68 (Sigma) per liter medium was added to form a stabile foam layer of about 2 cm height preventing excessive foaming in the conditioning vessel [221]. General cell protective traits have been attributed to its use [103, 158]. An increased amino acid uptake has been found for chicken fibroblasts at concentrations of up to 0.1 % [31]. Therefore, its use was considered to be beneficial to the overall performance of the process at concentrations of 0.1%.

Because of the varying nature of the experiments and their susceptibility to contamination at some instances, 10 ml PSN solution (Sigma) per liter medium were

added as a preventive measure. The final concentration was 50 $IU \cdot ml^{-1}$ penicillin, 50 $\mu g \cdot ml^{-1}$ streptomycin, and 100 $\mu g \cdot ml^{-1}$ neomycin. Tests for contamination and mycoplasma infection were performed on a regular basis in the cultures under absence of antibiotics. This includes testing for masked contamination when using PSN. It should be noted that the presence of neomycin might have helped stabilizing hCG productivity through selective pressure as genes for neomycin and ampicillin resistance have been originally co-transfected with the plasmid containing the hCG sequences into the genome of the CHO cells [147].

CHO-S-SFM II medium (Medium V; LTI) [76] was modified, besides the instructions given from the supplier, by adding PSN and Pluronic in the previously mentioned amounts. This medium was tested and used because of its low protein content (100 $\mu g \cdot l^{-1}$) and productivity enhancing characteristic [216], thus improving downstream-processing characteristics of the broth. The composition and preparation of each medium is given in Appendix IV.

3.4.1. Media Preparation

All media were prepared from powder using water of WFI quality, according to the instructions of the manufacturer unless specified above. Addition of sodium bicarbonate was according to recipe provided by the supplier with modifications as outlined (see Appendix V). After complete solution of the respective components the media were sterile filtered using a 0.2 µm sterile cartridge filter (Gelman) into sterile media bottles or tanks. All media were positively sterile tested prior to addition of PSN and use.

3.4.2. Serum

Foetal calf serum (FCS; FBS) is a complex solution of salts and proteins, including bovine serum albumin, immunglobuline and other growth factors. Depending on origin and donor animals the growth enhancing properties vary. In consideration of the current contamination of European herds with bovine spongioform encephalopathy (BSE) viruses (28 32 kDa) and FDA classifications only serum from USDA controlled

sources (class 1), provided by GIBCO/LTI and Cansera, was used. Growth properties of the lots were tested prior to use and charge protocols were established to control quality and provide consistency and tracability.

3.5. Analytical Methods

3.5.1. Sampling

20 ml sample volume were taken from the bioreactor through a sterile sampling valve into sterile serum bottles. Sampling was recorded electronically and protocolled. The sampling line was automatically steam sterilized prior and posterior to sampling with saturated steam from the autoclave, at 125 °C for 40 minutes. 4 ml of the sample were used for immediate quantification of pH with an external probe, cell density and glucose/lactate concentration. Further, 13 ml were stored at -24 °C and two times 1.5 ml at -80 °C.

3.5.2. Cell Density

Cell density was determined using an improved Neubauer counting chamber (hemocytometer) using the trypan blue exclusion staining method [123]. Cell density in the fluidized bed was not determined on a regular basis because of the associated error when using macroporous carrier and because of the reduction of bed volume, which was considered to be a major source of systematic error. In two instances the citrate method was used to bring immobilized cells into solution for counting [131, 132].

3.5.3. Glucose and Lactate

Glucose and lactate concentration was measured off-line using a YSI 2000 series glucose-lactate analyzer which uses the enzymatic conversion of glucose and lactate with the respective peroxidase (membranes 2365 and 2329) to O_2, which is quantified by polarographic electrodes. Internal calibration was done automatically using standard 2747 and buffer 2357.

3.5.4. Ammonium

The assay was an adaptation of the Boehringer Ammonium colorimetric method (Boehringer 1 112 732) for microplates. The underlying reaction principle is the

enzymatic (glutamate dehydrogenase) catalyzed conversion of NADH to NAD^+. The amount of oxidized NADH is stoichiometric proportional to the amount of ammonia. NADH is detected as change of absorbance at 340 nm. The concentrations used in the original kit were not changed, however the amounts used have been reduced by a factor of ten so that the test could be executed in 96-well microplates. Some substrate solution concentrations were optimized to improve reproducibility within the margins of pipetting errors.

3.5.5. Glutamate and Glutamine

The assay used was an adaptation of the Boehringer L-Glutamic Acid colorimetric method (Boehringer 139 092) for microplates. The underlying reaction principle is the enzymatic (glutamate dehydrogenase) catalyzed formation of NADH from NAD^+. NADH is subsequently stoichiometrically trapped in a reaction with INT to a formazan, a red dye detected at 492 nm. Secondly, the detection of glutamine becomes possible by converting it with L-asparaginase (Boehringer 102 903) to glutamate which has a 2 % activity for the glutamine/glutamate conversion. The concentrations used in the original kit were not changed. However, the amounts used were reduced by a factor of ten, so that the test could be executed in 96-well microplates. Some concentrations were optimized to improve reproducibility within the margins of pipetting errors.

3.5.6. Total Protein

The assay was an adaptation of the Bio-Rad Protein Assay (Bio-Rad 500-0006) for microplates. The underlying reaction principle is the shift in the absorbance measured at 595 nm when Coomassie brilliant blue G-250 reacts with protein (BRADFORD). Some amounts were optimized to improve reproducibility within the margins of pipetting errors. The standard used was bovine γ-globulin.

3.5.7. Calculation of Metabolic Rates

The steady state mass balance around the system can be formulated as:

$$Addition = Removal + Formation$$

or more precise:

$$Feed = Effluent + Change + Decomposition + Degradation$$

In terms of measurable variables this can be formulated as:

$$c_{i,Feed} \cdot V_{total} \cdot D = c_{i,Effluent} \cdot V_{total} \cdot D + \frac{dc_{i,CSTR}}{dt} \cdot V_{total} + k_i \cdot \bar{c}_{i,CSTR} \cdot V_{total} + qI \cdot V_{Carrier}$$

or:

$$qI = \left(\frac{dc_{i,CSTR}}{dt} + \left(c_{i,Effluent} - c_{i,Feed} \right) \cdot D + k_i \cdot \bar{c}_{i,CSTR} \right) \frac{V_{total}}{V_{Carrier}}$$

From this the consumption and production rates can be defined with respect to the initially inoculated volume of carriers equivalent to the volume of settled inoculated carries (40 ml unless specified), and were determined as follows. Note that qDO appears as a positive value although it is actually a consumption:

$$D = \frac{m_2 - m_1}{\left(t_2 - t_1 \right) \cdot V_{total}}$$

$$qDO = OUR = \frac{\left(c_{DO,CSTR} - c_{DO,FB_{out}} \right) \cdot \dot{m}_{recycle}}{V_{Carrier}}$$

$$qGluc = \left(\frac{c_{Gluc,2} - c_{Gluc,1}}{t_2 - t_1} + \left(c_{Gluc,2} - c_{Gluc,Feed} \right) \cdot D \right) \frac{V_{total}}{V_{Carrier}}$$

$$qLact = \left(\frac{c_{Lact,2} - c_{Lact,1}}{t_2 - t_1} + \left(c_{Lact,2} - c_{Lact,Feed} \right) \cdot D \right) \frac{V_{total}}{V_{Carrier}}$$

$$qhCG = \left(\frac{c_{hCG,2} - c_{hCG,1}}{t_2 - t_1} + \left(c_{hCG,2} - c_{hCG,Feed} \right) \cdot D \right) \frac{V_{total}}{V_{Carrier}}$$

Ammonia and glutamine kinetics were determined considering the first-order chemical decomposition of glutamine to pyrrolidone carboxylic acid and ammonia and the metabolic activity:

$$qGLN = \left(\frac{c_{GLN,2} - c_{GLN,1}}{t_2 - t_1} + \left(c_{GLN,2} - c_{GLN,Feed} \right) \cdot D + k_{GLN} \cdot \frac{c_{GLN,2} + c_{GLN,1}}{2} \right) \frac{V_{total}}{V_{Carrier}}$$

$$qNH_4 = \left(\frac{c_{NH_4,2} - c_{NH_4,1}}{t_2 - t_1} + \left(c_{NH_4,2} - c_{NH_4,Feed} \right) \cdot D - k_{GLN} \cdot \frac{c_{GLN,2} + c_{GLN,1}}{2} \right) \frac{V_{total}}{V_{Carrier}}$$

The decomposition rate constant k_{GLN} was assumed to be 0.0030 h^{-1} [71, 167, 168]. Yields were calculated as the ratio of the two respective metabolic rates for metabolite A from B:

$$Y_{A/B} = |qA/qB|$$

Values for steady states were calculated to allow for settling of transient changes after at least three residence times or three days, whichever was longer. The reported metabolic coefficients represent volumetric, meaning normalized to the volume of inoculated carriers, $V_{Carrier}$, metabolic rates and are therefore indicative of the efficiency of the system. Yields are dimensionless and represent cell specific values.

The dilution rate D represents the dilution rate of the whole 2300 ml reactor system. D based on total volume takes into account the necessity of the whole reactor system peripherals. In addition, there are two other dilution rates. First, the recycling dilution rate, D_{rec}, that is the reciprocal residence time of medium in the fluidized bed, which is 4 orders of magnitude larger than the reactor system dilution rate. Second, the dilution rate of feed with respect to the fluidized bed, which is by a factor of 60 to 80 times larger than the system dilution rate.

3.5.8. Estimation of ATP Production Rates

Following along the rationale of previous researchers the ATP production rate was estimated using lactate production rate and oxygen uptake rate [71, 153, 154, 172]:

$$qATP = 2 \cdot (P/O) \cdot qDO + f \cdot qLact$$

The fraction of lactate coming from the glycolysis f was assumed to be 1. The phosphorylation ratio (P/O) was assumed to be 3, according to the prevailing opinion in the literature [71, 154, 171, 172] (see chapter 7.4.3 for discussion). The NADH and ATP yield from glutamine were calculated as:

$$Y_{ATP/GLN} = 3 \cdot Y_{NADH/GLN} = 3 \cdot (2 \cdot qDO/qGLN)$$

4. Bioreactor for Non-Invasive Investigation of Metabolism

4.1. Reactor Design

The reactor needed to fit into a 20 cm horizontal bore biomedical magnetic resonance imaging instrument (Figure 4-1). This required custom design for optimized use of the limited space as well as special consideration of the NMR peripherals and electromagnetic interference (EMI).

4.1.1. Materials

For the construction of bioreactors several materials have been suggested, including, stainless steel, titanium, glass, polyethylene foils, and polymers such as PTFE. The construction material needed to satisfy the following requirements:

- repeated steam sterilization at 125 °C for 45 minutes
- biologically compatible, no toxicity
- no interference with radio-frequency pulses common to NMR
- no magnetic susceptibility, i.e. no steel
- acceptable transparency
- excellent machinability and design properties
- satisfactory tensile and yield strength

From the above listed material options only two polymers fulfilled all requirements, polysulfone and polycarbonate. Both materials come in qualities that are acceptable for use in biological applications according to the US pharmacopoeia, they are used in blood derivative production as well as for sterile filter membranes and filter housings. The polycarbonate Lexan was chosen for its availability and higher transparency. The reactor was gun-drilled out of a cylindrical block of Lexan and subsequently machined with no additives as those have been shown to penetrate into the material resulting in residual contamination [211] of the medium and toxicity for the

cells. The screws were brass as they do not come into contact with medium, seals were Viton (PDMF) O-rings and fittings were made from PTFE.

4.1.2. Design

The reactor design and dimensions were chosen based on modelling the metabolic degradation inside the reactor using a spreadsheet [152] (Appendix I & II). The reactor had a net volume of 120 ml with a maximum length of the cylindrical fluidized bed of 130 mm at an internal diameter of 30 mm. At the bottom, 12 ml glass spheres formed a static mixing element distributing the flow evenly. At the top, the tube widened, reducing the superficial velocity and thus slowing and retaining the carrier. The reactor could be opened by removing the head plate, which sealed via an O-ring flange to the bottom part. It was connected with PharMed tubing (Norprene) to the recirculation loop.

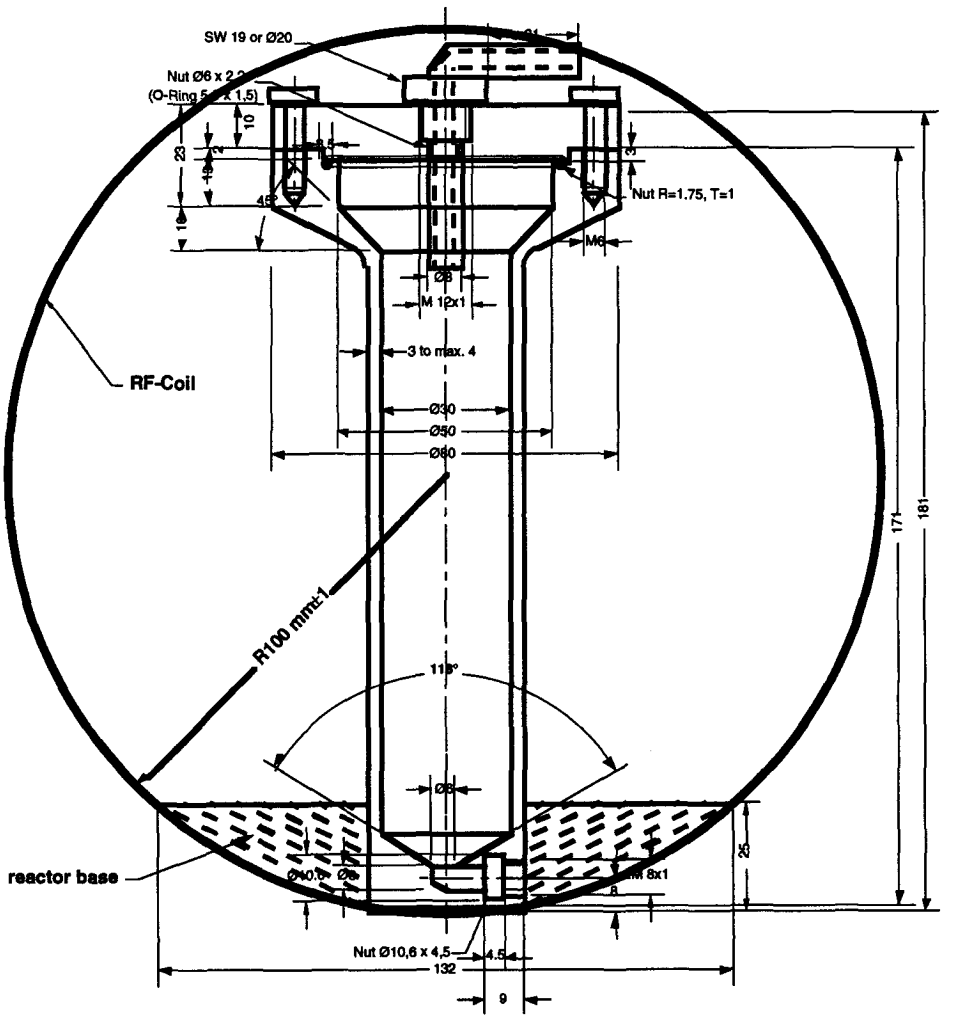

Figure 4-1. *Fluidized bed reactor fitted in MRI bore; material: polycarbonate, brass, PTFE*

4.1.3. Fluidization

Fluidization takes place as upward flow joins with buoyancy dragging the particle along the flow direction, overcoming gravity, dragging downwards. The equilibrium of forces has been used by STOKES to define the *terminal* velocity, u_t, of a single homogeneously solid particle in the endless laminar flow field [108]:

$$u_t = \sqrt{\frac{4 \cdot d_{particle} \cdot (\rho_{particle} - \rho_{liquid}) \cdot g}{3 \cdot c_W \cdot \rho_{liquid}}} \qquad c_{W,lam} = \frac{24}{\mathbf{Re}_{particle}} \qquad \mathbf{Re}_{particle} = \frac{u_t \cdot d_{particle} \cdot \rho_{liquid}}{\eta}$$

with c_W depending on $Re_{particle}$ this results in u_t for the laminar case (u_{lam}):

$$u_{lam} = \frac{d^2_{particle} \cdot (\rho_{particle} - \rho_{liquid}) \cdot g}{18 \cdot \eta}$$

For the transition from laminar to turbulent conditions, c_W requires iterative solution :

$$c_{W,transition} = \frac{24}{\mathbf{Re}_{particle}} \cdot \left(1 + 0.15 \cdot \mathbf{Re}^{0.7}_{particle}\right)$$

The *superficial* velocity, u_c, was found by RICHARDSON and ZAKI [183] when using spherical homogenous particles to correlate to the porosity of the bed ε and the terminal velocity u_t :

$$\log u_c = \log u_t + n \log \varepsilon$$

with n following for the transition from laminar to turbulent ($1 < Re_{particle} < 200$) :

$$n = \left(4.45 + 18 \frac{d_{particle}}{d_{tube}}\right) \mathbf{Re}^{-0.1}_{particle}$$

The real case, however, differs from the outlined relations and assumptions somewhat, thus that the results obtained differ from the values found in the literature. Firstly, the outlined relations have been found for solid, not macroporous, particles. This leads to erroneous results when neglecting the resulting lower density, as in the case of THÖMMES and KULA [214]. This can be corrected when considering the intra-particle porosity ε'' in addition to the overall porosity ε' and the bed voidage ε:

$$\varepsilon = \frac{V - V_{particle}}{V} = 0.48 \qquad \varepsilon' = \frac{V - V_{matrix}}{V} = 0.73$$

$$\varepsilon'' = \frac{V_{particle} - V_{matrix}}{V_{particle}} = \frac{V(\varepsilon' - \varepsilon)}{V_{solid} + V(\varepsilon' - \varepsilon)} = 0.47$$

resulting in a modified density of the particle in the fluidizing medium:

$$\rho_{particle} = (1 - \varepsilon'') \cdot \rho_{solid} + \varepsilon'' \rho_{void} = 1.642 g \cdot ml^{-1}$$

Secondly, size and density of the particles vary in biological fluidized beds over the population and the time, such that a field under changing conditions has to be considered rather than a singular case [108]. The varying density due to cell growth can be estimated:

$$\rho_{particle} = \frac{d^3_{carrier}}{d^3_{particle}} \cdot (\rho_{carrier} - \rho_{particle}) + \rho_{particle}$$

In the case of suspended SIRAN carrier, it was possible to model the terminal velocity field gradient with a viscosity, η, of 0.96 mPa·s [214]):

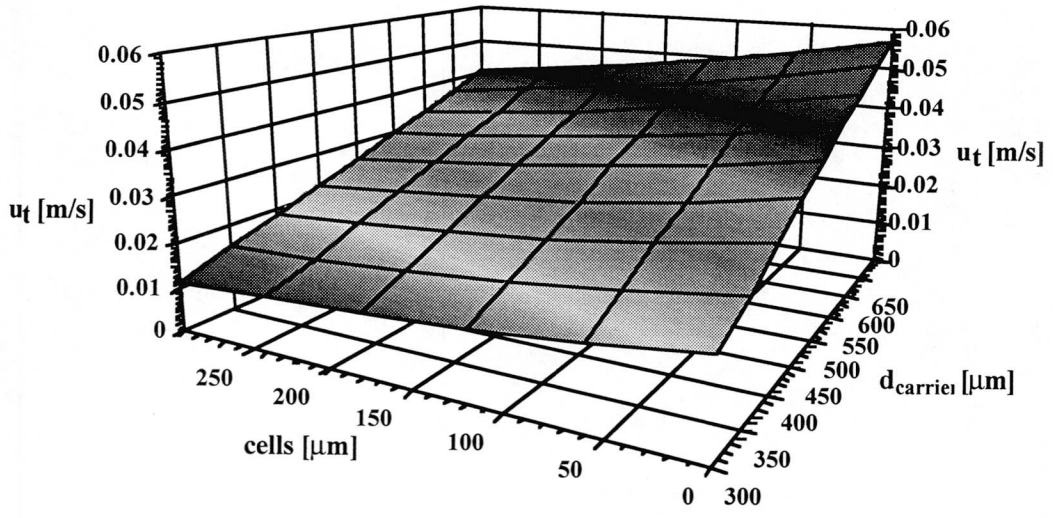

Figure 4-2. *Terminal velocity gradient; terminal velocity decreases with decreasing carrier diameter and increasing cell layer due to growth. Data are from Appendix III.*

Thirdly, the particles considered are in reality non-spherical, an analytical solution for such particle has not yet been found. Finally, the particles are by far not independent and not influenced by each other, including collision and mechanical abrasion phenomena [108]. The latter two reasons suggest a statistical-experimental or modelling approach for a solution. Yet, such an endeavour might be better suited during

cultivation of micro-organisms, rather than mammalian cells, involving lower costs. Therefore, such experiments were, a priori, not attempted.

4.2. Microcarrier

4.2.1. Carrier Selection

Since the first description of the use of micro-carrier [223] for the cultivation of immobilized adherent mammalian cells, several microcarriers have been developed and made commercially available. *Macroporous* microcarrier have been developed for increased cell density and to provide a protective micro-environment for the cells. Commercially available carriers are subject to success on the market and are sometimes only available for limited times, therefore necessitating a careful choice. Microcarriers found potentially suitable for high-density cell culture of adherent CHO cells included the VERAX VX-100 (formerly VERAX Corp., now Cellex, Inc.), PolyporE I and II (formerly IAM, Universität für Bodenkultur, Vienna now Cytoline by Pharmacia AB), CultiSpher-G (HyClone AB) [180], Cellsnow (Kirin, now Cytocell by Pharmacia AB) and SIRAN [128] (Schott AG). From those mentioned only PolyporE I and SIRAN borosilicate microcarrier were available in consistent quality on a continuous basis as required for industrial purposes [60]. PolyporE I is made from polyethylene, SIRAN from borosilicate glass as such both are biologically inert. Neither harboured the potential of tight additional regulatory conditions probable when using material from animal origin such as gelatine or collagen.

Comparison of their interference with the magnetic field and the radio-frequency field applied in a magnetic resonance spectrometer revealed a slightly superior performance for the SIRAN carrier, based on measurements of their magnetic susceptibility [125].

SIRAN carriers are manufactured in a proprietary process from Duran 50 the standard borosilicate glass (80 % SiO_2; 4 - 8 % Na_2O, K_2O; 12 -13 % B_2O_3; 2 - 7 % Al_2O_3) and are therefore of unmatched chemical resistance and inertness. The carrier

selected from the size fraction 300 to 1000 µm have a specific BET-surface of 0.22 $m^2 \cdot g^{-1}$, a total voidage of 73 %, and a maximal pore diameter of 120 nm.

4.2.2. Carrier Preparation

Prior to use, the carriers were boiled for 24 hours in 2.5 M hydrochloric acid with two intermittent washes until the boiling solution lost its initial yellow color. Then the carriers were boiled for 48 hours in 10 % nitric acid and for another 48 hours in deionized water with five to seven intermittent washes. After drying at 10^{-3} mbar and 120 °C overnight, the carriers were sieved into three fractions 300-500, 500-700, and 700-1000 µm. The carriers were sterilized three times in twice the volume PBS prior to any cell culture work. This treatment resulted in a hydrophilic hydroxyl surface modification (Si-OH) for improved cell attachment characteristics [131].

4.2.3. Inoculation

Pre-treated carrier, preferably of the 300-500 µm size fraction, were conditioned with cell culture medium (Medium III) containing 5 % FCS in sterile 200 ml ERLENMEYER flasks five days prior to planned inoculation with three intermittent media changes on a rotating shaker (130 rpm) in a humidifed incubator (5 % CO_2, 37.5 °C) following recommended procedures [14, 132].

Cells were grown from a MCWB in 3 to 4 passages to the exponential phase before transfer to carriers. Specifically, cells were passaged from stock cultures in T-80 flasks to T-175 flasks, which were subpassaged every four days with media change every two days. Cells were inoculated after trypsination from the T-flasks at a cell density of $2.5 \cdot 10^6$ viable cells per ml carrier with twice the volume of fresh medium for one day in ERLENMEYER flasks on a rotating shaker (120 rpm) in a humidified incubator to allow for a sufficient attached initial seed density of cells on the carriers. The next day the carriers were transferred under sterile conditions from the ERLENMEYER flasks to the fluidized bed. A second inoculum volume of $2.5 \cdot 10^6$ viable cells per ml carrier was added to the reactor. The recirculation pump was slowly started and the bed inspected from outside for bubbles and flow inhomogeneities until it stabilized with no

carry-over. The first day after inoculation the reactor recirculation speed was limited to promote bead to bead transfer and attachment of suspended cells. The bed entrapped suspended cells. After 48 hours the recirculation speed and bed expansion were calibrated and set to 80 - 95 % of maximal expansion to prevent carrier-bridging [46].

4.3. System Layout

4.3.1. Design

The system was designed as a classical continuous recycling loop with an MBR Mini 2.5 l reactor serving as conditioning vessel (Figure 4-3). The CSTR had inlets for pH, DO and temperature probe, heating and cooling, aeration via a ringsparger, medium and base supply, sampling, effluent, and ports for the recirculation loop connecting the fluidized bed and the second set of probes. Sterilizable couplings provided means of disconnecting lines and exchanging peripherals including, feed, product, and base.

The medium was supplied from ice-water cooled 10 l medium glass tanks (Schott) which had custom-designed in and outlet ports allowing supply of further additives and sterile venting. The peristaltic medium pump (Watson-Marlow) was setpoint controlled from the computer. The effluent was drawn via a peristaltic pump from the CSTR continuously by means of an U-shaped outlet keeping the level inside the reactor constant. The product (effluent) was collected in tanks equal in design to the feed tanks, and were placed on a balance connected via a RS-232 to the computer where the measurements were used to calculate the effluent dilution rate. Base addition (0.3 M NaOH) was controlled by the pH-loop controller via a peristaltic pump (Watson-Marlow). The exhaust gas was cooled to +4 °C to minimize loss of humidity and prevent humidity in the exhaust filter.

Aeration was achieved as outlined before by means of a ringsparger which was covered with Gore-Tex (GT30512, W. L. Gore & Assoc.) to minimize bubbling, which would in return cause foaming. This would change the magnetic susceptibility of the medium and then lead to erroneous measurements in the NMR [140]. Further, it was found that excessive bubbling would result in micro-bubbles in the recirculation loop,

which would serve as additional oxygen supply. This would disable the differential measurement of the oxygen uptake rate. The material used as diffusive sparger allowed an air diffusion of 3 $ml \cdot min^{-1} \cdot cm^{-2}$ and prevented bubbling effectively. The air influx was filtered via a 0.2 µm sterile filter before entering the reactor.

Sampling was possible through an automatically sterilizable sampling port at the bottom of the reactor into a sterile serum bottle cramped with a silicon stopper. This allowed taking sterile samples which could be used to prepare subclones, as well as perform further tests with the collected cells. Before and after sampling, the port was sterilized with flow through steam at 125 °C for 40 minutes; the pneumatic valve was driven directly from the computer.

The system was sterilized in two parts. All peripherals could be disconnected and separately sterilized three times at 125 °C for 40 minutes. The CSTR was sterilized in situ (sterile-in-place) three times with flow through steam at 125 °C for at least 2 hours, to achieve comparable conditions, prior to a sterile test of at least 48 hours. Common procedures were used for the connections.

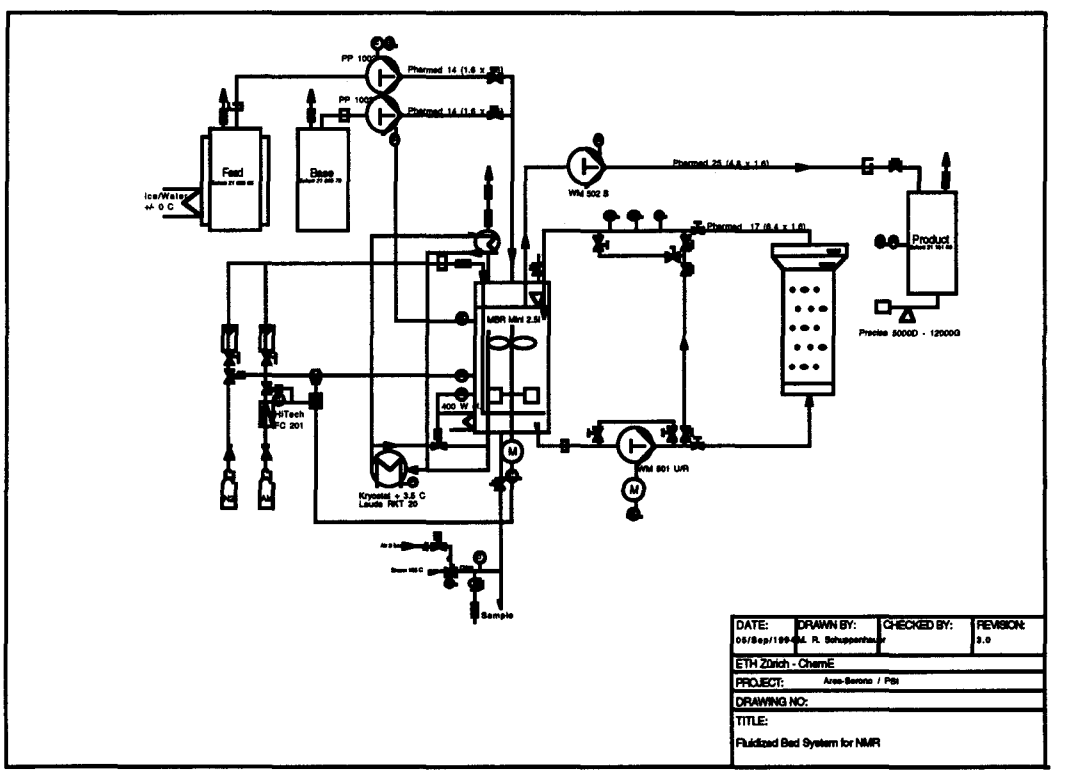

Figure 4-3. *P & I diagram of reactor system for metabolic studies; (see Appendix).*

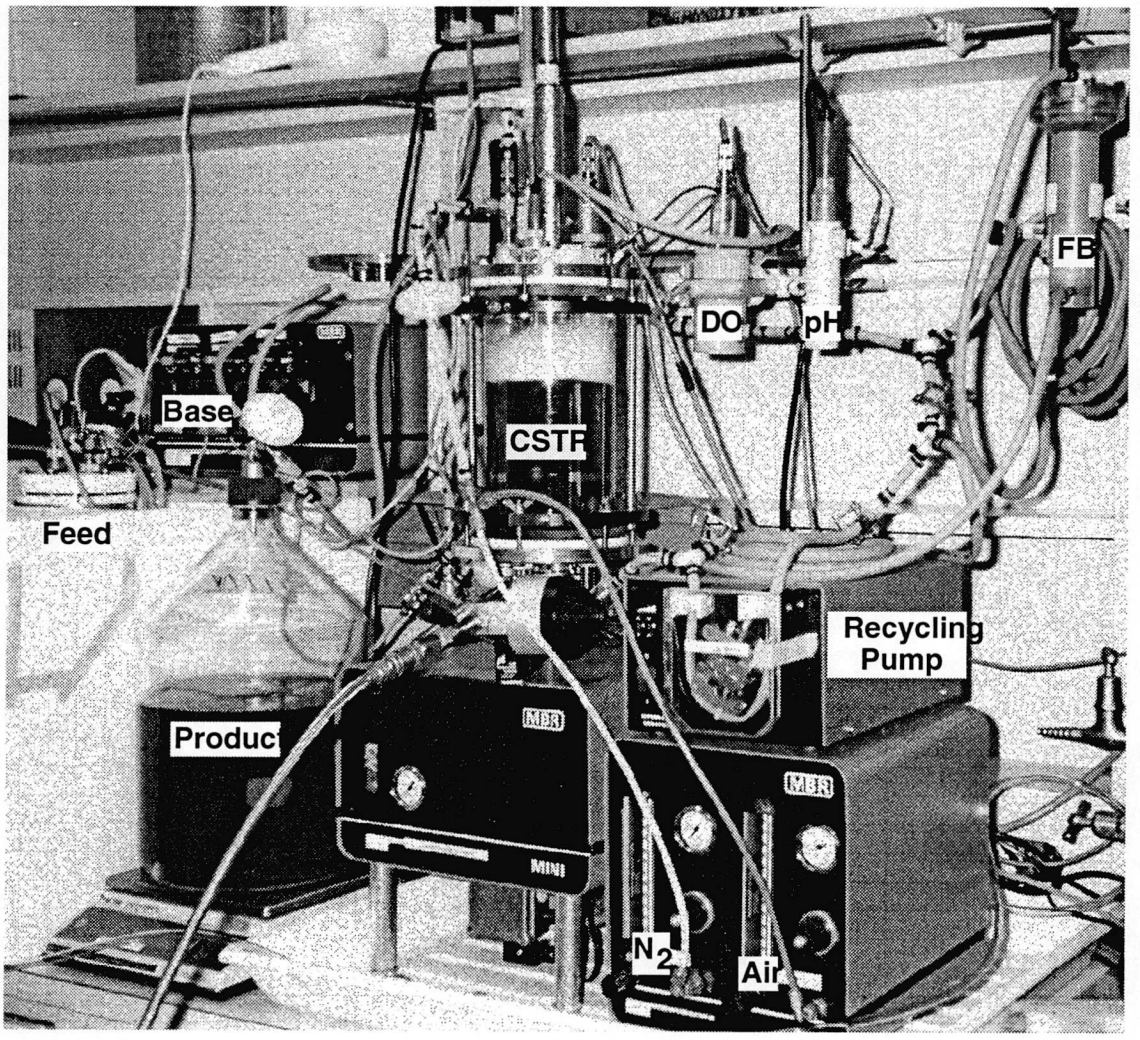

Figure 4-4. *Picture of plant*

4.3.2. Differential Measurements

The system was designed to have two sensor points to allow measurement of the (metabolic) gradient along the fluidized bed with respect to oxygen, temperature and pH. The first sensor point was inside the conditioning vessel, and the values generated were used by the set-point controller as outlined before. The second point was inside the recirculation loop before the spend medium exiting the fluidized bed entered the vessel. The total length of the recirculation loop was 6 m to have the conditioning vessel (CSTR) and its peripheral equipment, such as feed and waste supply, outside the critical vicinity of the MRI and its magnetic field. A connection between the lines leading to and from the fluidized bed allowed regular calibration of both probes. Thus, it

was possible to take on-line differential measurements and derive on-line the volumetric oxygen uptake rate, as a function of the bioprocess variables.

4.4. Transportation of a Bioreactor

The non-invasive MRI measurements were performed at the Paul-Scherrer-Institut (PSI) in Würenlingen-Villigen, which is located roughly 60 km (one hour drive) north-east of the lab. However, cell culture and start-up of the reactor had to be done at the ETH where the facilities were more suited. Hence, the reactor system needed to be transported under running and sterile conditions to the PSI. Crucial was especially the oxygen supply to the cells in the fluidized bed, as the oxygen inside the bed would be consumed within 2 minutes if turned off. Therefore stirrer, recycling pump and aeration had to be maintained at normal levels without interruption during the transport.

The system was therefore fitted on a conventional laboratory rolling-cart. Transport was accomplished using a truck with hydraulic lift (Mercedes-Benz 310 Eurovan). Power during transportation was supplied using a 2.2 kW emergency power unit delivering 2 x 220 VAC at 10 A (MAG 2000) obtained from the Swiss Army and separately mounted on the truck. It should be noted that all the systems were fully connected to all the peripherals and running during transport, thus demanding special care. The expansion was however reduced to 125 %, ensuring that no overflow from the fluidized bed into the recirculation vessel could occur. Transport was successfully accomplished in both instances.

4.5. Oxygen Transfer Considerations

4.5.1. Mass Transfer - Dissolved Oxygen

Due to its low solubility, the most important single nutrient, consumed by the cells is oxygen with an average solubility of 180 $\mu mol \cdot l^{-1}$ (100 % air saturation). The oxygen uptake rate (OUR) of mammalian cells can vary from 0.05 µmol per 10^6 cells·h to 0.5 µmol per 10^6 cells·h [61] when sparging with air. It is therefore important to optimize the oxygen transfer rate of a given aeration system. Based on the two film

theory, and using HENRY'S Law, the oxygen transfer rate (OTR), assuming neither sink nor source, for a batch reactor is defined as:

$$\frac{dc_{O_2}(t)}{dt} = k_l \cdot A \cdot \left(c^*_{O_2} - c_{O_2}(t)\right) = OTR \qquad c^*_{O_2} = \mathrm{He} \cdot pO_2$$

which can be solved as:

$$\ln \frac{\left(c^*_{O_2} - c_{O_2}(0)\right)}{\left(c^*_{O_2} - c_{O_2}(t)\right)} = k_l \cdot A$$

in which the k_lA the liquid mass transfer coefficient is, depending on reactor geometry, medium, massflow and stirrer speed.

When applying the dynamic method, that is applying a step-change in oxygen on a nitrogen-saturated medium or reverse, the following deduced equation can be applied to convert the values measured with the DO electrode directly into the respective k_lA value:

$$k_l \cdot A = \frac{\ln \frac{\left(c^*_{O_2} - c_{O_2}(t_1)\right)}{\left(c^*_{O_2} - c_{O_2}(t_2)\right)}}{t_2 - t_1}$$

in which c^*_{O2} can be replaced with the maximum value to which the electrode was calibrated and $c_{O2}(t_i)$ with the respective readings at the times t_1 and t_2.

4.5.2. Stirrer Geometry

For the CSTR used in the experiments, the reactor geometry was optimized according to findings by previous researchers [98], such that the OTR or k_lA would be maximized at minimal stirrer speed, resulting in the geometry sketched below. A marine impeller was mounted on top of a RUSHTON-turbine on the axis of the stirrer such that the flow regime of each stirrer was equally distributed in the mixing volume. Further to the shown arrangement the vessel contained a six bladed baffle gasket:

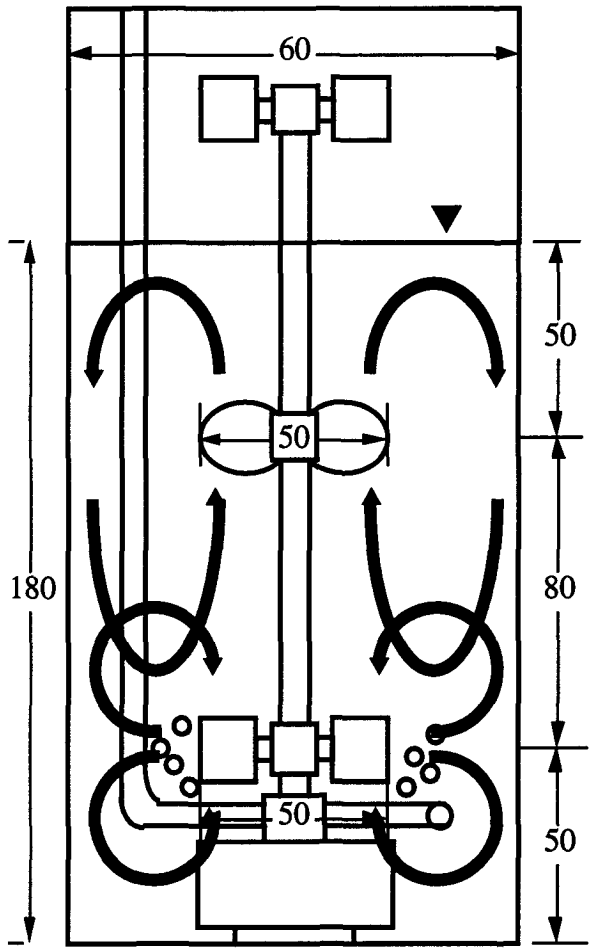

Figure 4-5. *k_lA-optimized stirrer geometry; baffles are not shown, arrows indicate flow regime. The top stirrer served to mix the air above the liquid as well as mechanical foam breaker preventing foam from spoiling the exhaust air outlet centred in the head plate.*

4.5.3. k_lA-Field

The klA was measured in the mass flow range of 0 to 10 ml·min^{-1} and the stirrer speed range from 250 to 1250 rpm using the outlined geometry. A low-bubble-sparger covered with Gore-Tex and inserts such as electrodes and baffle gasket all served as turbulence inducers enhancing the k_lA further. The medium used was the same as the one used for cultivation, e.g. Medium III or IV. The k_lA was found to vary with both parameters with an optimum of 42 h^{-1} at 750 rpm and 50 ml·min^{-1}. Increasing the stirrer speed did increase the power input, but it decreased the k_lA presumably due to de-mixing effects. The observation suggests that formation of bubbles resulted in bubble swarms leaving the reactor faster than they are able to contribute to an increase of

oxygen transfer (flooding). For the conditions which are relevant to the cultivation, 0-30 $ml \cdot min^{-1}$ and 250-500 rpm (based upon estimated and measured oxygen uptake, and bubble and foam limitation), the k_lA was found to increase monotonically between 1.6 and 8 h^{-1}. The system fulfilled the requirements with respect to oxygen transfer, low foaming and minimal bubbling characteristics for the planned cell culture cultivations.

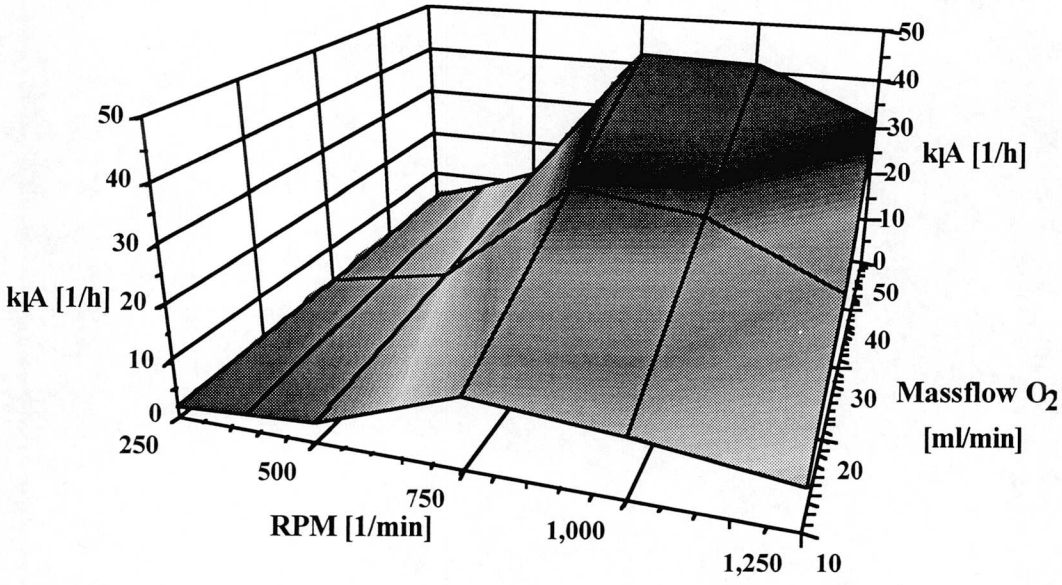

Figure 4-6. *k_lA as a function of stirrer speed and massflow for CSTR; The mass transfer shows an optimum above the conditions relevant for cell culture (0-30 $ml \cdot min^{-1}$ and 250-500 rpm) where the k_lA is between 1.6 and 8 h^{-1}.*

Process validation is establishing documented evidence which provides a high degree of assurance that a specific process will consistently produce a product meeting its predetermined specifications and quality characteristics. (21 CFR 210/211)

5. Process Monitoring and Control

5.1. Hardware

Process control was achieved using the modular, custom-designed, single-loop controller system IMCS 2000 (Process Control Systems AG and Rüegger-Elektronik AG, Switzerland) used also for the process industry, which is a derivative of the former MBR system of the same IMCS series. Signals from the sensors were preamplified, if necessary, conditioned, displayed and passed on as inputs for PI and PID controller (Figure 5-1). The resolution was better than 4000 units per full-scale (12 bit). The system featured further a dot recorder and analog data-out and remote-in of all actual values and set-points as 0 - 10 V signals, as well as the digital switches as TTL signals, respectively. There were also master/slave cascades, individual remote set-point control, guide control, and mode control options for the respective control parameters available [186]. The controller provided galvanically isolated voltage signals to be used as input for the supervisory control and data acquisition.

All connections from sensors to the IMCS and from the system to the data-acquisition circuitry were double-twisted double-shielded cables, with analog and digital lines separated to prevent electromagnetic interference from the expected strong magnetic field. Special care was taken for proper grounding. All potentially sensitive parts, such as switch boxes and controller, were placed inside FARADAY cages.

5.1.1. Stirrer

The stirrer was driven via a magnetic coupling from an electric motor providing a speed-meter output signal of 0 - 10 V, which was passed to the amplifier, display, data-out and the controller with PI characteristic driving the stirrer speed continuously.

5.1.2. Temperature

Temperature was monitored at two points. Inside the reactor a Pt-100 provided the signal for temperature control in the CSTR when hardware controlled. A second Pt-100 probe was inside the pH probe, located in the recycle loop, providing a second signal and the temperature gradient or heat loss along the recycling loop. This signal was used in setpoint-control mode (SCADA) to control the temperature in the fluidized bed, according to the setpoint, by slight upward regulation of the setpoint. A cooling finger (+4 °C) and a heater (400 W) inside the reactor vessel connected to the controller provided means of upward and downward control via on/off switching following PID characteristic. The temperature loss along the recycling loop was found to be less than 1 °C throughout all experiments. This is below the error caused by electrical resistance in the lines and at the connection contacts (1 Ω per additional contact corresponding to 2-3 °C). The recycling lines were isolated with polyurethane foam tubes to further reduce heat loss.

5.1.3. Dissolved Oxygen

Oxygen was measured inside the conditioning vessel and in the recycling loop before the recycled medium entered the vessel. Two polarographic/amperometric electrodes (CLARK'S Principle; Ingold) were used to measure the dissolved oxygen. They were freshly filled with electrolyte prior to sterilization and calibrated according to instructions in µmol oxygen per liter medium *after* sterilization. The saturation concentration was determined according to the methods outlined by SCHUMPE et al. [189-191]. For the media used, the saturation concentration was found to be 185 $\mu mol \cdot l^{-1}$ (corresponding to 100 % air saturation) at standard conditions when using a calibrated artificial air mixture (CO_2:O_2:N_2=5:20:75).

The sensor signal was preamplified, displayed and passed to the controller which drove either stirrer speed or mass flow continuously upward, or the nitrogen flow discontinuously downward, following PI characteristic. In reality, the maximum nitrogen flow was capped or turned off, and the controller was allowed to control the mass flow

of air with pre-set stirrer speed, because the triple-cascaded control (DO-massflow-internal massflow) was oscillating to strongly and showing unstable DO concentrations inside the CSTR (± 10 µmol with a frequency of 10 to thirty minutes). Using the modified scheme the DO inside the CSTR was constant at setpoint (± 0.2 µmol).

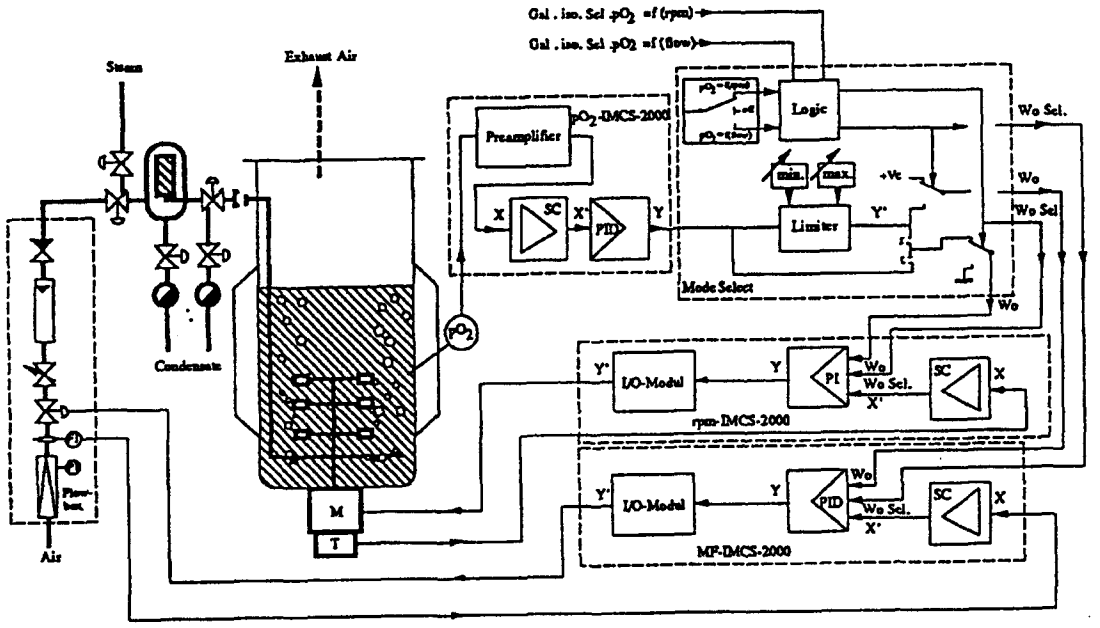

Figure 5-1. Design of cascaded DO hardware controller loop; [186]

5.1.4. Massflow

The air massflow was controlled with a cascaded controller. A thermic massflow meter with internal PID controller (Bronkhorst High-Tech F-201C-GB; 0 - 50 ml·min^{-1}) was used and monitored with a rotameter. The sensor provided a signal (0 - 10 V), which was displayed and used for a PI controller inside the IMCS 2000 to drive the setpoint of the first controller. The air was passed through a sterile filter (0.20 µm) prior to entering the reactor volume via a sparger covered with a Gore-Tex membrane providing theoretically diffusive aeration, but in reality limited bubbling occurred.

5.1.5. pH

pH monitoring was performed using sterilizable gel electrodes from Endress + Hauser. The electrodes needed no pressurization prior to sterilization and were stabile during extended and repeated cultivations. The electrodes were calibrated prior to sterilization against pH buffer pH 4 and pH 7. One electrode (CPS11-1DA4-

GCA) was placed in the conditioning vessel and served as signal for the pH controller, which drove continuously a base pump adding 0.3 $mol \cdot l^{-1}$ NaOH for upward regulation. The other electrode (CPS12-1DA2-TSA) was a combined pH-temperature electrode and was placed in the recirculating loop. The signal was used also to control the accuracy of the first control loop, as the pH gradient of the bed was generally below 0.2 pH units. Further the temperature signal from the combined electrode was used to monitor the temperature at the fluidized bed exit.

However, it was found that the electrodes showed different calibration response before and after sterilization. Also the values of the two probes differed on average by 0.3 pH units directly after sterilization. This was accounted for by recalibration and slope adjustment at two pH values which were referenced to an external measurement after sampling. pH shift was achieved using carbondioxide and nitrogen sparging. It was observed that samples taken from the reactor generally had externally a pH value of 0.2 pH units above the value measured inside the reactor. This can be explained with the loss of degassed CO_2 after decompression through the needle into the sterile sample bottle and subsequent change of the equilibrium in the sample. It is reasonable to assume an average deviation of 0.1 pH units from the actual value. Reproducibility was better than a deviation of 0.3 pH units.

5.2. Software

A process control system needed to be developed for the on-line control of a fluidized bed system for the cultivation of mammalian cells that is as comprehensive as existing systems. Yet reprogramming and adapting the system to changing needs must be easy and quickly accomplished. Various control schemes need to be accessible. Export and post-process analysis should be platform and software independent and compatible with existing simulation and statistics packages. The user interface needs to be intuitive and easy to learn for multi-user environments. Additional peripheral instruments with various interfaces (balance, pump) also need to be accommodated. It was intended to develop a system that has large potential for industrial use.

5.2.1. Regulatory Requirements and Validation

Source code and its supporting documentation for application programs used in drug process control, e.g. control of biopharmaceutical processes, such as cultivation of mammalian cells, are considered to be part of master production control records, within the meaning of 21 CFR parts 11, 210 and 211. Accordingly, those sections of the cGMP regulations which pertain to master production and control records will be applied to source code, testing, documentation records and vendor responsibilities [55] and hence constitute the law [23]. As a result [54] computerized systems, including soft- and hardware, are subject to close scrutiny by regulatory bodies such as the FDA and the EMEA. Particular, recently cases occurred in which, not only financial damage, but also loss of human life could be traced back to malfunction of computerized systems, which is an unacceptable situation [36]. Although cGMPs specify the minimum acceptable level of system control, no effort should be spared that ensures that the system will perform its intended function accurate, reliable and consistent. Crucial points comprise:

- hardware specifications and operational limits
- hardware testing procedures
- hardware documentation
- re-validation

For the software side, modular development or the *system life cycle approach* is suggested [56, 176]. This comprises six phases:

- Development, including the definition of the user requirements (URS), *design qualification* (DQ) , system specification and documentation,
- Implementation, the actual coding and documentation of the code,
- Testing or *software qualification*, including input-output checks, compliance with specifications, strategies, error-handling, boundary conditions, critical decision paths and algorithms, data integrity, accuracy and reliability, where the purpose is not to show that there are no errors but to find them as well as documentation,

- System installation and *installation qualification* (IQ),
- *performance qualification* (PQ),
- Maintenance or *operational qualification* (OQ), including regular calibration checks, inspections, backup, input/output verifications, change control, upgrades, adaptation, and enhancements, all well documented.

In all these phases, the crucial point is the documentation, or as 21 CFR puts it, the *documented evidence* which has to be provided. It has been shown that co-current documentation and validation is cheaper and faster than retrospective validation.

In the event of system failure, a backup must be provided.

These outlined requirements resulted in the formation of the Good Automated Manufacturing Practice (GAMP) published in May 1995 by the ISPE. This document covers all soft- and hardware aspects of validation. The GAMP defines five different categories of software with increasing intensity of validation:

- operating systems, such as the MacOS or Windows,
- standard instruments and micro controller, such as single-loop controller
- standard software packages, such as Microsoft's Excel,
- configurable software packages, such as distributed control systems (DCS) and supervisory control and data acquisition packages (SCADA), as well as LIMS and MRP_2 packages,
- custom built or bespoke systems, such as code written in low-level languages.

Besides compliance with existing legal requirements, the value of conforming to such standards, and the ISO9000 series is complementing, is the increased inherent quality, cost reduction and provision of confidence about the data integrity, also in an academic environment. Further, closing the gap between academic education and industrial reality with respect to quality control, and the development of applications and processes, which can be used in production through technology transfer, therefore contributing to current issues in the engineering domains. Hence, validation not only puts a burden on process control software development, but offers also and

opportunity for intelligent solutions that provide quality, data integrity, security and confidence, as well as increased options for process validation.

5.2.2. Graphical Programming

In long-term cultivations, large amounts of data need to be acquired, conditioned (filtered and averaged), and stored. Further, continuous cultivations require automated, unsupervised event handling through an event-driven approach. This suggests newer graphical platforms (Windows 3.1, MacOS, SunOS) as suitable programming environments.

This is where LabVIEW [111] combines two previously unrelated programming methodologies - structured and data flow programming - and embeds them in a graphical editing and execution system (Figure 5-2). The Virtual Instrument (VI) paradigm was adopted, whereby software for laboratory automation is viewed as a hierarchy of instrument-like modules, containing interactive front panels and programs in the form of block diagrams [9, 110, 217]. Sub-VIs are placed as icons on the diagram and connected with wires. Each sub-VI has its own front-panel and block diagram, ultimately applying a modular approach - the *Babushka principle*.

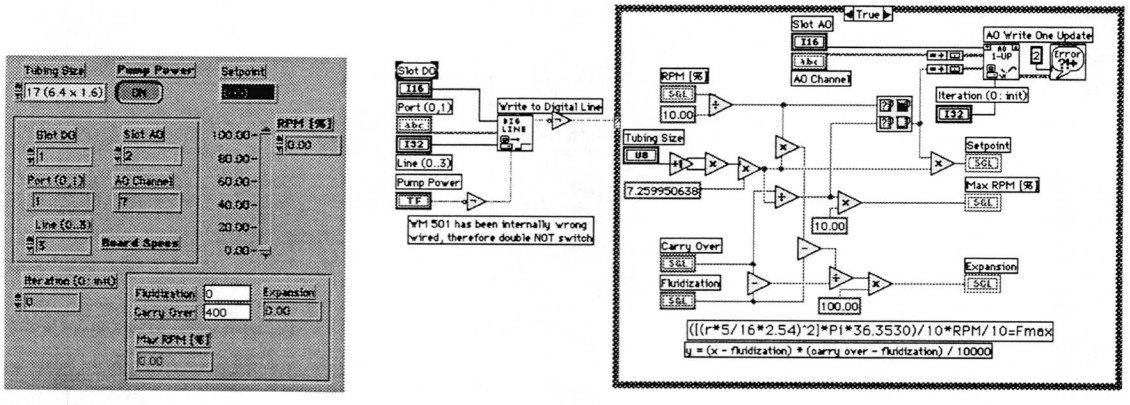

Figure 5-2. *Virtual instrument (VI) controlling the recirculation pump; front panel (user-interface, left) and data flow structure (code, right)*

In a recent study on the fault rate of object-oriented programming in a non-medical application, it was found that the rate was only 15 to 30 % of conventional programming, thus creating better quality code [119]. Further modularity, required for successful validation is inherent to object-oriented programming. Tracability from

requirements to the code can be shown by logically associating requirements with the objects intended to fulfil the requirements to implementation. It can take up to 40 man-years to trace and document a 1.5 million line code, a process that is fairly straight forward in self-documenting object-oriented languages. Further, inherent advantages are shorter code and hence fewer sources of error. This suggests that current validation requirements can be met with distinct advantages over conventional text-based programmes.

5.2.3. Results

Using the graphical programming environment, the coding time for an inexperienced user was reduced by a factor of five. The first version of a comprehensive process control system was commissioned and running after two weeks programming. Translation of the P & I Design to similar event-driven data flow programs is close to the process engineers vision, with the abstract model picturing the logic of the real system. Structured programming techniques [102] increased readability, and quick transfer to a program was achieved. By simultaneously designing interface (panel) and code (data-flow) it was possible to directly meet user requirements and documentation (performance qualification)

The hardware process control system IMCS 2000 was interfaced via analog circuitry (0 - 10V). Serial instruments (balance, modem) were interfaced using RS-232 connections. Additional networking was programmed via Windows' DDE. A 486DX2 system running Windows 3.1 was chosen to feature up to 64 analog input channels, 12 analog output channels and 16 digital channels. In addition, alarm options have been incorporated to call remote operators as well as send reports. The code comprised about fifty subroutines, plus the standard routines from the main libraries, with a total of 1.3 MB code executing at the speed of C programs. The system allowed access from remote locations via a telephone link. Data were acquired in two second intervals from the IMCS 2000 system as 0 - 10 V or TTL signals, from the balance as RS-232 input in 30 second intervals, and setpoints were sent out to the IMCS2000 (analog and digital),

the recycling and feed pump, which were directly driven, and the pneumatic valve in two second intervals. Further, off-line data from samples were logged in a separate spread-sheet. Visualization was possible either on the virtual instrument interface, or using graphing software. The acquired values, one record totalling 27 variables, were averaged over a period of three minutes and stored to a tab-delimited (ASCII) file. The new records were only appended to the file, and the file was not kept open during the run. The log-file did not allow any alterations from other parts of the control software to insure data-integrity. A central error handling routine notified the operator, also when at home (watchdog). Via a telephone link it would dial in appropriate cases a remote phone to send pre-programmed messages. Error messages were automatically logged to file. In the worst possible scenario, the reactor would be left hardware controlled and the computer would reboot to recover from crash, which however never occurred.

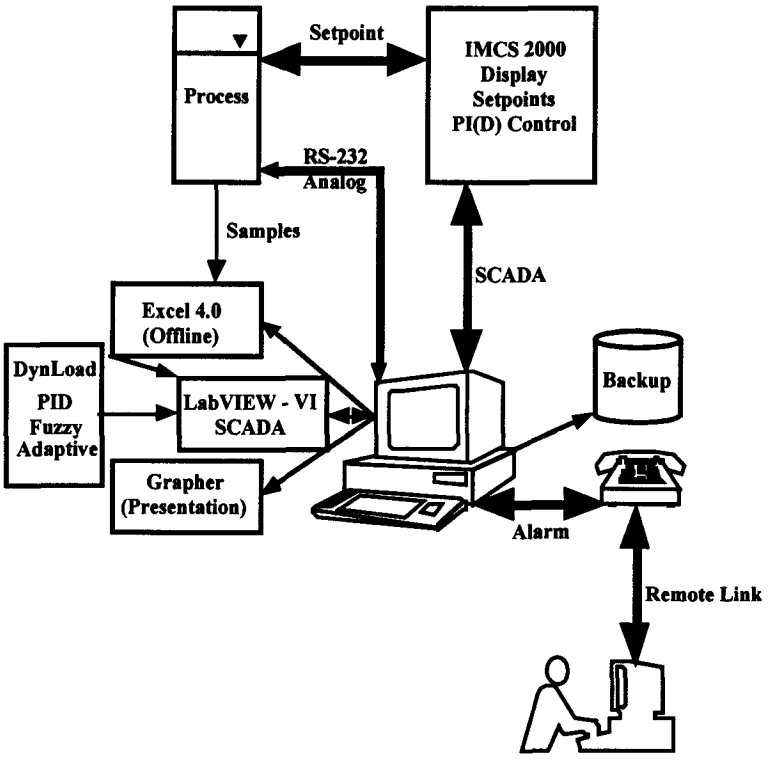

Figure 5-3. *Scheme of data flow and lay-out of SCADA-IMCS system*

From the gathered values, variables such as metabolic coefficients and bed expansion were calculated, displayed on-line in sub-level VIs, and stored. Various ways of displaying historic data, as well as exporting them, were implemented in further

subroutines. A library of subroutines was thus established that allowed subsequent projects to progress more quickly.

From pre-existing libraries, the necessary control schemes, including PI/PID control algorithms, adaptive algorithms [16], fuzzy controller, sequential batch processes (start-up), and sequential recipe-based processes, can be dynamically loaded when a change in the cultivation strategy is required. The system featured enhanced stability through hardware redundancy. As hardware backup, PI/PID controllers were used on the hardware side to off-load real-time critical tasks to the set-point controller. On the software side supervisory control and error-handler were provided.

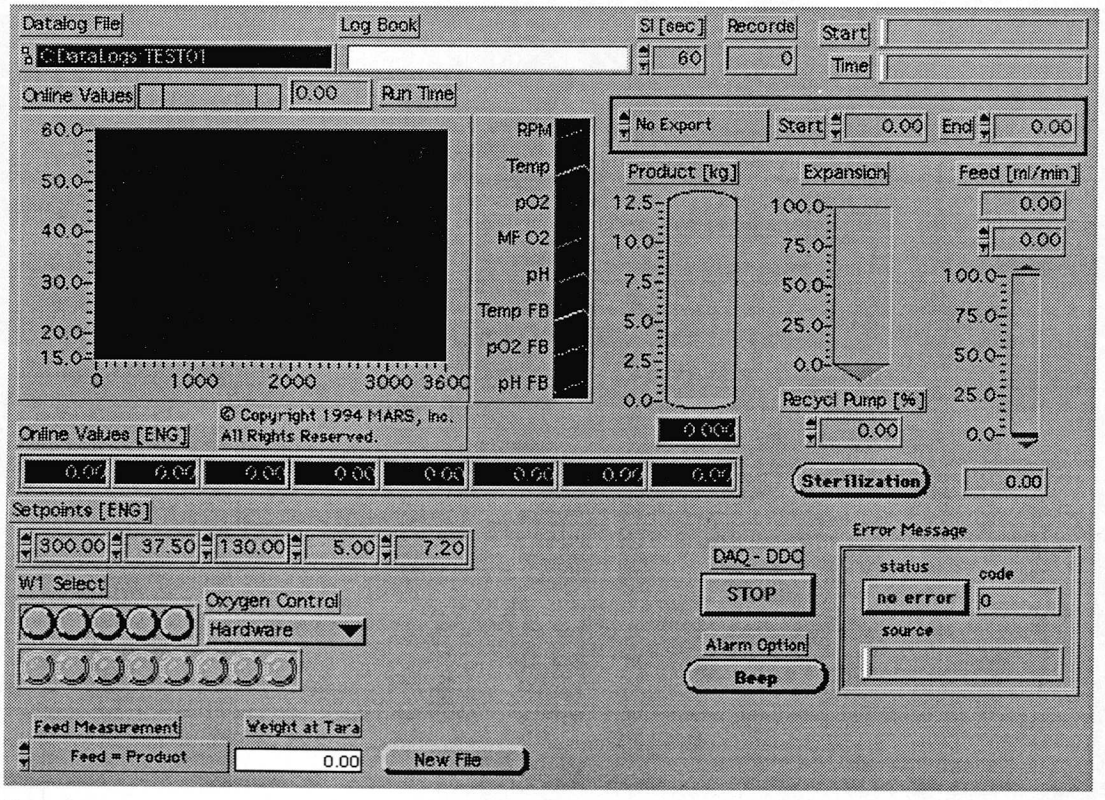

Figure 5-4. *Man-machine-interface (MMI) for control of the reactor*

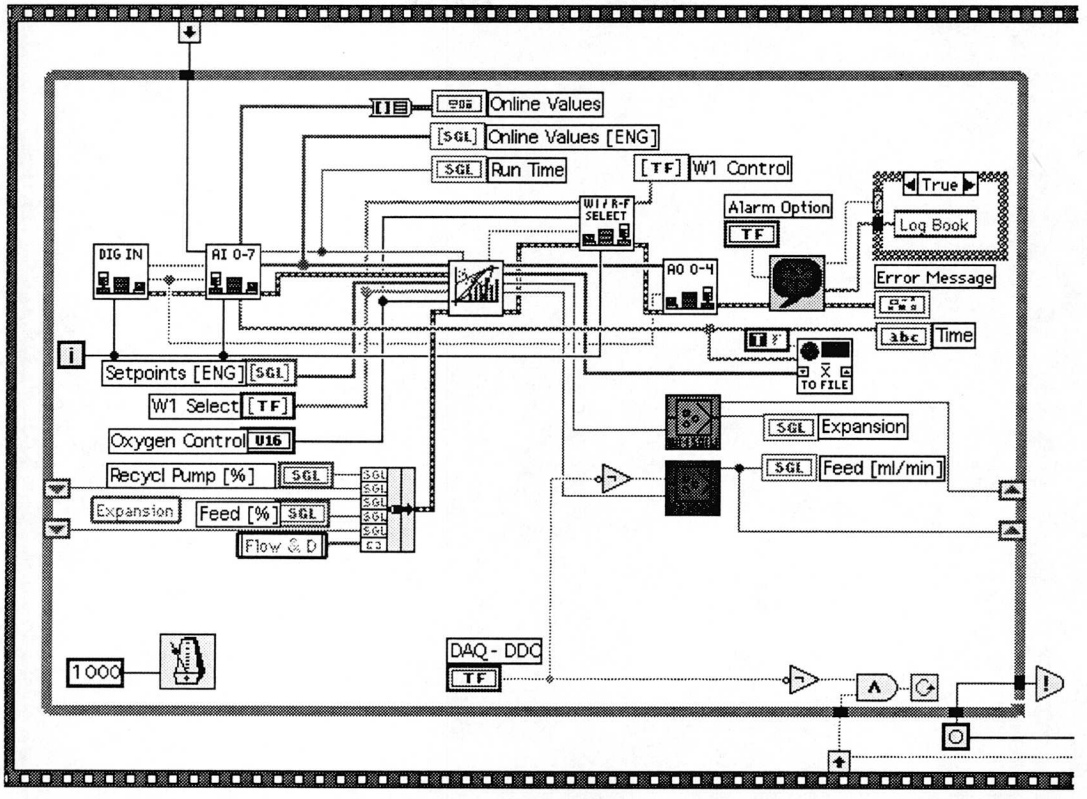

Figure 5-5. *Data flow structure of main VI; data acquisition and set-point control VI*

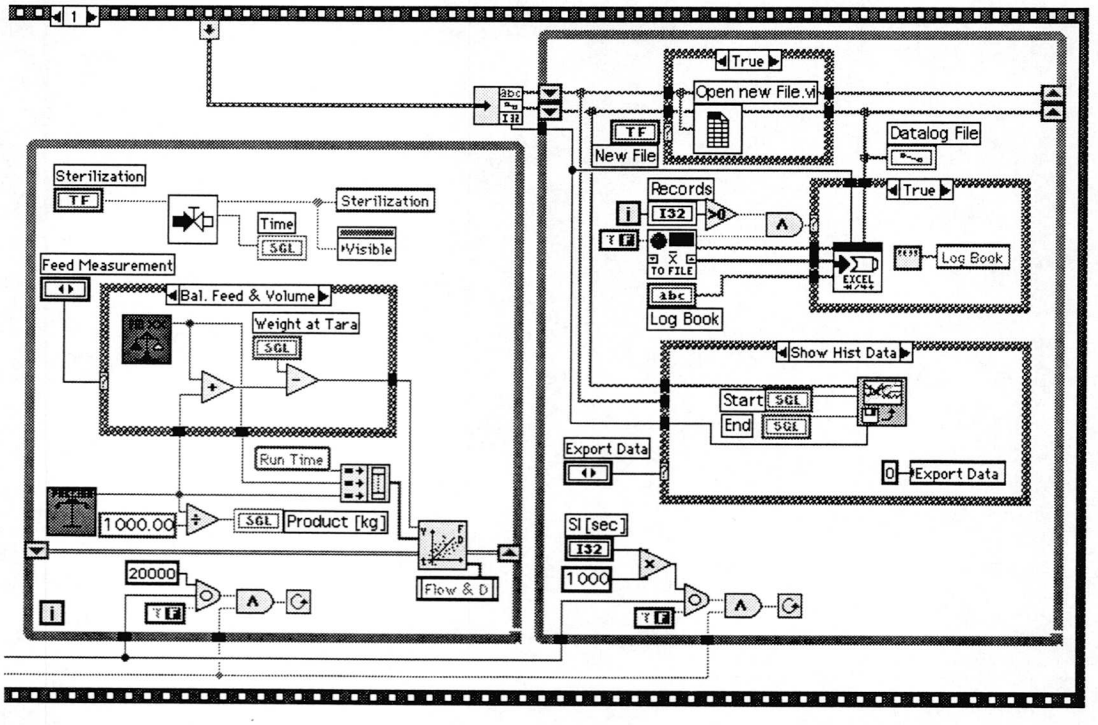

Figure 5-6. *Data flow structure of main VI; balance, sterilization, data storage and historic trending subroutines (VI)*

5.2.4. Conclusion

Implementation of a process control system using a graphical programming language (LabVIEW) proved successful for comprehensive data acquisition, analysis, control and documentation (SCADA) in the long-term continuous cultivation of animal cells. The system allowed 12 or 16 bit on-line data acquisition of various sources, serial data transfer, as well as off-line value handling. Flexibility, modularity, and an interactive graphical user interface (Figure 5-4) enhanced transparency and control of the complex bioprocess at every instance for the operator, as highlighted by previous researchers [203]. Multitasking, asynchronous-processing capabilities of the system provided direct interaction with more sophisticated control strategies, adaptive controllers, dynamic modelling and reporting for publications. Similar systems were implemented for the feed-back control and integration of instruments such as GC and HPLC [80, 218]. Especially because of the integrative approach, the graphical environment reduced hardware and complexity.

The 486 and 386 processor-based systems under Windows 3.1 proved to be stable for as long as 1400 h in process control and data acquisition of large volumes (> 7 MB). LabVIEW represents a programming environment to create a platform independent, open process control software with easy and intuitive graphical user interfaces. Object-oriented programming effectively reduced complexities of process control systems, thus increasing performance and productivity in real-world control tasks. In a laboratory environment the modular approach allowed maximal flexibility, fast re-configuration and re-engineering on the wire [15, 81]. An extension of this trend is expected, in the future integrating other analytic systems that still require their own computer system.

Modular programming mirrors industrial programmable logic controllers (PLCs) and fieldbus technology on the software side. Drivers for all relevant PLC systems exist. Non-standard instruments can be easily integrated and supplied with a standard interface . Interfaces are also available to incorporate C code, as well as to establish

direct dynamic links to Matlab, Mathematica, Igor, HiQ and a SQL server. Export to Excel formatted tables opens the world of spreadsheeting and enables the user to stay on known paths and environments. This integrates well into corporate wide information systems and technology strategies.

Plant-wide use of this approach on distributed control-systems is possible, especially as modular program libraries are becoming established [15]. Although significant validation issues inherent to networked environments have to be addressed. The modular design approach reflects the modular development structure required by regulatory bodies. Further, using the built-in history protocols and checklists, the process control system can be manufactured according to the ISO 9000 series [102]. Validation of object-oriented software differs, however, significantly from traditional script-based software with respect to the integrity of the code. Check-sum profiles, write-once-read-many (WORM) program and data storage, history protocols and checklists are present solutions. Systems generally should be dedicated exclusively to process control when working in validated environments; this excludes networked environments with physical connections to other computers.

Science is merely a process of information gathering with the true quantum-leap being the coincidence rather than a co-ordinated and directed effort.

6. NMR Spectroscopy of Bioreactors

6.1. Introduction

Many elementary metabolic pathways inside the cells have been *qualitatively* described, however, the *quantitative* understanding and regulation, that are the fluxes and reaction kinetics, remain to be elucidated. Measurements outside the cells provide only indirect information, in the case of metabolic networks they yield no information on fluxes along branches and alternative paths where the net change is zero. Protocols for intracellular measurements after extraction always bear uncertainty about the influence of the sampling procedure on the result. Intracellular ATP measurement after trichloracetic acid extraction, as commonly used, requires extremely fast sampling, as the total turnover rate of ATP in the cell is below one second. In addition, each sample can only be analyzed once, and controls, reproducibility and consistency are difficult to achieve when considering sample variability in complex systems. Further, non-invasive sampling techniques are preferred since drawing representative samples from the ports of the reactor is not possible, without causing a substantial disruption of the culture.

To overcome these severe limitations, nuclear magnetic resonance spectroscopy (NMR) and magnetic resonance imaging (MRI) have been suggested as non-invasive, repetitive and successive techniques. The studies on various organisms, including archae, prokaryotes and eucaryotes, such as animals and humans and their organs, have challenged existing metabolic theories, finding new pathways and unexpected metabolic conversions [188, 199]. Hence, the questions relevant to biochemical engineering tackled by NMR spectroscopy and MRI promise to further our understanding of metabolism, energy states and product formation, influence of the environmental conditions on the intracellular state, reaction kinetics, and metabolic pathways as well as mass transfer.

The present research attempts to elucidate the influence of oxygen and pH, as well as their gradients in a typical high-density reactor system, such as the fluidized bed, on cellular metabolism. Of particular interest is the energy state of cells in culture in their bioprocess environment the bioreactor, in this case a fluidized bed. Step changes were applied to obtain dynamic metabolic responses.

6.2. Principles of Magnetic Resonance Spectroscopy

Nuclei posses a *spin* due to impair neutron or proton number and thus have associated with them an angular momentum. Because certain nuclei have a charge and a spin, they also have a magnetic momentum associated with them. In a strong external magnetic field B_0, the magnetic momentum vector aligns either with or against the external magnetic field, with the first case representing a lower state of energy. The energy difference ΔE between the two quantum states is proportional to the magnetic field strength and is dependent on the magnetic behaviour of the nuclei. Expressed by the gyromagnetic constant γ:

$$\Delta E = h \cdot \nu_0 = \hbar \cdot \omega_0 = \hbar \cdot \gamma \cdot B_0 = \frac{h}{2\pi} \cdot \gamma \cdot B_0$$

A transition from the lower energy state to the higher energy state (resonance condition) occurs if the incident photon has an energy equal to the energy difference between the two states, which is for the magnetic field strengths used in NMR spectroscopy in the order of radio-frequencies:

$$\nu_0 = \frac{\gamma}{2\pi} \cdot B_0$$

The distribution of nuclei between the two energy states in the magnetic field is given by the BOLTZMANN equation:

$$\frac{N_\downarrow}{N_\uparrow} = e^{-\frac{\Delta E}{kT}} = e^{-\frac{\gamma \cdot \hbar \cdot B_0}{k \cdot T}} = e^{-\frac{\gamma \cdot h \cdot B_0}{2\pi \cdot k \cdot T}}$$

As ΔE is very small, only a very small number of nuclei contribute to the observable net magnetization. This makes NMR spectroscopy inherently insensitive,

requiring preferably a large amount of nuclei in the measuring volume. Specifically, in the case of ^{31}P-NMR at 4.7 T, the BOLTZMANN equation indicates that only 13 nuclei out of one million will resonate when excited at the LARMOR-frequency (80 MHz). After applying a short electromagnetic impulse at the LARMOR-frequency, thus exciting the nuclei, the nuclei relax and fall back to the lower energy state, emitting the energy as damped cosine oscillation or *free induction decay* (FID). Multiple excitation and relaxation, and then addition of the resulting FIDs, increases the signal intensity and the average signal to noise ratio (SNR). The FID signals are converted from the time-domain to the frequency-domain via Fast-Fourier-Transformation (FFT), resulting in a spectrum. In the spectrum each frequency signal (peak) represents a nucleus in a different chemical environment, e.g. in the molecule. The slight difference in the resonance frequency and its resulting chemical shift can therefore be assigned to it. The area under the peak is proportional to the number of nuclei excited, and is thus proportional to the concentration of a metabolite in the measuring volume. Absolute quantification becomes possible when a calibrated standard is used during spectroscopy in the sample. The main nuclei of interest, by virtue of their magnetic moment and biological occurrence are ^{1}H, ^{13}C, ^{23}Na, ^{15}N and ^{31}P.

Nuclei	Abundance	γ	ν	Sensitivity	min. Conc.	Application
1H	99.98%	26.75	200.12	1	0.01 mM	MRI, mass transfer
13C	1.11%	6.73	50.33	0.016	1 mM	glycolysis, gluconeogenesis
14N	99.64%	1.94	14.47	0.001		amino acid metabolism
15N	0.37%	-2.71	20.29	0.001		amino acid metabolism
19F	100%	25.17	188.28	0.833		cell volume, flourinated comp.
23Na	100%	7.00	52.36	0.093		intracellular sodium, cell density
31P	100%	10.84	81.09	0.067	0.05 mM	energy metabolism, pH, (Mg)

Figure 6-1. *Nuclei suitable for NMR applications; characteristics with respect to ^{1}H, ν is the LARMOR-frequency [MHz] when applying a magnetic field B_0 of 4.7 T, γ is given in [0.1 MHz·rad·T^{-1}]*

6.3. MR Techniques in Biochemical Engineering

6.3.1. ^{31}P-NMR

^{31}P, with 100 % abundance and fair relative sensitivity, is the preferred nuclei chosen for NMR spectroscopy, mainly, as it is the only nuclei of metabolic relevance

not requiring addition of labelled compounds. It is therefore likely to be the first nuclei tried, when applying NMR spectroscopy to a sample. Yet the low sensitivity, as compared to ^{13}C enriched samples, requires a more stable and homogeneous magnetic field. ^{13}C nuclei are important, considering the increased wealth of possible information, for further metabolic studies [140]. The metabolic investigations with ^{13}P NMR all aimed at elucidating the influence of extracellular environmental changes, preferably glucose and glutamine, on the energy state of the cell, expressed as contents of high-energy phosphates such as NTP, NDP and NAD(H), or the intracellular pH. Several reviews have been published recently [32, 58, 105, 184, 185].

Individual research on mammalian cells, such as CHO and hybridoma cells, both relevant to bioprocess engineering focused on the determination of cell density based on:

- the assumption of a constant NTP concentration and non-invasive measurement of NTP [141],
- the differences in intracellular inorganic phosphor content when changing the substrate from glucose to glutamine [206],
- the determination of transfer rates from one energy metabolite to another [162],
- the determination of NTP and NDP levels under presence and absence of nutrients and oxygen [219],
- the early response of glioma cells to hyperosmotic stress [121] resulting in a decrease of cell volume and an increase in NTP concentration.

The intracellular pH can be deduced from the change in chemical shift of phosphocreatine and inorganic phosphor, or between two NTP peaks. The peak positions are influenced by pH, and these shifts can be used to calculate intracellular pH levels [72, 106, 114]. As ATP forms a complex with Mg^{2+} intracellularly, the intracellular pH depends on the Mg^{2+} concentration, which also needs to be measured [86]. If neither phosphocreatine is present, nor the Mg^{2+} concentration can be determined, as in the case of immobilized CHO cells, intracellular pH cannot be determined.

The peak areas correlate well with cell density and growth rates assuming a constant intracellular ATP concentration and therefore cell-density and growth rates can be estimated. ATP/ADP ratios, indicators of energy and metabolic state, can also be obtained from ^{31}P spectroscopy [206].

Similar measurements as with mammalian cells have been performed on micro-organisms such as *E. coli* [1, 24, 35], *Zymomonas mobilis* [209] or *S. cerevisiae* [29]. Though micro-organism are orders of magnitude easier in practical handling, they feature similar metabolic pathways.

6.3.2. ^{13}C-NMR

The most interesting metabolic studies on isolated cells were made using ^{13}C, because of the central role carbon plays in the metabolism, specifically, glycolysis, TCA and oxidative phosphorylation. Unfortunately, ^{13}C in nature occurs in very low concentrations ($\approx$ 1%) at a relative sensitivity half of that from phosphor. It must therefore be added as enriched ^{13}C labelled medium, such as glucose or glutamine.

^{13}C-NMR spectroscopy is a powerful means to track metabolic pathways. Due to its low abundance in nature however (<1%), labelling is required, which means adding to the medium a metabolically-active compound with ^{13}C at one position in the molecule. The analysis requires then identification of all the ^{13}C peaks, which involves all the metabolically-related compounds. Prediction of the possible locations that could be taken by the original ^{13}C nuclei can be made from prior biochemical knowledge. Thus, after postulating the principle pathways, the location of the ^{13}C nuclei starting from a specific source, e. g. glucose and glutamine, can be predicted [127]. Absolute quantification is often difficult, but relative measurements for different carbons in the same intermediate and relative changes with time can be measured, thus allowing to calculate fluxes and flux partitioning [204]. The slow dynamic changes throughout the metabolic network (5 to 20 hours for full saturation with ^{13}C) cause a loss of intracellular ^{13}C to extracellular compounds, especially CO_2. In addition, a dilution of the ^{13}C at each location in the pathway is caused by the metabolism of unlabeled

compounds through side paths. All these changes give valuable insight into the rates and pathways. Assuming steady state, it is possible to equate the rates of formation and consumption for any one compound. Additional balances can then be written for any specific ^{13}C location in a single compound, which is produced from more than one ^{13}C source, by using prior knowledge on the structural rearrangements. Using measured fractional and relative labelling as well as external and internal concentrations and global fluxes, it is possible to establish a sufficient set of algebraic equations to calculate all the intracellular fluxes [195]. NMR can thus be used to obtain intracellular information that cannot be deduced by the more conventional analysis using only extracellular rates. Because of the specificity for location, it is a more powerful tool than radioactive labelling, but at the same time less sensitive.

Tracer studies with 1-^{13}C glucose and 3-^{13}C glutamine in continuous hybridomas cultivated in hollow-fibre reactors revealed significant activity of the malate shunt and showed that the flux through malate dehydrogenase was substantially larger than that through citrate synthetase. 2-^{13}C glucose was used to determine the relative fluxes of the pentose phosphate network and glycolysis. Further, it was possible to calculate the fluxes through all the metabolic pathways under feed glutamine concentrations of 4.0 mM and 1.7 mM glutamine [142, 197].

6.3.3. ^{15}N-NMR

Nitrogen is elemental to the amino acid metabolism and should therefore be, after carbon, the nuclei of most interest for the non-invasive investigation of metabolism in animal cells. However, its sensitivity is two orders of magnitude lower than that of ^{31}P and the lowest of the relevant molecules, further the abundance of 0.37 % necessitates the use of labelled compounds. Therefore, only limited research has been conducted involving ^{15}N. Research mostly involved the investigation of the behaviour of various active enzymes in solution and their reaction mechanisms. Applications in vivo are because of the outlined disadvantages not very attractive [104].

6.3.4. ^{23}Na-NMR

^{23}Na features 100 % abundance with a relative sensitivity better than that of phosphor and would therefore be a suitable nuclei, however its metabolic relevance is limited and the peaks are rather broad and difficult to resolve. Sodium is metabolically relevant mainly in the cellular ion balance. Assuming a known sodium ratio between inside and outside, thus a stabile transport mechanism, one can calculate from the intracellular and the extracellular sodium concentrations, which both can be determined by NMR, the cell volume or the cell number, also in immobilized cells [85, 141]. To do so, one has, however, to add a shifting agent (dysprosium(III)-tripolyphosphate) to separate the two peaks (intra-/extracellular), potentially altering the cellular metabolism [85, 198]. Further, the calculation relies on a small difference between two very large numbers, introducing an error comparable to other cell density measurements [140].

6.3.5. MRI

Magnetic resonance imaging (MRI) applies spatial magnetic field gradients to align the nuclei in all three dimensions allowing the acquisition of a spatially resolved matrix of spectra or image. This is enhanced by using mathematical algorithms to resolve the FIDs. Traditionally, this is done with whole body ^{1}H MRI in medical diagnostic applications (tumour detection), for which it has been approved, and only very limited information of adverse effects of such strong magnetic fields is available [126].

Flow patterns have been investigated using MRI after applying special pulse sequences. Measurements of the flow induced phase shifts and applying fast FOURIER echo imaging sequences, flow in the aorta has been analyzed, The velocity profiles and the instantaneous flow rates have been determined. Refining the technique it was possible to analyse also more complex flow pattern at bifurcations [21].

In a cell free hollow-fiber reactor, a 3D Fourier flow imaging technique yielded the fluid velocity profiles. This included phenomena such as STARLING flow, which occurs as a convective leakage flow along the fiber-axis due to a transmembrane hydrostatic pressure difference. MRI is in this case supportive to reactor design, as mathematical

modelling would necessitate detailed information, such as fiber placement and construction, not readily available [89, 92].

6.3.6. Reactor Systems

NMR spectroscopy has been established as a non-invasive tool for the elucidation of cellular metabolism in vivo. Yet, it is inherently insensitive and requires therefore a high cell density and a system to maintain it to produce a sufficient signal to noise ratio (SNR > 2.5). The first designs were based on analytical NMR spectroscopy (wide-bore) systems and attempted to immobilize the cells either by entrapment in alginate [136], collagen or dialysis tubing [59], and on microcarriers [161]. Further developments yielded simple NMR-tube airlift reactors [115] or sparged tubes with improved oxygen transfer. With their simple design they are convenient and still favoured [136, 160]. They lack resemblance to industrial bioreactors because of limited peripherals, such as pH and DO probes, and their very small total volume below 10 ml, resulting in rather short cultivations.

Further design improvements yielded hollow-fiber reactors [25, 140] and specially designed reactors (CSTRs) combining high flux of detectable nuclei through the coil [45] or with internal coils [150], with large numbers of nuclei in the measuring volume. They have been used to monitor the energy state of cultivated cells in long-term continuous cultures [51, 68, 137, 196].

However, all previous systems were rather designed to allow metabolic studies using NMR spectroscopy than to investigate bioreactors. Only recently the interplay of cells *and* reactor, with related issues such as mass transfer, metabolic pathways and reactor heterogeneity, has found interest [47, 89, 140]. Further, the abundance of biomedical MRIs led to the increased use of these systems, with less geometrical constraints offering more realistic bioreactors, such as loop reactors and fluidized beds [192, 193].

6.4. Localized MR Spectroscopy

To obtain information non-invasively in a predetermined small volume it is necessary to either excite or relax a specific volume. This is possible by using surface

coils directly attached to the volume of interest (localized spectroscopy) or by using volume selective methods, such as image selected in-vivo spectroscopy (ISIS) or volume selective refocussing (VSR) based on a combination of complex excitation pulse sequences and magnetic field gradients. Localized spectroscopy is simple and has a high sensitivity and signal to noise ratio, it is however limited to volumes close to the surface and spherical measuring volume and intensity. Volume selective methods solve these problems, but are very complex and require a highly homogenous magnetic field in order to apply very narrow field gradients on narrow samples. For ^{31}P, the spatial resolution possible at 4.7 T is above 1 cm using volume selective methods. It was therefore more favourable, given the current state of such developments and the potential sample geometry, which would require a full gradient over the diameter of only 3 cm, to pursue with a set of surface coils than developing new excitation and gradient pulse algorithms.

6.4.1. Bioreactor Design

Besides the conventional bioreactor design considerations outlined above, a bioreactor for MR investigations has to fulfil the requirements from this analytic technique. The system must provide a suitably high concentration of nuclei, e.g. cells in the order of 4 to 7 per cent cell volume per measured volume ($50 \cdot 10^6$ cells per ml) [150], to provide a sufficiently strong signal (SNR >2.5). The SNR for whole-cell NMR is a function of many variables, proportional to the square root of the acquisition time, the number of scans and the sample density. The interdependence of these two quantities was emphasized [44] and it was shown that for the β-phosphate of ATP, the acquisition times rise sharply above 10 seconds for cell densities less than 10^8 cells/ml.

The material chosen for the reactor hull was polycarbonate, with the fittings made from PTFE and the screws providing an O-ring seal were brass, which has superior properties with respect to influencing the magnetic field as compared to the biological first choice titanium. A reactor column of polycarbonate with an effective vertical length of 125 mm and 30 mm horizontal diameter, was constructed to fit inside the 20 or 30 cm horizontal bore of the biomedical MRI (Figure 6-2).

Two main uncertainties could not be assessed up-front. Firstly, the presence of steady flow and continuously moving particles inside the coil, potentially disturbing the magnetic field such that no meaningful result can be achieved. Secondly, the necessary cell density required an optimal growth of the cells in a high-cell density system, with no growth-limiting conditions, such as contact inhibition.

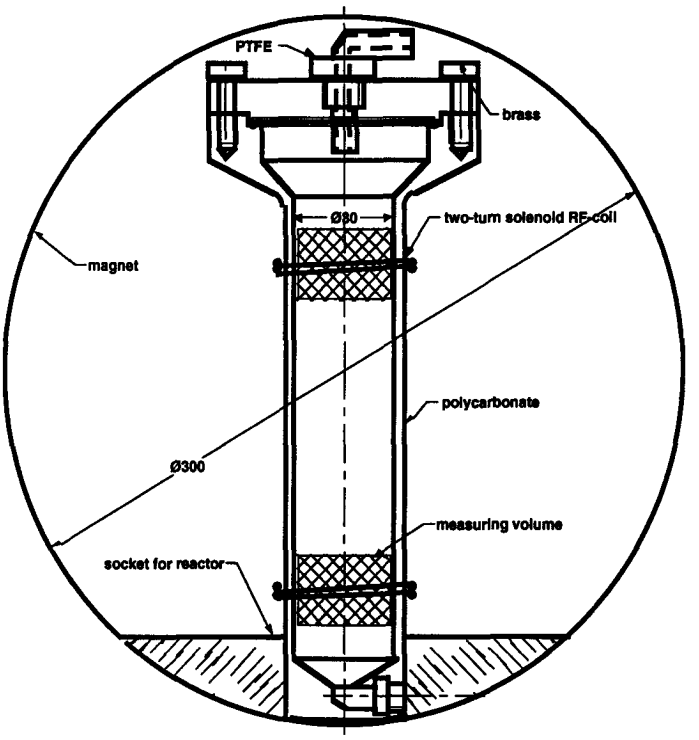

Figure 6-2. *Fluidized bed reactor for localized NMR spectroscopy; cross-hatched area indicates approximate measuring volume*

6.4.2. RF-Coil

To acquire localized ^{31}P-MR spectra, two separate RF surface coils - one at the bottom and one at the top of the reactor (Figure 6-2) were used. These coils were designed to transmit and receive the ^{31}P RF signals (80 MHz). In order to optimize the receiving signal, the same coils were used for magnetic field shimming. This was done by detuning the surface coils to the ^{1}H resonance frequency using a separate tune/match circuit and varying the local magnetic field in order to maximize the receiving ^{1}H signal. Detuning the coils to the ^{1}H resonance frequency allows to do the shimming in a reasonably short time due to the 15 fold sensitivity of ^{1}H compared to ^{31}P (Figure 6-1).

Two two-turn solenoid coils with an inner diameter of 40 mm were made from 1/16" PTFE coated wire. Solenoid coils feature good homogeneity of the RF (B_1) field and allow free positioning in the magnet's bore as long as their axis is orthogonal to the main field axis [124]. Care was taken that the wires were intertwined in one plane to focus the field. The solenoid coils were arranged perpendicular to the axis of the fluidized bed column, such that the column was located inside the coil and the medium flow went through it in direction of the B_1-field. Geometrically, it was therefore also a mixture of solenoid and slotted-tube resonator, combining their advantages [159].

The two circuits, that are the two tuneable capacitors (Polyflon VC 10-12-05/07) for each circuit and the grounding to the case were, placed in a 1 mm wall thickness cooper shielded case protecting from EMI, and the two cases were stapled on top of each other. This allowed the selection of one of two measuring volumes at the top and bottom of the fluidized bed column. Due to coupling it was however necessary to fine-tune every circuit using the tuneable capacitors before a measurement was taken, leaving room for future improvement. Further, measurements in different levels were taken a few minutes apart as the MRI instrumentation did not allow simultaneous measurements in both circuits.

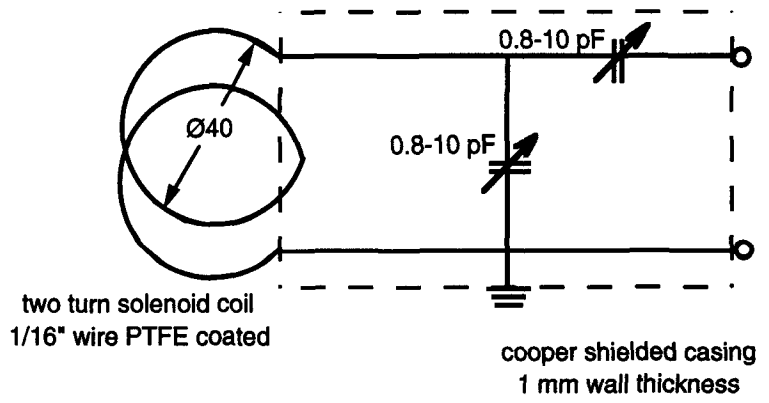

Figure 6-3. *RF-circuitry used for localized MR spectroscopy*

6.4.3. NMR Spectroscopy

The system used for localized NMR spectroscopy was a SIS 200/330 NMR Imaging Spectrometer (transmitter/receiver/amplifier) from Siemens/Varian Associates with a 4.7 T / 200 MHz Magnet from Oxford Instruments and a Sun SPARCstation

330GX for acquisition and processing (24 MB RAM, 1 GB mass storage) located at Paul-Scherrer-Institut. ^{31}P NMR spectra were acquired at 80.98 MHz with 6336 data points. Spectra were either acquired under fully-relaxed conditions with respect to the high energy phosphates (HEP) (9.5 s acquisition time, 70 or 400 scans) or under forced conditions (0.5 s acquisition time, 700 scans). The acquisition of one spectrum took a minimum of 10 minutes. 4096 data points were processed with 10 Hz line broadening. The RF pulse angle θ was determined using the acquisition software supplied by Varian and was found to be 45 °.

6.4.4. Quantification

Quantification of spectra is possible when carrying a standard of known concentration along during the measurements. An *internal* standard has to be metabolically inert and non-toxic, with a chemical shift distinctly different from any relevant nuclei, and it must be present in a concentration in the order of the observed nuclei. In the case of ^{13}C NMR spectroscopy, this is commonly achieved by referring all concentrations to the carbon contained in the metabolically inactive HEPES, which is commonly used as buffer in cell culture media at concentrations of 10 to 30 mM. In the case of ^{31}P NMR spectroscopy, several standards have been suggested for internal or external reference, including dimethylphosphonic acid (DMMP) [10, 121], methylenediphosphonic acid (MDPA) [67, 99, 227, 228] and trimethyl phosphate (TMP) [109]. The crucial question of toxicity and biocompatibility is for most cases not solved when an internal standard is used, as they are commonly only used in short-term experiments [10]. Based on an assessment of the potential toxicity [50, 95, 143] to cell growth and metabolism, and the convenient location of the peaks at 39 ppm, DMMP was used as an *external* standard.

A solution of DMMP in PBS was sterilized and a 0.5 mm NMR tube (Willmad) was filled with this calibrator. The tube was sealed and attached to the outside of the fluidized bed column so that equal amounts of phosphorous nuclei stemming from DMMP and from the cells and the medium were placed inside the measuring volume.

The DMMP standard was calibrated on a Bruker AMX-200 NMR spectrometer under identical conditions as outlined above against a known phosphate buffer of pH 7.4 to calculate absolute concentrations c_{Pi} :

$$c_{P_i} = A_{P_i} \cdot \frac{c_{DMMP}}{A_{DMMP}} \cdot \frac{d_{Tube}^2}{d_{FB}^2}$$

Thus it was also possible to correct forced spectra [140] :

$$c_{P_i,calibrated} = c_{P_i,measured} \cdot \frac{A_{relaxed}}{A_{forced}}$$

The areas under the peaks were quantified after assignment of the chemical shift of the peaks [222]. The deconvolution algorithm providing a Gaussian fit for calculated single model peaks [26], respectively, was provided by the acquisition software from Varian.

The concentration of the nucleoside triphosphate (NTP), mainly ATP, was calculated from the area under the peak assigned to β-NTP (that is the intermediate phosphor), and the concentration for NDP was determined from the difference between the area assigned to the β-NTP peak and the average of the area assigned to the α-NTP/NDP and the β-NDP / γ-NTP peak. Assignment of the phosphor nuclei in the nucleoside phosphates (ATP) was:

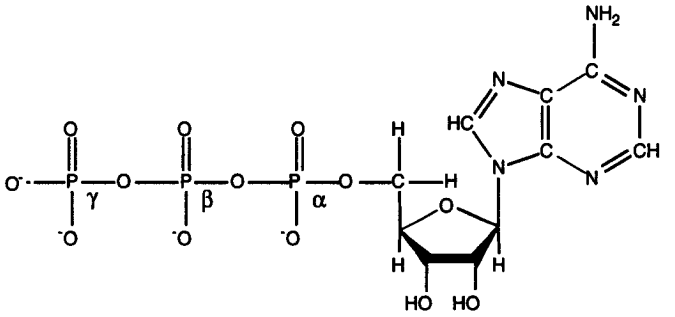

6.5. Results and Discussion

Recombinant CHO cells [144] were cultivated in IMDM/Ham's F-12 (1:1) medium supplemented with 1% FCS on 40 ml macro-porous unmodified borosilicate SIRAN carriers (Schott) of 300 to 500 µm diameter according to the methods outlined in Chapter 4. After three days of batch culture and subsequent four days of continuous culture the reactor assembly was transported to the site of NMR spectroscopy (Paul-

Scherrer-Institut). Cultivation continued for a total of three weeks. ^{31}P-NMR Spectroscopy was performed using the two horizontal two-turn-solenoid RF-coils in the upper and lower region of the upright fluidized bed column.

6.5.1. ^{31}P Sensitive Metabolites

^{31}P NMR spectra exhibited resonances due to inorganic phosphate (P_i), the combination of nucleoside diphosphates (NDP) mainly from ADP, nucleoside triphosphates (NTP), mainly from ATP, pyridine nucleotides (NAD(H)), mainly from NAD, NADH, NADP, and NADP(H). Further, resonances from unidentified phosphodiesters (PDE), phosphomonoesters (PME), and phosphoenolpyruvate (PEP) were visible. The DMMP reference showed two peaks, one from DMMP and one from a decomposition product that forms after sterilization [10]. Due to the lower concentration of the decomposite, it was used as convenient second reference when quantifying low concentrations. A typical ^{31}P NMR spectra is given below.

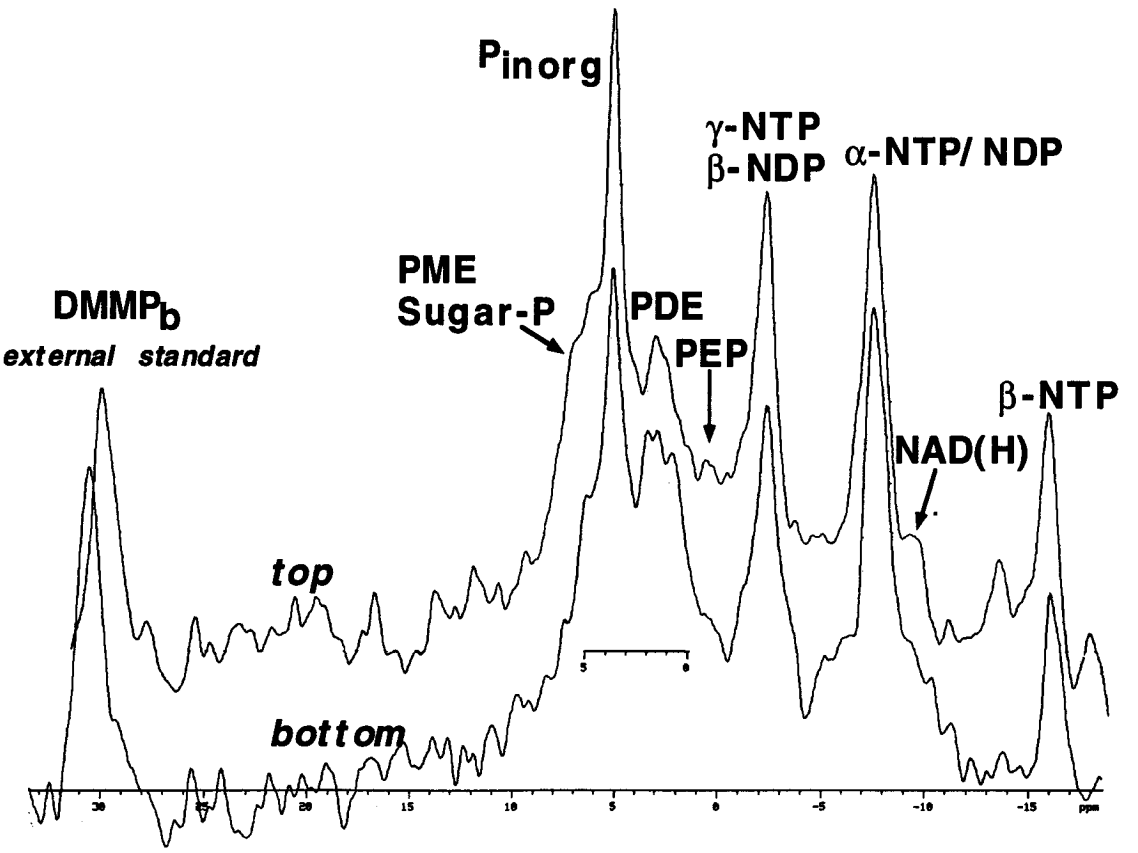

Figure 6-4. *Localized ^{31}P NMR spectrum; comparison of bottom and top section of fluidized bed reactor with respect to NTP concentration. The y axis is indicating intensity.*

Localization of the spectra and observation of two distinct areas was possible using two coils in two different sections of the bed. Fast spectra were possible with less than 10 min acquisition time and low noise pickup, compared to the expected noise due to flow and moving particles. In fact, the apparent T_1 relaxation time was reduced as medium, and carriers with excited nuclei were to some part moved out of the *sweet-spot* of the coil, thus allowing faster pulses, higher SNR and shorter acquisition time. Localized NMR spectroscopy therefore provides a powerful non-invasive tool for process and metabolism monitoring of cells in the reactor.

6.5.2. Axial Cell Density Gradient

NTP and NDP concentrations were generally found to be higher at the top of the reactor than at the bottom. Quantification of the spectra revealed up to two times more NTP in the upper region than in the bottom. Carrier samples taken after the cultivation showed up to one order of magnitude higher cell concentrations in the upper region of the bed (Figure 7-4). In the upper half of the reactor, we observed *bulging-out* [60] of cells around the carriers in the order of 10 to 15 cell layers, which could be confirmed in SEM pictures, as well as by thorough visual inspection of the reactor.

Figure 6-5. *SEM of microcarrier from fluidized bed; top (right) section shows several cell-layers (bulging-out) around the carrier, while under higher mechanical stress (bottom; left) growth occurs only on the inside of the macroporous carrier.*

This phenomenon termed stratification, was confirmed by the different volumetric ATP contents in the upper and lower region of the bed. However, reports are scarce as the common understanding of a fluidized bed is rather crude compared to a conventional CSTR or plug-flow tubular reactor. Previously, it has been considered to be similar to a stirred reactor [65] as well as modelled as a tubular reactor [122]. Reality lies somewhere between the two, judging from experimental data, such as a residence time distribution in a hydro-dynamically very similar system [214]. Moreover, in expanded bed adsorption, such as Pharmacia's Streamline process, a density gradient has been employed to achieve a stabile expansion with a near plug-flow characteristic [53]. It was observed that a well-mixed zone at the bottom exists, suggesting higher degrees of collision and mechanical stress, and decreased turbulence in the upper part of the column, suggesting gentle conditions with low mechanical stress.

It is reasonable that microcarriers used for cultivation show similar behaviour and that after long-term cultivation stratification occurs due to a widening density and size distribution (see Chapter 4). In further investigations [200], it was found that stratification varies with cultivation conditions, such as dilution rate, which in return influences the cell density in a continuous reactor system and on the carrier. Low mechanical stress in the upper region explains growth of cells in layers around the carrier, additionally lowering the density of the particle while increasing the hydrodynamic cross-section and therefore lowering the terminal velocity u_t. Whereas in lower regions, cells can only be found in the cavities, keeping those carriers in the lower region and pronouncing stratification. It is not clear why two equally extended distinct zones could be visually observed. It might be just a perception of a non-gradual transition than a measurable phenomenon, as the carrier appear slightly yellowish when covered with cells.

Assuming that the axial position of a carrier in the bed is proportional to the density difference and the square of the diameter of the carrier (the hydrodynamic cross-section as the area offered for drag), a normalized terminal velocity represents the axial distribution of the carriers - the bed gradient (Figure 6-6; see Chapter 4.1.3). The

apparent phenomenon that high cell density reactors are inherently inhomogenous has recently also been observed by other investigators using various reactor systems, such as hollow-fiber reactors which grew from top to bottom [140], fluidized beds growing also from top to bottom [60], and stirred reactors in continuous or batch mode. It was suggested to increase the number of sensors, specifically DO sensors, to gather a broader database [38] about the assumed inhomogeneities.

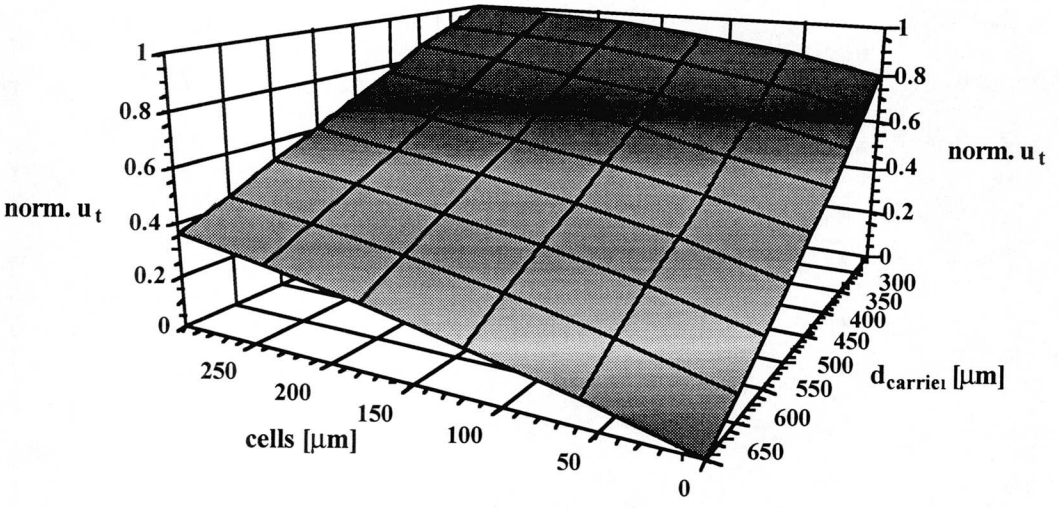

Figure 6-6. *Axial distribution of carrier; the normalized location of the carrier along the axis in the fluidized bed varies with size and cell layer thickness supporting that small carriers with several cell layers are most-likely to be found in the upper region.*

For the practical application of fluidized beds this suggests for DO a controller at the effluent, rather than one which would control the flow *into* the fluidized bed column. This is reasonable since the larger part of the cell mass and therefore the larger metabolic gradient is in the upper half, due to the heterogeneous fluidized bed population.

6.5.3. Response to step changes in DO and pH

Oxygen is one of the key cellular metabolites. Changing concentrations of dissolved oxygen and pH have been found to influence specific metabolic rates and productivity of mammalian cells in culture [154], thus influencing the performance of a reactor system in an industrial context. A step change was applied for DO from 130 µM to 30 µM as well as from pH 7.4 to pH 7.1. The responses of the phosphor-metabolites, the high-energy phosphates [HEP] such as NTP and NDP, were observed.

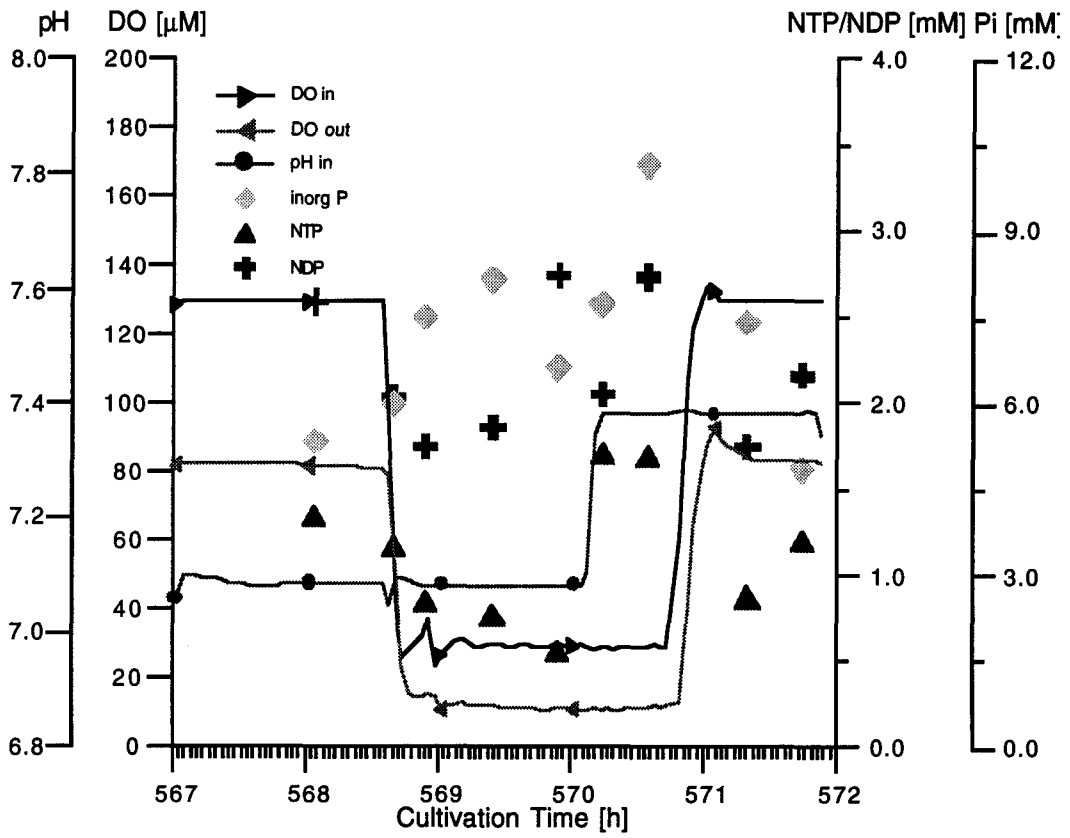

Figure 6-7. *Response of phosphates to step changes in oxygen and pH; NTP decreased due to lower available oxygen for oxidative phosphorylation. A pH shift upward increased the NTP concentration suggesting energy gain due to a favourable pH gradient across the membrane.*

NTP and NDP decreased when lowering the dissolved oxygen from 130 $\mu mol \cdot l^{-1}$ to 30 $\mu mol \cdot l^{-1}$. The decrease in NTP was higher than that for NDP. Whereas NTP decreased continuously from 1.3 mM to 0.5 mM very rapidly, already during the step change, NDP decreased only in the initial phase from 2.5 to 1.8 mM during the first 20 minutes. NDP recovered after one hour. This correlates to the conversion of NTP to NDP and inorganic phosphor (P_i), which increased as NTP decreased. After one hour when NTP reached its low level and NDP increased, P_i decreased, suggesting the renewed formation of NDP from P_i and sugar-monophosphates. NTP did not recover and stayed on the lower level. Returning to 130 $\mu mol \cdot l^{-1}$ dissolved oxygen after 2 hours, returned the NTP and NDP levels to the initial concentrations too.

Further, it was observed that the volumetric OUR decreased from 5 $\mu mol \cdot ml^{-1} \cdot h^{-1}$ to 2 $\mu mol \cdot ml^{-1} \cdot h^{-1}$, as can be calculated from the decreased difference between DO_{in} and

DO_{out}. The OUR recovered rapidly after the DO was raised again. This corresponds well with findings of previous researchers [141], who found that hybridoma cultures that the NTP concentration was proportional to the OUR, and that below 120 µM the OUR dropped proportionally. To further substantiate this, the OUR was plotted as a function of inlet dissolved oxygen (Figure 6-8). It was found that with lower dissolved oxygen the cells would apparently consume less oxygen, suggesting a cell internal mechanism regulating the metabolism as function of the nutrient concentration, e.g. dissolved oxygen, available.

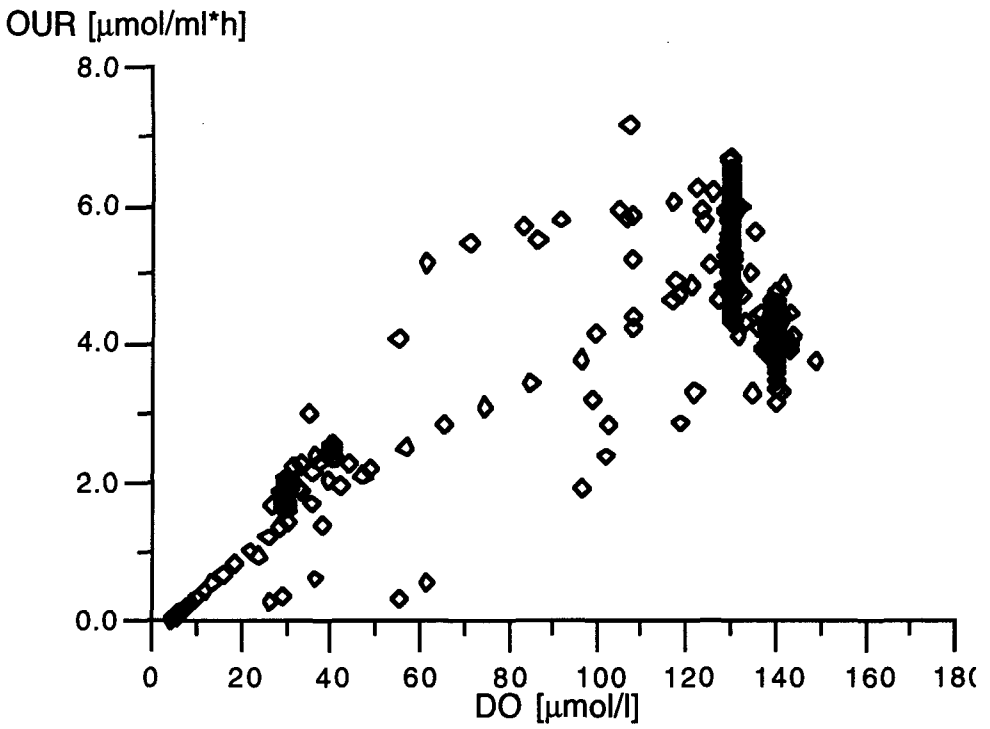

Figure 6-8. *OUR as a function of inlet dissolved oxygen (DO_{in})*

The results are consistent with the previous finding, that the concentration of NTP in cells responds quickly to the changes in oxygen concentration, suggesting that the cells obtain a large portion of their energy from oxidative phosphorylation, as opposed to other energy producing pathways, such as glycolysis. The concentration of oxygen was lowered by about a factor of four with the NTP concentration dropping only by a factor of two. This difference suggests that other pathways contribute significantly to the energy production of the cell, and/or that cells modify their metabolism in response to the reduced availability of oxygen [57]. Although the

concentration of oxygen is expected to be well regulated within the cell [163, 202], the immediate drop in NTP suggests, that the regulatory processes are inadequate to maintain the levels during such changes in extracellular conditions.

The metabolic rates, such as the energy state resulting from glucose, glutamine and dissolved oxygen conversion were higher at high pH values. The increase in glucose and lactate metabolism at high pH values is well-known for tumor cells [138, 153]. One possible explanation lies in the increase of the activity of glycolytic enzymes. It is known that hexokinase has an optimal pH value of 8. Another explanation is that increased pH alters the membrane potential, changing the glucose transport rate through the membrane [172].

The apparent ATP production increased with high pH. This increase was due to the increase in glycolytic flux. A 3-fold increase in ATP concentration did however not lead to a higher growth rate. Cells seem to dissipate energy for unknown reasons [172]. At elevated pH, cells do not use the extra energy generated from glycolysis and glutamine oxidation. Oxidative phosphorylation has been reported to contribute decreasing percentages of ATP with increasing pH [172].

As part of a planned scheme of experiments, the pH was changed subsequently from 7.1 to 7.4. The pH step caused a rapid increase of NTP at the apparent expense of NDP, which was however supplied quickly after depletion. This suggests that pH 7.1 is energetically a worse state for the cell than pH 7.4, which confirms the optimal pH range for exponential growth of CHO cells [77]. The apparent increase in inorganic phosphor remains unexplained. The oxygen uptake rate was not influenced by pH and remained at 2 $\mu mol \cdot ml^{-1} \cdot h^{-1}$, corresponding to findings of previous investigators [155, 172].

The applied increase in DO_{in} after the pH increase should have led to a further increase in NTP content due to more favourable conditions, reversing the first step-change. However, a transient decrease of NTP content was observed, which may be in part due to the sensitivity of the deconvolution algorithm for broader peaks, thus decreasing the apparent concentration of NTP. Yet, the final energy state of the cell

represents very closely the starting conditions with respect to NTP, NDP and P_i concentrations, therefore no permanent damage was caused in the cell metabolism.

6.5.5. Radial Mass Transfer

The apparent decrease of the volumetric oxygen uptake rate (OUR), which is in fact an average over the whole cell population in the fluidized bed, suggests a mass transfer limitation, thus possibly resulting in only a part of the population contributing to the metabolism and the net oxygen uptake and therefore mimicking a lower OUR This has been studied extensively by previous researchers, including the diffusion in the solid phase (cell layer) [34, 84, 108]. KELLER [108] specifically modelled the effects of cell growth around macro-porous SIRAN carrier in the range from 400 µm to 1000 µm and found that with carriers smaller than 500 µm at DO concentrations down to 27 $\mu mol \cdot l^{-1}$, and otherwise highly similar circumstances, no limiting conditions occurred inside the carrier. Further, the diffusion limitation has been found to be only important for diameters greater than 600 µm [33, 84]. The diffusion influence was only of minor importance with carriers smaller than 500 µm as judged from the THIELE-Module.

It is however stated that the model as well as the practical side suffer uncertainties with respect to the effective diffusion in dense cell aggregates and the exact specific oxygen uptake rate. Both are limited by the experimental procedures available [205].

6.6. Conclusion and Outlook

It was shown that NMR is a non-invasive method to investigate cell metabolism and to measure the influence of reactor conditions on metabolism and the energy-state of the cells. Fluidized bed reactors for animal cell culture have a sufficiently high cell density to permit NMR measurements and neither the moving particle nor the upward flow influences the measurement. In fact, the flow out of the measuring volume, reduces the T_1 relaxation time and therefore faster pulse sequences were possible when acquiring fully relaxed spectra [45, 150], further increasing the SNR. Application of NMR spectroscopy could be extended from hollow-fiber reactors successfully to fluidized beds. This opens the possibility for further investigations to support mathematical

modelling with non-invasive data [238], and to improve bioreactor design and understanding of mass transfer.

Using ^{31}P NMR spectroscopy, it was possible to measure the difference in cell density between the top and bottom of the column and to evidence stratification at the superficial velocity under which the cultivation was performed. Oxygen decrease results in rapid loss of energy for the cell within twenty minutes, which can be monitored in vivo by following the NTP and NDP concentrations.

However, it would be desirable to monitor quick dynamic changes, that occur within minutes or even seconds, with shorter acquisition times, for which stronger magnets and faster pulse sequences are required. Further, the quantification needs refinement, especially the deconvolution algorithms were found to need prior knowledge and tedious work to prevent arbitrary results. Although substantial changes were observed, the relationship between the uptake rates, phosphorylated metabolite levels, and protein production remains to be determined. Among the questions that remain therefore to be solved are: How does the nutrient situation influence the choice of different metabolic pathways ? What would be an optimized feeding strategy to meet the energy requirements of the cells ? How do internal metabolite concentrations correlate with the yield of protein production ?

Again, the use of ^{13}C labelled compounds should improve the SNR as outlined in the introduction. The use of combined ^{13}C and ^{31}P NMR studies together with external flux measurements will enable determination of internal fluxes and the resulting net energy changes thus giving a picture of both layers, the carbon and the energy flux. Particularly, the technique is necessary for elucidating branch points and exchange pathways, as no net fluxes are detectable from other measurements.

Another potential application of increasing interest in the medical community is the investigation of primary cells, such as hepatocytes and cells of other organs, by either ^{13}C or ^{31}P NMR spectroscopy, but preferably MRI, to monitor artificial organs and their endogenous or xenobiotic kinetics [137].

7. Influence of Bioprocess Conditions on Production

7.1. Introduction

Identification of factors influencing glycosylation in batch culture is complicated by simultaneous changes in several variables during cell growth. Chemostat culture enables the study of cell physiology at steady state, where environmental parameters remain constant with time. This technique has been used in the study of mammalian cell physiology before [62, 63, 91, 153, 155].

Although the basic concepts of the fluidized bed reactor and of cell metabolism are clear, the interplay between the environmental conditions, as pO_2, nutrients (glucose, fatty acids, glutamine, and other amino acids), reactor variables (recirculation rate, microcarrier, expansion of bed) and productivity, and the detailed metabolism is not fully understood.

Gradients within the reactor in axial direction, due to metabolism, as well as within the particles due to diffusion are implicit and not only of scientific but even more of industrial interest. Those gradients may result in changes of metabolism from bottom to top as differences in nutrient situation (oxygen, glucose vs. glutamine) and limiting metabolites (lactate and ammonia). This may result in the preference of different metabolic pathways. This in turn may influence both, the overall productivity of the cell and the biochemical structure of the product (glycosylation). FDA and industry require that proteins from processes are fully bioactive, efficient, safe, and consistently produced for successful validation.

In the present research the chosen product gives possibilities for variations in the degree of complete formation of the protein backbone as well as in the carbohydrate domain. In order to achieve the highest yield of optimal, that is correctly assembled and glycosylated, product, the fermentation conditions (environment) need to be

investigated and optimized based upon variables measured by, for instance, electrophoretic and immunoblotting techniques. The metabolic relationships during steady-states in a chemostat and the effects of step changes in the lead nutrient glucose on the glycosylation pattern are analysed in the present research.

When using a lead substrate, such as glucose, as input to control the dilution rate, the reactor system (CSTR and fluidized bed) is rather a nutristat (stationary with respect to a nutrient). However, the fluidized bed reactor immobilizes and contains the cells and is therefore a reactor in itself. With its dilution rate, D_{FB}, directly proportional to the controlled concentration(s) in the CSTR, the fluidized bed as such represents a continuous culture (chemostat [8, 17, 49, 229]) at steady-state.

7.2. Product Detection

7.2.1. hCG Quantification

The recombinant product, hCG, was assayed using a solid-phase, two-site immuno-enzymetric assay. Specifically, an adaptation of the commercially available Hybritech Tandem-E hCG kit for the immuno-enzymetric detection of αβ-hCG was used. It uses two different antibodies, each directed to a different epitop of the hormone (sandwich). A subsequent enzymatic reaction with one of the antibodies allows photometric detection at 405 nm. The absorbance was directly proportional to the concentration of hCG. The concentrations used in the original kit (Hybritech 4115BE and 4005BE) were not changed, nor were the amounts changed. However the photometric detection was executed in a microplate reader. A possible cross-reaction of the antibody was irrelevant, as only recombinant hCG and none of the other three hormonal glycoproteins were expressed by the cell line used [147]. Samples were diluted prior to execution to have results within the detection range of 25 - 400 $mIU \cdot ml^{-1}$ [100].

The positive reference and the 200 $mIU \cdot ml^{-1}$ calibrator have been standardized to the WHO 3rd International Standard of CG (WHO 3rd IS #75/537, originating from CR-119). In as much as the kit measures only immunologically active hCG molecules, it also measures the 2nd International Standard (2nd IS 61/6) equivalently [208]. According to the

standard 9.2857 IU are equal to 1 μg of pure hCG. The interstitial cell stimulating potency of this preparation was 13,450 $IU \cdot mg^{-1}$.

7.2.2. Concentration

Samples were taken as previously described. A total of 13 ml sample volume were ultrafiltrated in multiple fractions using micro-concentrators from Amicon (Centriprep/Centriplus-10; Microcon-10) with a cut-off of 10 kDa. Samples were centrifuged at +4°C for 50 minutes at 3100 g (Centriprep-10, Centriplus-10) and 30 minutes at 8000 g (Microcon-10) respectively.

The filtration membranes were blocked using bovine γ-globulin followed by three PBS washes to prevent excessive loss of protein prior to loading with samples. After saturation the membranes were stored at 4°C filled with WFI-water to prevent rupture until further use. Although the units are reusable, they were discarded to avoid sample carry-over and increase consistency.

7.2.3. Isoelectric Focusing

Isoelectric focusing (IEF) was performed using methods common to the art [234]. Specifically, the concentrated samples were applied to commercially available Ampholine PAG-plates with a pH of 4.0 to 6.5 (Pharmacia) on a Multiphor-II (Pharmacia) connected to a MultiDrive XL (Pharmacia) and water-cooling (+4°C). pI calibration was performed against IEF marker (Pharmacia) with a low pI from 2.5 to 6.5. Buffers for anode, 0.1 M glutamic acid in 0.5 M H_3PO_4, and cathode, 0.5 M NaOH, were prepared fresh. After pre-focusing for 20 minutes at 500 V 20 or 40 μl sample were applied at one third of the total running distance. Subsequent focusing was done with a gradual power increase from 500 V to 1500 V over a time of 130 minutes.

7.2.4. Reference Proteins

Reference preparations of hCG (CR-125, CR-127), the α-subchain CG (CR-119), the β-subchain (CR-121) and a hybrid CG (AB1ER-CR-1XY), a combination of Canfield's α-hCG-CR-123 and β-hCG-CR-123, were obtained through the National

Hormone and Pituitary Program from the NIDDK, the NICHHD and the USDA. The potency was determined by radioreceptor and rat uterotropic assays by the NIH.

7.2.5. Staining

Several protocols for Coomassie, Alcian-Blue and silver staining were, though unsuccessful, established based on common procedures [200, 234].

7.2.6. WESTERN Blot

Based on several protocols from collaborating groups [151, 201], a suitable method was established. The proteins were semi-dry blotted for 20 minutes at 10 V immediately after IEF on Bio-Bind nitro-cellulose 0.2 µm membranes (Whatman) using a Nova-Blot unit (Pharmacia) and a transfer buffer (3.03 g TRIS, 14.4 g glycine, 200 ml methanol in 1000 ml WFI).

7.2.7. Membrane Staining

After blotting, the membranes were transiently stained with 0.1 % Fast Green FCF (Fluka) in 1 % acetic acid in order to detect and note the pI of the marker proteins for future reference and calibration. Destaining was possible under running tap water.

7.2.8. Immuno Detection

For the primary detection of the blotted isoforms, an antiserum containing polyclonal antibodies against both hCG subchains (Sigma C-8534) developed in rabbits was used. A possible cross-reference was irrelevant as only recombinant hCG and none of the other three hormonal glycoproteins were expressed by the cell line used. The secondary antibody was a biotinylated goat-anti-rabbit-antibody used in an amplified alkaline phosphatase system (Bio-Rad 170-6412). Positive, and negative controls were 2 µg hybrid-hCG and media samples, respectively. The membranes were blocked after blotting using 5 % dry powdered milk in TTBS prior to incubation. Immunoreaction followed with the primary and secondary antibody, each for one hour. The amplification with a streptavidin-alkaline phosphatase conjugate was carried out according to instructions supplied by the manufacturer [200]. The blots were scanned at

256 grayscales using a Hewlett-Packard ScanJet IIcx and stored as compressed TIFF file for compatibility in open platform systems.

7.3. Results

7.3.1. Cultivation

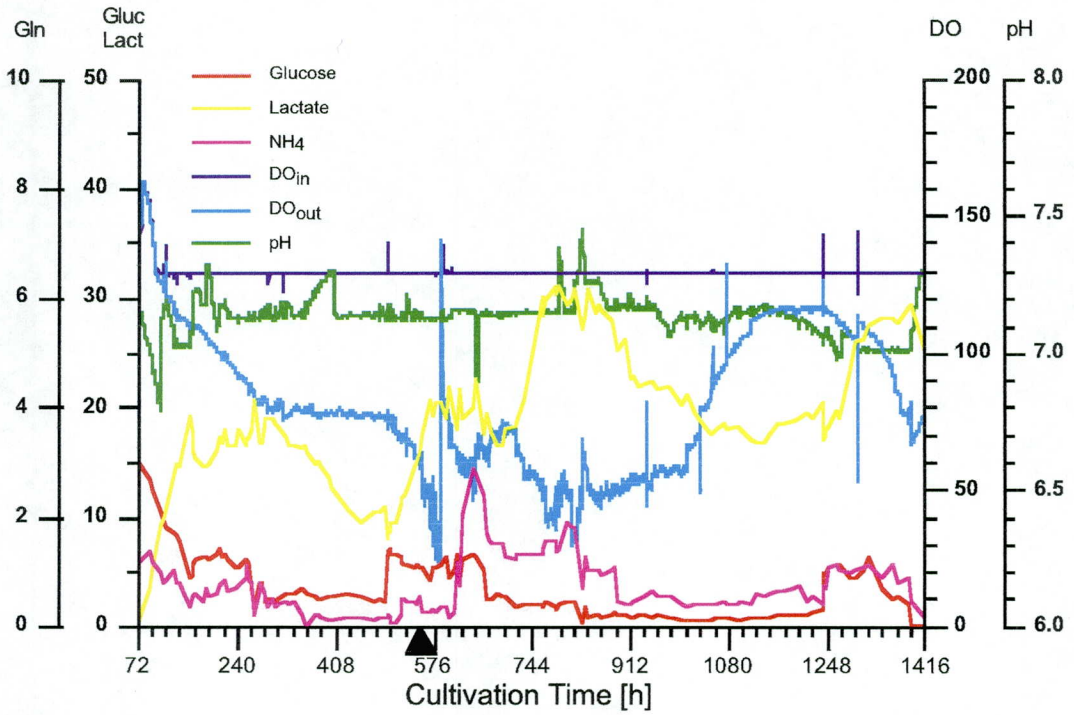

Figure 7-1. *Residual concentrations profile; 1500 h cultivation of CHO-αβhCG cells ▲ CHO-S-SFM-II, concentrations in the CSTR are in mM for Gluc, Gln and Lact, and in µM for DO.*

The reactor was inoculated with 40 ml preseeded carriers of the size fraction 300-500 µm, following the outlined inoculation procedure. It was intended to run a continuous cultivation at limited and unlimited growth conditions in several steady-states. The aim was to investigate the influence of reactor variables (nutrients, *D*) on metabolism and productivity, as well as to elucidate if and how growth, metabolism and production are influenced by a proprietary medium (V) opposed to the standard medium (III).

The cultivation (Figure 7-1) was initially run as batch culture until the glucose concentration dropped at 100 hours below 10 mM from initially 15 mM, indicating

metabolic activity. Temperature, pH, and DO control loops were adjusted (DO_{in} 130 µM, pH_{in} 7.2 + 0.2, T_{in} 37.5°C) to be met throughout the cultivation.

	Time h	D 1/d	Cells c/ml	Glucose mM	qGluc µmol/ml*h	Lactate mM	qLact µmol/ml*h	Y(Lac/Gluc) mol/mol
1	165-257	1.28	3.9 E+5	6.29	-25.40	16.44	49.47	1.95
2	284-334	0.48	4.0 E+5	2.71	-16.49	18.24	23.89	1.45
3	382-482	0.20	5.4 E+5	2.78	-6.01	11.92	2.40	0.40
4	577-663	1.76	3.4 E+5	5.77	-85.12	20.10	107.67	1.26
5	691-814	0.91	6.0 E+5	2.17	-56.18	26.08	78.27	1.39
6	858-950	0.32	9.2 E+5	1.10	-21.67	25.28	17.85	0.82
7	1030-1174	0.13	2.6 E+5	0.91	-8.36	17.98	6.38	0.76
8	1264-1341	0.53	5.5 E+5	5.17	-27.86	24.42	50.92	1.83

Figure 7-2. *Steady-state phases of continuous rhCG cultivation; glucose, lactate*

The dilution rate was tuned to hold the first steady-state (*D* 1.28 d^{-1}, c_{Gluc} 6.3 ± 0.5 mM; phase **1**). The growth rate which is in a chemostat represented by the dilution rate at steady-state matched the growth rate found in the exponential phase of the same cell line when grown in T-flasks. Metabolic activity was observed as lactate, ammonium and hCG concentrations increased and glutamine and glucose were consumed. The continuing increase in the oxygen gradient indicates increase in cell number. Growth of the cells led to expansion of the bed which in turn necessitated the reduction of the recirculation flow (superficial velocity). This state was designed to represent an unlimited state with respect to nutrients [90, 94, 197]. the lactate from glucose yield was with 97 % close to the theoretical maximum of 2.0. Ammonia yield from glutamine was about 1.7 which is 85 % of the maximum. The hCG titer reached 1500 $mIU \cdot ml^{-1}$ at a hCG yield of 177 mIU per mol glucose.

At 257 hours the next steady-state (**2**, **3**; c_{Gluc} 2.8 ± 0.3 mM) was tuned in and maintained from 286 to 495 hours. This state was designed to represent a limitation in glucose for a prolonged period of time, ultimately exhausting the internal reservoirs of the cell and therefore potentially affecting the protein and glycosylation capabilities of the cells. The oxygen gradient stabilized with an volumetric OUR of 6.3 $\mu M \cdot ml^{-1} \cdot h^{-1}$ throughout the whole steady-state. The cell number did not increase, and the expansion stayed constant. An increase in suspended cells was observed. Although the glucose

concentrations stayed constant over the whole period, a transient metabolic response was observed in the beginning such that an initial phase, **2**, and a late phase, **3**, were observed with distinct metabolic states.

The initial phase **2** with a steady state from 284 to 334 hours, at a lower dilution rate of 0.48 d^{-1}, correlated decreased metabolic activity with decreased glucose consumption. Specifically only 73 % of the maximal possible glucose was converted to lactate, indicating that more glucose entered the TCA cycle. Ammonia from glutamine yield increased to nearly the theoretical maximum. Volumetric hCG productivity dropped by 10 % at a titer of 2200 $mIU \cdot ml^{-1}$. However, yield from glucose increased when compared to the unlimited state (phase 1).

After 380 hours, the dilution rate stabilized at 0.20 d^{-1} (phase **3**). Metabolic activity stalled with only 20 % converted to lactate, and most of the pyruvate from the glycolysis, 80 % of the glucose, entering the TCA cycle. Residual glutamine concentration dropped below 0.20 mM at nearly complete conversion yield of ammonia from glutamine. Volumetric hCG productivity likewise ceased, resulting in a decreased yield from glucose (70 mIU per mM glucose). Factors indicating a glutamine deprivation. Ammonia can be ruled out as inhibiting, with a residual concentration of 3.56 mM, well below a detrimental level which would be expected at 5 mM. The recirculating cell density had increased by 35 % thus indicating a *stressed state*.

	Time h	D 1/d	Glutamine mM	qGln µmol/ml*h	Ammonia mM	qAmm µmol/ml*h	Y(NH4/Gln) mol/mol
1	165-257	1.28	0.73	-4.76	2.48	8.12	1.71
2	284-334	0.48	0.48	-3.43	3.54	6.80	1.98
3	382-482	0.20	0.17	-1.17	3.56	2.32	1.99
4	577-663	1.76	1.25	-23.31	2.50	12.66	0.54
5	691-814	0.91	1.51	-13.31	2.47	7.50	0.56
6	858-950	0.32	0.70	-5.98	2.83	2.73	0.46
7	1030-1174	0.13	0.50	-2.04	2.77	1.07	0.52
8	1264-1341	0.53	1.06	-8.62	2.77	4.43	0.51

Figure 7-3. *Steady-state phases of continuous rhCG cultivation; glutamine and NH_4*

At the end of this phase, the residual glucose concentration was raised above 6 mM with a dilution rate of 0.9 d^{-1}. This led to increase in residual lactate

concentration. It is not clear if the cells used the available glucose to build up energy storage within the cell, as no ATP or NTP measurements were available. Yet, the following 48 hours marked a recovery of the metabolism with renewed increase in the oxygen gradient and cell growth. Stratification of the bed developed in two distinct zones the lower apparently only with cells in the cavities and the upper layer with cells bulging-out around the carrier.

Two changes to the system were made. Firstly, the medium was changed at 550 hours to Medium V (CHO S-SFM-II) apparently inducing growth also around the carrier, and ultimately necessitating a lower superficial velocity eventually leading to stagnating zones. Secondly, to increase the relative expansion and allow higher superficial velocities, 10 ml carrier from the lower section - the bottom of the bed - were removed under sterile conditions. It was assumed that, as those carriers did not show the bulging-out phenomenon [60] they were less populated and assumed to be less productive. Therefore, it was attempted to increase the overall performance of the reactor and eliminate the stratification by removing the bottom layer. Both aims were achieved as the average volumetric oxygen uptake rate increased by 18 %, and only carriers with varying degree of outer cell layers were left in the system.

Steady-state conditions for phase **4** were determined at an average dilution rate of 1.76 d^{-1} with a resulting average glucose concentration of 5.77 mM. Judging from the lactate from glucose yield (63 %), only 37 % of the glucose entered the TCA. The ammonia yield from glutamine dropped to only one mol ammonia per two mol glutamine, which is metabolically not readily explainable. This suggests a different metabolic path for glutamine. Washout of Medium III and replacement with Medium V enhanced specific hCG productivity to 11,500 $\mu IU \cdot ml^{-1} \cdot h^{-1}$. Further, the medium change increased the volumetric oxygen uptake rate, suggesting increased growth. The lower protein content increased the broth (effluent) purity by an order of magnitude from 0.07 to 0.91 mg hCG per mg protein.

Reduction of the residual glucose level to 2.17 mM by means of a briefly interrupted feed flow (phase **5**) during the following steady-state from 691 to 814 hours resulted in a dilution rate of 0.91, twice as high as with the previous medium at similar residual concentration. The specific lactate production rose, so that only 30 % of the glucose entered the TCA with the rest forming lactate. Ammonia from glutamine yield stayed at 0.56, suggesting a correlation with the different medium composition. The resulting residual glutamine concentration was at a higher level at 1.25 mM, however, the feed glutamine to glucose ratio also increased. The volumetric oxygen uptake rate increased slightly suggesting only minor growth. Stratification increased such that at 760 hours a similar distribution prevailed of bulged-out carriers and carriers with cells only on the inner cavities of the macroporous carrier. Both, specific hCG productivity and yield from glucose increased to 13,000 $\mu IU \cdot ml^{-1}$ and 230 $IU \cdot mol^{-1}$, respectively.

Phase **6** at 1.1 $mmol \cdot l^{-1}$ residual glucose prevailed from 858 to 950 hours with a resulting dilution rate of 0.32 d^{-1}. Glucose consumption dropped, but less than lactate production, resulting in 60 % glucose entering the TCA cycle, leaving only 40 % incompletely oxidized to lactate. Ammonia from glutamine yield remained constant at 0.46, however at lower rates. Product titer and yield increased, yet not specific production rate, suggesting a transient state. Increasing volumetric oxygen uptake rate suggests further cell growth, at low level however.

Reduction of the residual glucose concentration after a prolonged period from 1030 to 1174 hours (phase **7**) to 0.91 mM resulted in a dilution rate of 0.13 d^{-1} and a depletion of a nutrient, however not necessarily glucose or glutamine. 62 % of the glucose was converted to lactate, as calculated from the lower specific lactate production rate, resulting in a lactate from glucose yield of 0.76. The residual glutamine level dropped to 0.5 mM, the ammonia from glutamine yield stayed constant at 0.52. Volumetric hCG production declined, however yield from glucose and titer increased. Considering an increased suspended cell number, this suggests a loss of immobilized cells, which may however mean excretion of stored protein due to nutrient depletion

which may have caused a stress-situation. Loss of cells was also documented by a decreased oxygen uptake rate of 4.6 $\mu mol \cdot ml^{-1} \cdot h^{-1}$. Further, the bed expansion decreased allowing for higher recirculation and superficial velocity. This decrease does however not account for all the reduction of metabolic activity, as the respective OUR-normalized values also decreased.

The final phase **8** involved a step change with respect to the residual concentration of the lead substrate glucose to above 5 mM with a resulting dilution rate of 0.53 d^{-1}. The lactate from glucose yield returned to a high 1.8 and a contribution of only 8.5 % to the TCA cycle from glucose, the larger part therefore covered from glutamine at a residual concentration of 1.06 mM. The ammonia from glutamine yield remained at 0.51. Productivity remained constant, although hCG from glucose yield declined. Metabolic activity increased transiently, whereas volumetric oxygen uptake rate, indicative for increased cell density, increased much more slowly. Cell growth started to revive. Purity level of the broth reached 1.63 mg hCG per gram protein.

At 588 hours, 10 ml carriers from the bottom section of the bed were removed, and at the end of the cultivation at 1416 hours carrier samples from top and bottom section were taken to determine the cell density. The differences in both cases between top and bottom section was found to be one order of magnitude, underlining the stratification phenomenon under unlimited conditions. However, it remains to be noted that the method, as acknowledged previously, can have a significant error of up to one order of magnitude associated with it. This is common to all cell density measurements for immobilized cells [131, 202]. However, it becomes clear that there is a difference between top and bottom layer with respect to volumetric cell density and specific carrier density - stratification.

Time h	Top cells/ml	Bottom cells/ml
588.1	3.7 E+7	4.1 E+6
1415.7	1.1 E+7	1.0 E+6

Figure 7-4. *Cell density in different sections of the bed; determined with the citrate method* [131]

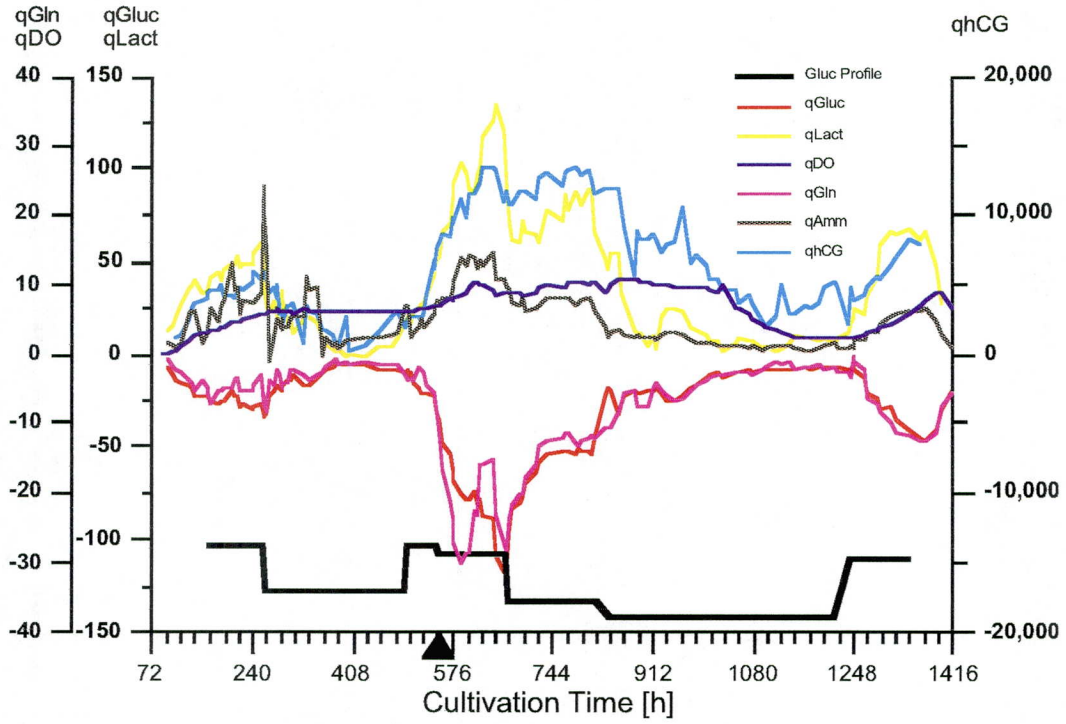

Figure 7-5. *Metabolic rates; 1500 h cultivation 9407 of CHO-αβhCG; ▲ CHO-S-SFM-II, all metabolic rates q are in μmol·ml^{-1}·h^{-1}, and μIU·ml^{-1}·h^{-1} for hCG.*

7.3.2. Metabolic Conversion

Glucose and glutamine are major nutrients for cellular growth. Most of the *glucose* is converted via glycolysis to lactate, and only a limited amount enters the TCA cycle via pyruvate. Glucose further provides the penta-saccharides for nucleotide synthesis via the pentose phosphate pathway, and it is the carbon source for many amino-acids. The metabolic fate of *glutamine*, which is used as major energy source for cells in culture is considerably more complex than that of glucose. Glutamine is initially converted to glutamate. The δ-amino group is either donated for nucleotide or for another biosynthesis or released as ammonia. The second amino group is then removed by transamination or released as ammonia, with the remaining carbon skeleton entering the TCA cycle as α-ketoglutarate. One half of the glutamine is oxidized to CO_2, with the remainder going to lactate or cell mass via TCA cycle intermediates or direct synthesis [148, 181, 236].

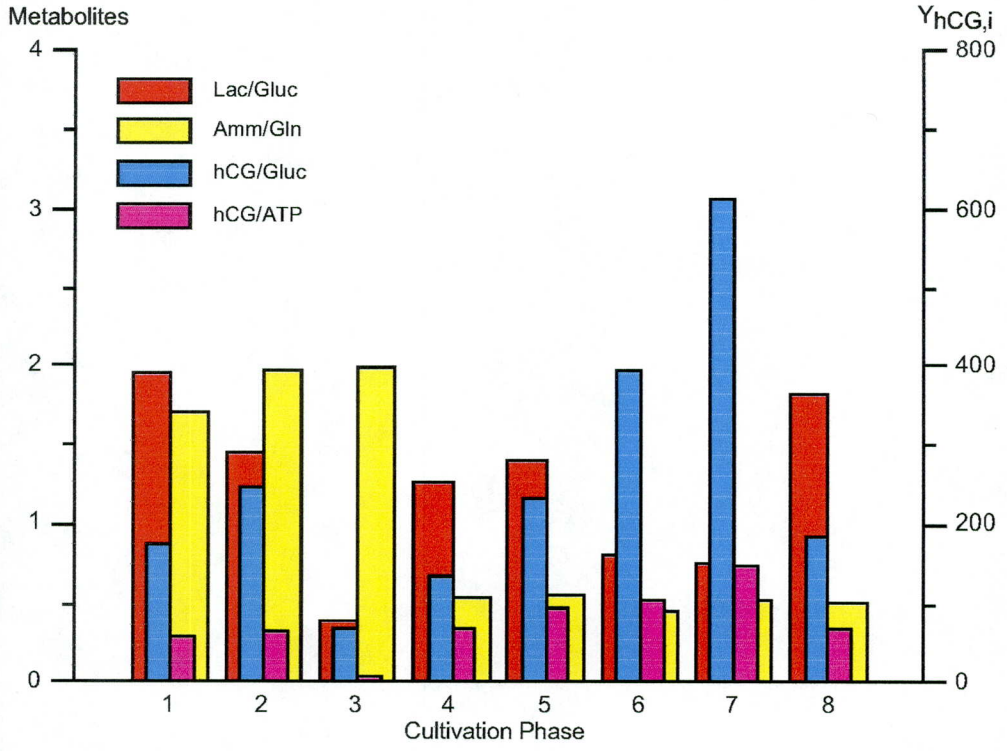

Figure 7-6. *Metabolic conversion yields at steady states; productivity averaged at eight steady-states, yields are dimensionless and only for hCG in IU·mol^{-1}. Ammonium from glutamine indicates a metabolic pathway shift after medium change (**4-8**). hCG yield increases after the medium change.*

The lactate from glucose yield (Figure 7-6) was not constant, indicating changing metabolic pathways. Specifically, during growth phases $Y_{Lact/Gluc}$ was about 1.8 or 90 % of the theoretical possible value, during maintenance 1.3, at limiting conditions 0.8 and at harmful conditions (**3**) below 0.4. Whereas the ammonia from glutamine yield apparently depended rather on other medium components than the metabolic path. Glucose entrance from glycolysis via pyruvate to TCA and high-energy metabolism depends on the nutrient situation. At high glucose steady-states (above 5 mM) there was no accumulation of storage and waste to lactate. In low glucose steady-states (below 3 mM) there was complete oxidation via TCA and oxidative phosphorylation to CO_2, and possibly re-entrance of lactate due to cellular energy demand. Transient changes were observed when looking at time profiles.

The OUR-normalized metabolic rates (OUR-yield) (Figure 7-7) represent cell-specific metabolic rates, based on the assumption that the OUR is constant and not

influenced by the applied changes to the system [154]. This normalization shows that phases **2** and **3**, as well as **6** and **7**, are metabolically different states with reduced metabolic activity in glucose, lactate, glutamine and ammonia. hCG production was lower when using Medium III but not when using Medium V. In fact, hCG productivity remained fairly constant with the latter medium and was not correlated to metabolic activity, the dilution rate or residual concentrations, suggesting growth-independent hCG production.

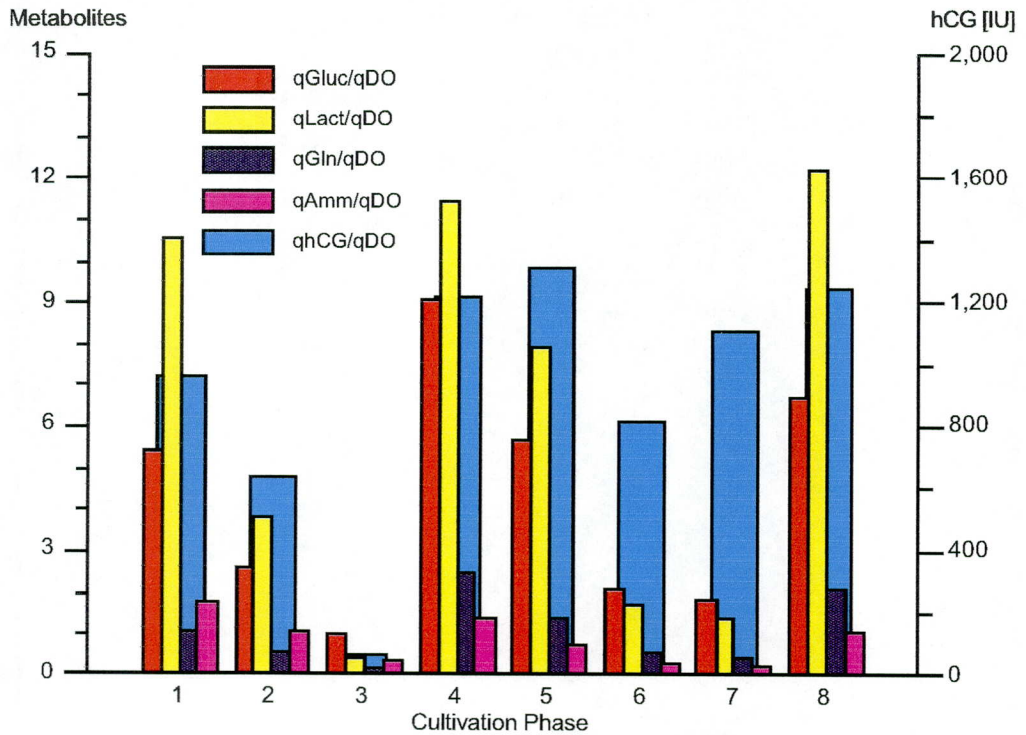

Figure 7-7. *Specific cellular yields during steady states; Glucose, lactate, glutamine, ammonium, and hCG normalized (dimensionless) against oxygen uptake rate. Cell specific productivity increases when medium is changed (**4-8**), however glucose and lactate yields show similar behaviour in both cases.*

Again, the metabolic activity for all considered variables depended on availability of substrate, with growth only occurring when excess substrate was available (phases **1**, **4**, **5**, **8**). There was more efficient use of substrate, e.g. less lactate production during substrate limited periods. It should be noted that phase **5**, with only the medium changed, represented a metabolically more active state as compared to phase **2**, with both phases featuring similar residual glucose concentration.

The glutamine limitation of glucose consumption from phase **3** caused q_{Gluc} and q_{Gln} to rise transiently after the step change (from phase **3** to phase **4**) in dilution rate and in residual glutamine. This is not unprecedented, and is attributed to a substrate-limited enzyme [155].

Using Medium V results in the production of one mol ammonium per two mol glutamine, suggesting a pathway for degradation such as a biosynthetic coupling for pyrimidine and purine base synthesis, instead of simple deamination. The removal of the α-ammonia from the glutamate can also be accomplished by less active transaminases to the glycolytic intermediate 3-phosphoglycerate to form serine and later glycine [171]. The reason for this change is most likely to be found in one of the growth factors or undefined components in Medium V.

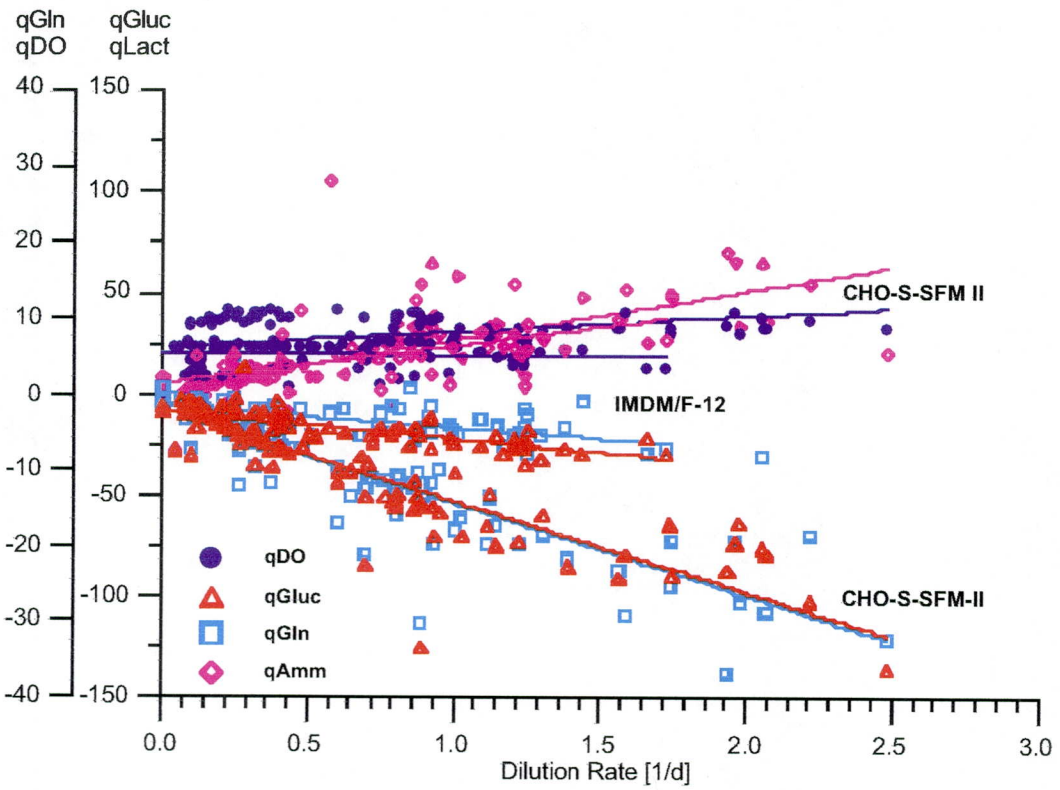

Figure 7-8. *Effect of dilution rate on metabolites; short lines indicate Medium III (IMDM/F-12), long lines Medium V (CHO-S-SFM II), metabolic rates are volumetric and in $\mu mol \cdot ml^{-1} \cdot h^{-1}$. Glucose and glutamine consumption show similar dependence on dilution rate but higher metabolic activity when changing to Medium V evidenced by larger slopes. Oxygen uptake rate is independent from dilution rate and nutrients (constant). Ammonium production rate increased with dilution rate.*

The oxygen uptake rate shows a near linear increase with dilution rate (Figure 7-8), yet with the smallest slope. Volumetric glutamine and glucose uptake rate both increase with dilution rate, however with different slopes depending on the medium, whereas ammonium production rate shows *equal* dependency on the dilution rate for two *different* media, requiring a switch in pathway and a decoupling of ammonia and glutamine metabolism.

7.3.3. Energy Metabolism

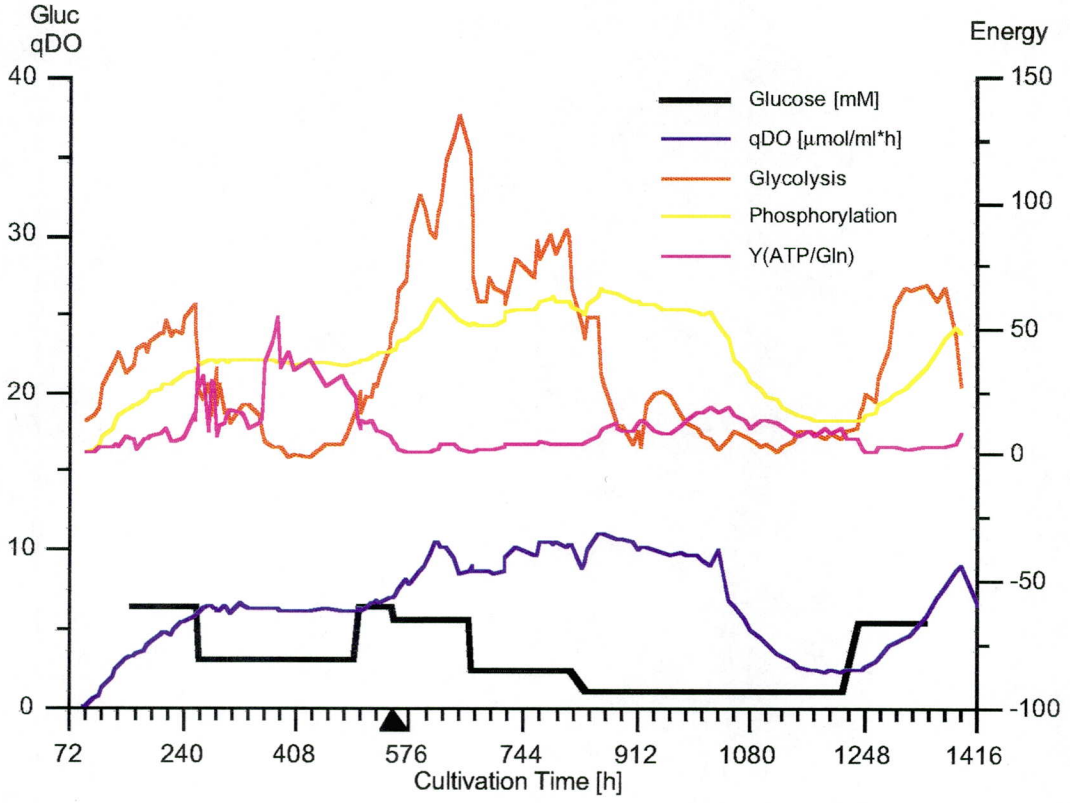

Figure 7-9. *Calculated transient energy states; contributions from glycolysis, oxidative phosphorylation, and glutamine (via TCA) to total ATP production at different steady-states (glucose profile, ▲ start of CHO-S-SFM-II perfusion). Glycolysis and oxidative phosphorylation sum up to total calculated ATP and represent the energy state as function of the nutrient situation.*

Cells used glucose and glutamine for energy production (Figure 7-9). Oxidative phosphorylation, a major supplier to ATP production, contributed varying percentages to the total energy production, with a minimum of one third of total ATP generation during growth or unlimited phases (**1**, **4**, **5**, **8**). Similar results have been found also by

previous investigators [153-155, 171]. During limitation (phases **2, 3, 6, 7**) contribution from oxidative phosphorylation increased to 95 %, suggesting a more efficient use of the available resources and a higher flux of pyruvate into the TCA than for lactate yield. ATP production showed dynamic dependency on the nutrients available, in contrast to findings by other investigators [172]. It has also been found that up to 80 % can be contributed by oxidative phosphorylation under unlimited high glutamine steady-state conditions [197]. Further, ATP production and contribution from glycolysis varies with a pH varying from 6.9 to 7.65 [172].

Calculated ATP production (Figure 7-10) increased sharply after a step-change up from a limiting condition (**3** to **4**, **7** to **8**), which was followed by a delay of about 24 to 48 hours before cell density increased. Less intensive glutamine oxidation after the step change suggests that glutamine was used for biosynthesis.

	Time h	qO2 µmol/ml*h	qATP µmol/ml*h	TCA	OxP	Y(NADH/Gln)	Y(hCG/ATP) IU/mol
1	165-257	4.68	77.53	64%	36%	1.97	58.15
2	284-334	6.34	61.93	39%	61%	3.69	65.72
3	382-482	6.19	39.56	6%	94%	10.63	10.63
4	577-663	9.40	164.05	66%	34%	0.81	69.95
5	691-814	9.86	137.45	57%	43%	1.48	94.49
6	858-950	10.44	80.51	22%	78%	3.49	105.94
7	1030-1174	4.63	34.15	19%	81%	4.53	149.98
8	1264-1341	4.16	75.88	67%	33%	0.97	68.21

Figure 7-10. *Glycolysis and oxidative phosphorylation; correlation to productivity*

The NADH from glutamine calculation showed varying contributions, suggesting that in situations where glucose is less abundant (phases **2, 3, 6, 7**) more energy is derived from glutamine, whereas in unlimited situations more energy is derived from glucose. Yet, glutamine was not completely oxidized, as the theoretical attainable value of 7 mol NADH from glutamine was only reached in phase **3** with an overshoot at 10.6, suggesting considerable contribution from other metabolites, such as glucose, amino acids, lipids and maybe re-incorporation of lactate [155]. As cells obtain more energy from glycolysis, they use less glutamine oxidation with a NADH yield from glutamine

between 1 and 4.5. Such regulation in energy metabolism has been reported in the literature [236].

More specifically, in limited conditions the glutamine consumption rate was less than an order of magnitude smaller than the lactate production rate. Thus neglecting the lactate derived from glutamine may not be justified. To account for those intracellular fluxes, however, non-invasive measurements at the respective branch points would be necessary, e.g. using ^{13}C NMR spectroscopy flux analysis. That would permit finding the exact cause-function rationale, to be searched for ideally in a metabolic model.

7.3.4. Productivity

	Time h	Sample	D 1/d	hCG mIU/ml	qhCG µIU/ml*h	Y(hCG/Gluc) IU/mol	Protein g/l	Purity mg/g
1	165-257	11-24	1.28	1480	4508	177.49	3.89	0.04
2	284-334	36-41	0.48	2220	4070	246.87	3.40	0.07
3	382-482	50-54	0.20	2258	421	69.94	3.47	0.07
4	577-663	72-81	1.76	2072	11476	134.82	0.31	0.72
5	691-814	88-97	0.91	3943	12988	231.19	0.27	1.57
6	858-950	107	0.32	5541	8530	393.54	0.49	1.23
7	1030-1174	128-133	0.13	8111	5121	612.74	0.61	1.43
8	1264-1341	148	0.53	4580	5176	185.78	0.30	1.63

Figure 7-11. *Broth properties in steady-states; product titer, productivity, product yield, total protein and broth purity*

hCG production (Figure 7-11) was not directly growth, as determined by the dilution rate at steady-state, correlated, and the cells exhibited transient responses to step changes with respect to specific productivity. The more surprising result was an increase in productivity, following environmental stress during phases **6** and **7**, as opposed to phases **4**, **5**, and **8**. Similar effects have been shown by several researchers in case of stress, caused by low pH, hyperosmolarity or low dilution rate [153, 166, 170]. It seems that such an effect can be caused by decreasing the concentration of a key nutrient, not only for hybridomas [197], but also for other mammalian cells.

During the cultivation of eight weeks, in contrast to long term cultures at 1 % FCS [101], no loss of productivity was found. This can be in part due to the continued

selective pressure of Neomycin on the cell population, since its resistance gene was incorporated as amplifier in the hCG vector.

When applying Medium V, volumetric productivity was inversely proportional to yield at constant cell specific productivity (combining Figure 7-7 and Figure 7-11). This means that for production an optimization needs to be undertaken, with respect to time, unused medium and titer, rather based on an economic evaluation, than on a biochemical.

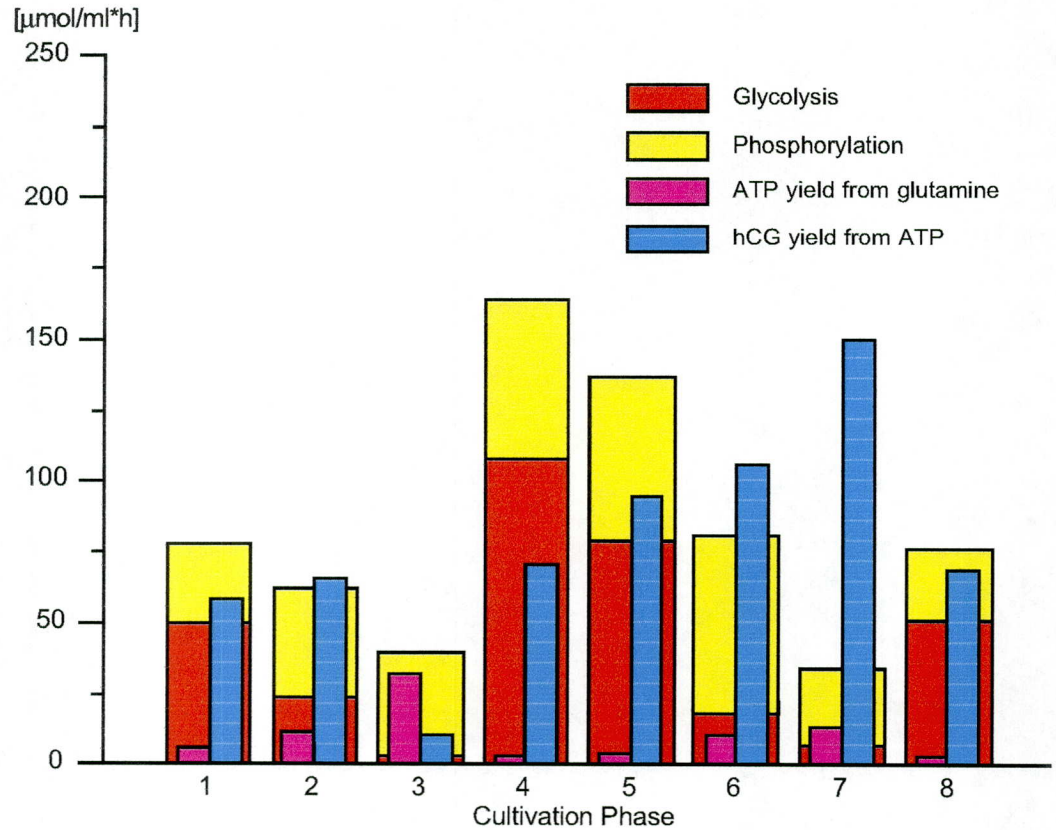

Figure 7-12. *Energy correlated to hCG yield; Comparison of glycolysis, phosphorylation, and TCA. Phase* ***3*** *indicates a low energy-state due to nutrient limitation. An energy limitation with a changed medium* ***(4-8)*** *in phase 7 does however not lead to a reduced product yield.*

As hCG production increased, despite a decrease of glycolytic metabolism and glutamine uptake, hCG production appeared to be not energy limited, except when metabolism was overall severely nutrient-limited (phase **3**). Productivity seemed to be uncoupled from the energy-state. Newsholme et al. [163] suggested that high rates of glycolysis and glutaminolysis in proliferating cells are not caused by a need for energy,

but rather permit high proliferation when required. Therefore, an increase in production, despite decrease in glutamine uptake, is not unreasonable [195].

7.3.5. Isoform Detection

The selected staining methods, including Coomassie, Silver, and Alcian-Blue, were only able to stain the hybrid hCG not native, subchains or samples on the gels. Staining as detection method therefore was abandoned, and direct WESTERN blotting was carried out. The ultrafiltration step yielded on average a 43 fold concentration from 13 ml to 300 µl as well as desalting, advantageous for electrophoresis.

Based on the cultivation strategy and off-line measurements of hCG concentration and protein content, an initial 26 samples, and in a subsequent analysis another 14 samples, were selected for concentration and immunodetection. For each blot 1 or 2 µg hybrid hCG, 40 µl negative control (fresh medium) and 30 or 40 µl sample were applied. The protocols developed revealed on the blots up to seven bands in the reactor samples, five bands in the positive control and none in the negative control. Measuring the running distances of the sample bands and the marker proteins permitted the assignment of pI values to the different isoforms on the blots based on linear regression.

Hybrid hCG	9407/16	9407/41	9407/54	9407/65	9407/79	9407/133	9407/154
	4.70	4.70	4.65		4.70		4.70
4.52	4.48			4.48	4.56	4.48	
4.39	4.34	4.43	4.43	4.39	4.43		4.43
4.25		4.25	4.30	4.30	4.25	4.25	4.25
4.16		4.16	4.16		4.16	4.12	4.16
4.07		4.07	4.07		4.03	3.99	4.03
					3.94		3.94
							3.90

Figure 7-13. *pI values of hCG isoforms detected by WESTERN blot; selected samples.*

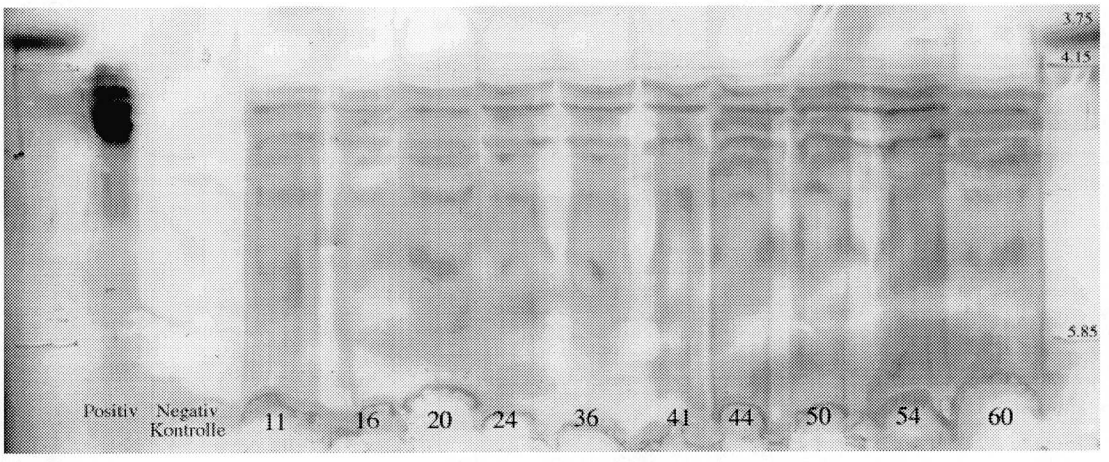

Figure 7-14. *Western Blot, samples 9407/11-60; Positive control contains 1 µg hybrid hCG (AB1ER-CR1XY, NHPP), negative control contains 40 µl CHO S-SFM-II, 40 µl total sample volume.*

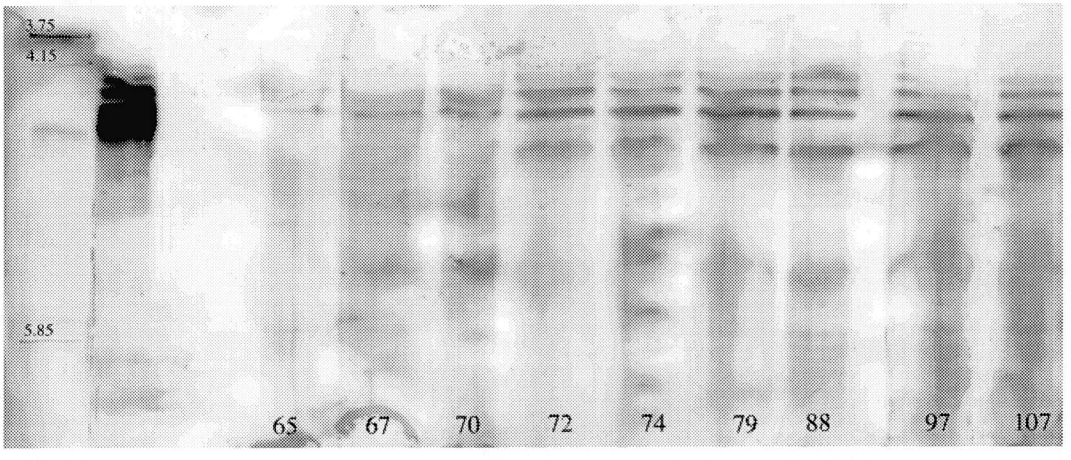

Figure 7-15. *Western Blot, samples 9407/65-107; Positive control contains 2 µg hybrid hCG (AB1ER-CR1XY, NHPP), negative control contains 40 µl CHO S-SFM-II, 40 µl total sample volume.*

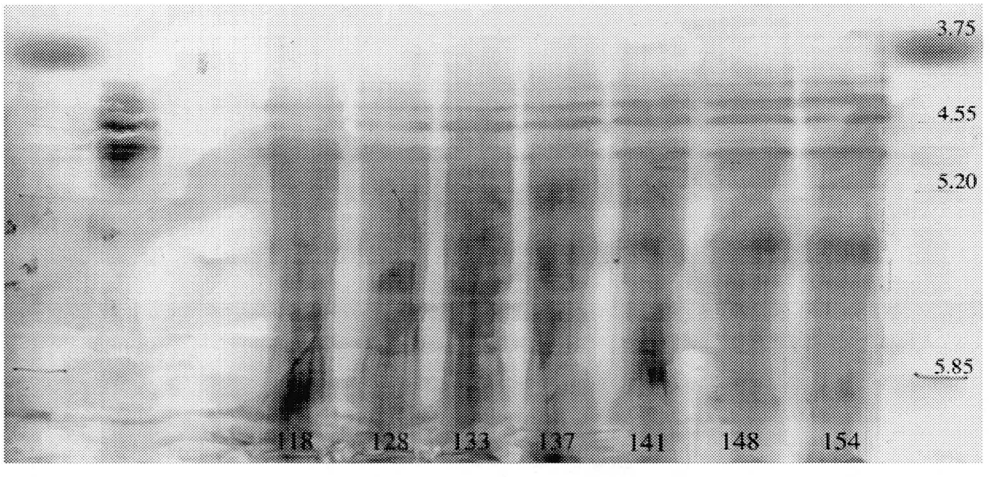

Figure 7-16. *Western Blot, samples 9407/118-154; Positive control contains 1 µg hybrid hCG (AB1ER-CR1XY, NHPP), negative control contains 30 µl CHO S-SFM-II, 30 µl total sample volume.*

7.3.6. Product Quality

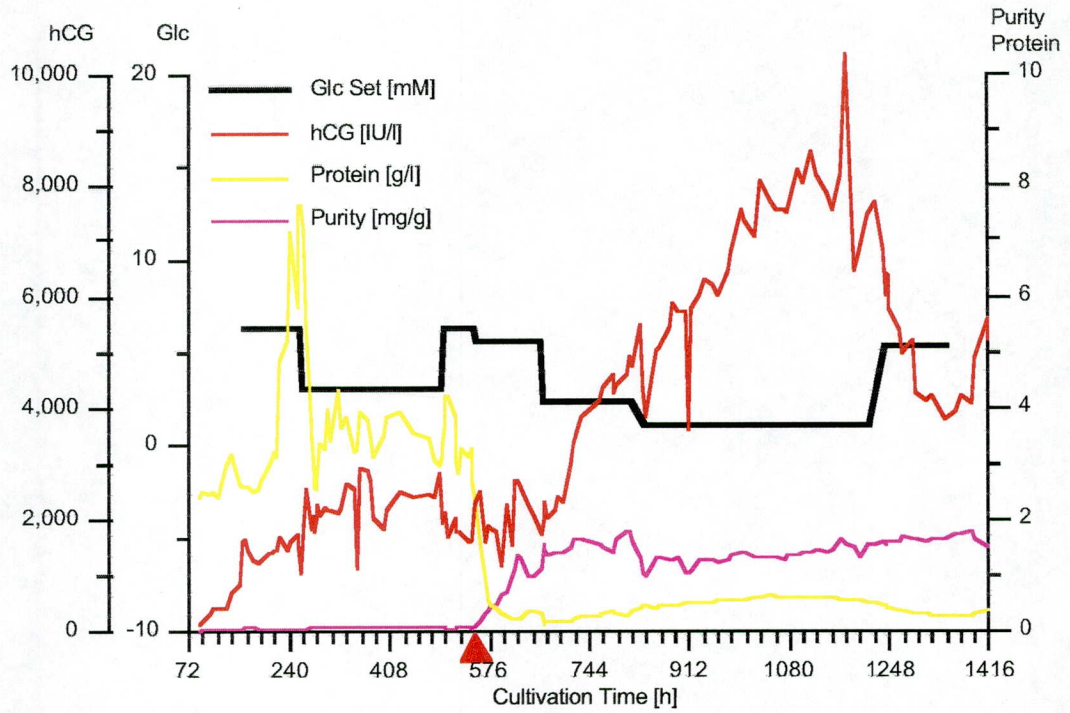

Figure 7-17. *Downstream properties of broth; Change to serum-free and low-protein medium suggesting improved process with higher relative purity and increased titer. (▲ start of CHO-S-SFM-II perfusion)*

The purity of the broth (Figure 7-16), that is the content of hCG per gram protein, increased by two orders of magnitude from 0.05 $mg \cdot g^{-1}$ to 1.6 $mg \cdot g^{-1}$ after changing to low protein medium at 550 hours. This is equally due to the decrease of protein in the feed, from 1 % FCS to a residual concentration of 0.1 µg, to the increase in titer from increased specific production and to the increased residence time allowing higher accumulation. Some of the protein in the effluent was from cell debris, which would necessitate an initial separation step in downstream processing. The variation of dilution rate showed only minor influence on the pattern compared to change in medium.

Using immunodetection (Figure 7-14 to 7-16), it was possible to detect 7 isoforms at a pI from 3.9 to 4.7 plus a broad band appearing at pI 5.5. This compares well with the 6 bands found by collaborating groups in the range from 4.0 to 5.2. Using similar protocols [151] other groups found considerably fewer bands in the same range [220]. Also,

the isoform pattern was similar to the reference materials from natural resources, with the hybrid showing only five bands. Specifically, no band was missing in the recombinantly expressed pattern. The varying dilution rate and associated metabolic states showed no detectable influence on the isoform pattern.

Switching to the low protein medium increased metabolic activity and productivity, but not at the expense of product quality, e.g. isoform pattern (Figure 7-15). The productivity did however increase. The low-protein medium induced expression of 2 isoforms at pI 4.7 and pI 5.5, more towards the alkaline, less sialated region. This may be rather an advantage than a disadvantage when evaluating the feasibility of the process, due to the physiological implications (see below). The relative purity of the medium was enhanced (Figure 7-16), allowing for better downstream processing and detection.

It is possible that the two more basic isoforms are nicked forms of the original hCG due to post-expression digestion [79], but the ammonium level was below the detrimental level of 6 mM [2, 5], and alkalisation and inhibition of glycosyltransferases can therefore be ruled out.

When evaluating the process as a whole, post-expression processing is hard to influence, unless by genetic means, as dilution rates, resulting in hold-up inside the reactor which allows post-expression processing, are inherent to the system. They are shorter in continuous systems as compared to batch systems and can be reduced when eliminating the holding volume of the recirculation vessel during scale up.

7.4. Discussion

7.4.1. Reactor Performance

Using the 300 - 500 μm fraction of the borosilicate SIRAN carrier provided, at least in the upper part of the reactor, a high density system capable of producing the recombinant product over extended periods of time. This fraction seems to be optimal for the chosen reactor geometry and cell line. The reactor performance, based on cell density and productivity, was two orders of magnitude greater than a batch reactor. The

main issue for axial scale-up seems to be the axial oxygen gradient. Further, the amount of medium necessary is proportional to the amount of cells and not the size of the fluidized bed or cell density therein. Therefore the media preparation capacity will further limit the process scale.

Also, it should be noted that, as the system is more sophisticated than a conventional batch run reactor, it requires more attention from the operator. A high degree of automation reduced the intensity of labour associated, but for industrial applications the system needs to be fail-safe in every detail by virtue of improved design, specifically considering the high degree of low-caliber work force in production.

Two aspects require particular attention. Firstly, the containment of the carrier in the defined fluidization area, allowing for bed expansion by a factor of 3, but preferably a factor of 5. In fact, the limited tube length constrained the maximum height, ultimately requiring to reduce the bed volume. The initial inoculated volume should therefore be 30 % of the total reactor volume. This will also insure that carriers will not circulate in sensitive areas, such as pumps. Peristaltic pumps, still preferred in biopharmaceutical production, but even more so pumps with internal moving parts are very sensitive to abrasive solid particles [60]. Single column designs without pumps are preferable [180].

Secondly, the oxygen gradient over the length of the bed has to be handled when scaling up. There are essentially two ways of dealing with it. One possibility is to add oxygen along the axis by either micro-bubbles running co-currently with the upward flow of media, e.g. by using micro-sparger [179] potentially necessitating protective additives in the medium [158], or by running oxygen supply through the bed, e.g. in tubing [88], possibly disturbing the advantages of the fluidized bed, its mixing behaviour and adding design complexity. Alternatively, it is possible to reduce the height so that the maximal oxygen gradient tolerable ultimately leads to a very short fluidized bed of, e.g. 5 cm height. Then the main issue would be the equal distribution of the medium over the radius cross-section. Significant stratification after bulging-out, as previously

described in Chapter 6, was confirmed in this cultivation. It did not adversely affect the metabolism or production in any way.

7.4.2. Media

The expected effect of replacing glutamine with asparagine [235] to prevent ammonia inhibition did not outweigh the apparent glutamine limitation during cultivation in phases **2** and **3**. As the subsequent medium showed massively better performance, the evaluation of this exchange is of minor importance, in fact rather suggesting to increase the glutamine content and thus the glutamine/glucose ratio.

The low protein medium doubled productivity and diversified the isoform pattern by specifically enhancing the biosynthesis metabolism due to one of its components. The growth and metabolism promoting effect of the proprietary media formulation may be due to the bovine glycoprotein contained in it.

A bovine glycoprotein, fetuin, which is often an important supplement to many serum-free media, has been shown to inhibit trypsin activity and promote cellular attachment, growth, and differentiation in many different culture systems. In addition, fetuin associates with various growth factors or growth-promoting substances [52, 93, 224, 237]. However, whether the growth-promoting activity of fetuin preparation is due to fetuin per se or to its minor contaminant(s) has been a long-standing puzzle, and recent research rather attributes the effect to the minor contaminants found in the Pederson-Fetuin fraction usually used [164, 165]. It therefore appears to be a rather complex and less well defined medium additive, maybe containing the sought-after essential growth factor. Which one that is, still remains to be elucidated.

On the other side, the important role of fetuin can also be to function as a donor of blocks to form carbohydrate side-chains glycosylated proteins with the glycosylation pathway not only being dependent on the supply of sugar moieties but also nucleotide and lipid precursors [90]. The specific effect of such precursors to steady-state cultures remains to be tested.

7.4.3. Metabolism

The variations and differences in the here reported quantitative metabolic values from previously reported values should be seen in the light of cell line differences, hybridoma vs. CHO, and other systematic differences. For instance, when calculating the ATP produced by the cells, the phosphorylation ratio (P/O) was assumed to be 3, according to the prevailing opinion in the literature [71, 154, 171, 172]. One investigator however uses, for unknown reasons, a value of 2 [156]. Further, the value for the correction for decomposition of glutamine to pyrrolidone carboxylic acid was found to be 0.0023 h^{-1} in one lab[168, 171] and 0.0048 h^{-1} in another lab [71]. Values for the specific oxygen uptake rate (OUR) differ in the literature for mammalian cell lines by an order of magnitude from 0.05 to 0.5 µmol per 10^6 cells per hour [19, 61, 71, 155, 169, 172]. Such differences, considering propagation of variance, may not necessarily interfere with the consistency and conclusions of single studies within established groups. However, they hinder the comparison and consolidation with conventional wisdom, and the extrapolation outside the scope of those groups.

7.4.4. Isoform Detection

Staining methods were abandoned after it became clear that the reference proteins did not react positively with any of the chosen methods, including Coomassie, Alcian-Blue, and Silver. Such obstacles have been associated with highly-glycosylated proteins [151, 234]. The steric configuration of the carbohydrate side-chains attached to the backbone [118] (Figure 2-6) suggests that the protein may actually be shielded by the sugars against the stain. This shielding will increase with carbohydrate content and number of glycosylated sites. In addition, the surface charge of the glycoprotein is under the acid conditions negative in the uncharged gel and should therefore reject likewise anionic stains such as Coomassie and Fast Green. WESTERN-blotting served as tool yielding improved information content over staining methods. The quality of the blots was apparently better than in competing groups [118], where common issues such as

smearing over the full length of the blot prevailed; yet there is still room for improvement.

Only little is known about the exact steric configuration and the extent of guard of the protein backbone by the carbohydrate moieties. X-ray crystallography, leading to the three-dimensional picture, is commonly done from deglycosylated backbones. As a result, the carbohydrate structures are missing and have to be digitally *attached* during image processing and visualization at the presumed sites. NMR structure analysis can help if the currently available techniques will be further refined.

7.4.5. Product Quality

The possibility of achieving a constant hCG isoform pattern at steady-states has been demonstrated using chemostat cultures. Specifically, in this work, it was demonstrated that the hCG isoform pattern remains constant over an extended period of time, with different cell physiologies and a wide range of physiological conditions, such as glucose limitation, glutamine limitation and varying dilution rates. But the isoform pattern was diversified when changing the medium composition.

Dilution rate influences the metabolic rates more than the glycoform pattern. In a similar study to assess the effect of the dilution rate on CHO cell physiology and recombinant IFN-γ production in glucose-limited chemostat culture, a similar result was found. Despite changes in the IFN-γ production rate and cell physiology, the pattern of IFN-γ glycosylation was similar at all except the lowest growth rates, where there was increased production of unglycosylated IFN-γ [91]. We did not look at the non-glycosylated protein, as its pI of 9 is very distinct and would allow a separation during downstream-processing. Furthermore, the biological activity differs significantly, as outlined in Chapter 2, and it is therefore not the protein of pharmacological interest rather an undesired by-product.

The changes in cell concentration that accompanied changes in the glucose feed concentration indicated that the cells were glucose-limited during some steady-states. There was a decline in residual glucose concentration and a reduced lactate yield from

glucose in those stages of the culture. The specific rate of hCG production was significantly lower at the higher glucose feed concentration. This equals the results from IFN-γ expressing CHO cells under glucose limitation [90]. However under glucose limitation, the proportion of fully glycosylated hCG produced by the cells was not different than before, which contrasts the findings with IFN-γ. Further, the proportion of fully glycosylated hCG did not increase during transient periods of glucose excess, suggesting that the culture environment did not influence the glycosylation as in the mentioned case [40]. Therefore, changing metabolic states and conditions does not necessitate changes in patterns.

In contrast, a transiently transfected CHO cell line expressed hCG with several isoforms towards the acidic region at changing metabolic states without change in the isoform pattern. Only the complete removal of serum, when changing from growth (2.5 % FCS) to production (0 % FCS) medium, shifted the isoform pattern towards the acidic region with at least one band changing the location [60]. This underlines the potential of serum, more specifically of one of its components, for shifting the isoform pattern into more neutral regions, e.g. by virtue of increasing the terminal sialic acid content, i.e. from the blot or gel bands.

The number of isoforms found, did not match the theoretical possible number of glycosylation variants, which is somewhere between 10^8 and 10^{18} possibilities. It would therefore not be very surprising to find multiple glycoforms in one isoform. Differentiation would require sequencing of the sugar side-chains.

To assess the quality of the product with respect to pharmaceutical use, one has to first determine the desired glycoform pattern, or even better, completely determine the structure of protein and carbohydrate structure. For this protein, however, only the basic structure-function relationships are clear (Chapter 2.3). Variations in the isoform pattern occur at the will of nature, apparently to allow subtle metabolic regulation, which is yet not fully understood. Variations in the natural glycoform pattern exist over

the time course of the pregnancy, the sampling place and over the population [97, 220]. Further, specifically the clinical effect and application of a biopharmaceutical preparation can vary distinctly from the pharmacologically defined one. Very recently, it has been found that cAMP release, indicating full and correct biological function, can be achieved by isoforms in the pI range 4 - 6. Isoforms with lower pI, indicating high terminal sialylation in the pI range below 4, were found in pathologic cases and are not desired. Isoforms with high pI were found to stimulate thyrotropic activity, an undesired side effect [97]. Subsequent studies with hCG, asialo-hCG, asialoagalacto-hCG and deglycosylated hCG revealed that removal of sialic acid caused a marked increase in both its affinity for hTSHr and its cAMP-releasing potency, whereas removal of more carbohydrates, although slightly enhancing receptor binding, was detrimental to adenylate cyclase activation [96].

Therefore, it may be desirable to have a mixture of glycoforms, with a high-degree of glycosylation and lower degree of terminal sialylation in a pI range of 4 - 6. Increased affinity to the ASHWELL-receptor is not relevant, as the major clearance path is the kidney and not the liver. The addition of two isoforms, when using the optimized medium, might be beneficial for the intended therapeutic application, as it offers a wider spectrum of diversity for more metabolic fine-tuning and targeting within a pI range.

Overall changes in the isoform pattern due to alkalisation of cellular compartments [5], extracellular sialidases (they might even be desired) [79], removal of serum leading to low pI isoforms [60], or overall variability [4, 41, 42, 73, 87] would not be an adverse issue in this process. Limitation on a high level via constrained feed seems to provide the best control options for restrained growth [69] and most efficient productivity [90].

7.5. Outlook

The feasibility of attaining constant glycoform pattern at various metabolic steady state has been demonstrated clearly. This will facilitate the determination of limiting parameters in the glycosylation pathway by manipulation of the cell environment in

such steady state cultures. Using chemostat cultures, it was shown that the hCG glycosylation pattern remains constant over a wide range of physiological conditions, but is altered when medium composition is changed.

This product can be delivered by the outlined process, using CHO-S-SFM-II medium at a dilution rate of 0.9 d^{-1} with a residual glucose concentration of 2.2 mM, thus contained limitation, at a titer of 4400 $IU \cdot l^{-1}$ (bands 88 and 97) in a consistent way. This should serve as a basis for refinement of the process conditions and a systematic investigation of the role that the bovine glycoprotein plays. Using ion-exchange chromatography and preparative capillary electrophoresis, it will be possible to separate the pI range 4 - 6 from the undesired fractions. Further manipulation of the purification conditions may allow a specific ratio and combination of variants to be selected, depending on the exact therapeutic application required.

For an industrially viable and attractive process, it will be necessary to reclone the cell line with higher amplification numbers aiming at a two orders of magnitude higher expression rate, as the highest titer reached in continuous culture was 10,000 $IU \cdot l^{-1}$, more than one order of magnitude lower than what can be found in blood serum of pregnant women (280,000 $IU \cdot l^{-1}$). A higher titer would be necessary as possible losses of product during subsequent downstream processing will determine the feasibility of the final process, whose product sells rather on the low end of biopharmaceuticals for therapeutic use.

Da steh' ich nun, ich armer Tor,
Und bin so klug als wie zuvor!
Heisse Magister, heisse Doktor gar
Und ziehe schon an die zehen Jahr'
Herauf, herab und quer und krumm
Meine Lehrer an der Nase herum -
Und sehe, dass wir nichts wissen können!

nach J. W. von Goethe, Faust, Der Tragödie erster Teil

Appendix

Data					
Carrier Volume	V[PB]	**30**	ml (cm3)		
Expanded Bed Volume	V[FB]	69	ml (cm3)		
Fluidized Bed Height	H[FB]	9.76	cm		
Settling Zone Volume	V[Sett]	**10**	ml (cm3)		
Expansion	Expansion	**230%**			
Porosity	e	0.57			
Diameter	d	**3.00**	cm		
Cross Section Area	A	7.07	cm2		
Total Liquid Volume	V[Tot]	**2300**	ml		
Recirculation Rate	F[Rec]	**250**	ml/min		
Mean Residence Time FB		0.32	min		
Dilution Rate FB	D[FB]	189.87	1/h		
Surface Velocity	u	0.59	cm/s		
Feed Flow	F[Feed]	**1.46**	ml/min		
		2.10	l/d		
Effluent Flow	F[Prod]	1.46	ml/min		
Vessel Volume	V[CSTR]	**1700**	ml		
Dilution Rate Feed	D[Feed]	0.038	1/h		
		0.914	1/d		
Mean Residence Time	t	26	h		
Dilution Rate Recycle	D[Rec]	8.824	1/h		
Mean Residence Time Recycle		6.80	min		
Stirrer Speed	RPM	**450**	1/min		
Volumetric Mass Transfer	klA	**17**	1/h		
Oxygen Equilibrium Concentration	C[O2,*]	**0.182**	mmol/l		
Inoculation Density	x0	**2.50E+06**	cells/ml Carrier		
Immobilized Cell Density	x[Immob]	**5.00E+07**	cells/ml Expanded Bed		
Suspended Cell Density	X[Susp]	**5.00E+05**	cells/ml Medium		
Percent suspended		25.00%			
Total Cell Number		4.60E+09	cells		
Growth Rate	μ	0.91	1/d		
Doubling Time		1.09	d		
Oxygen Uptake Rate	qO2	**-0.320**	μmol/Mcell*h	qATP	2.37
Glucose Consumption Rate	qGluc	**-0.336**	μmol/Mcell*h	Y(Gluc/Gln)	4.15
Glutamine Uptake Rate	qGln	**-0.081**	μmol/Mcell*h	Y(ATP/Gln)	23.70
Lactate Production Rate	qLact	**0.450**	μmol/Mcell*h	Y(Lact/Gluc)	-1.34
Ammonium Production Rate	qAmm	**0.045**	μmol/Mcell*h	Y(Amm/Gln)	-0.56
hCG Production Rate	qhCG	**70.0**	μIU/Mcell*h	Y(hCG/Gluc)	-208.33

APPENDIX I. Modelling of phase 5 from cultivation 9407; Data

Mass Balance		Oxygen	Glucose	Glutamine	Lactate	Ammonia	hCG
Feed							
Concentration 0	mmol/l	0.18	21.66	6.25	0.00	0.00	0.00
Flow 0	mmol/h	1.13	1.90	0.55	0.00	0.00	0.00
Conditioner							
q[A,CSTR]	µmol/Mcell*h	-0.32	-0.34	-0.08	0.45	0.05	70.00
r[A,CSTR]	mmol/l	-0.16	0.00	0.00	0.00	0.00	0.04
Concentration 1	mmol/l	**0.13**	**2.13**	**1.54**	**26.15**	**2.62**	**4068.15**
Flow 1	mmol/h	1.95	31.99	23.08	392.29	39.23	61022.26
Fluidized Bed							
q[A,FB]	µmol/Mcell*h	-0.32	-0.34	-0.08	0.45	0.05	70.00
r[A,FB]	mmol/l	-15.24	-16.00	-3.86	21.43	2.14	3333.46
Consumption	%	61.67%	3.95%	1.32%	-0.43%	-0.43%	-0.43%
Concentration 2	mmol/l	**0.05**	**2.05**	**1.52**	**26.27**	**2.63**	**4085.71**
Flow 2	mmol/h	0.75	30.73	22.77	393.98	39.40	61285.60
Effluent							
Concentration 3	mmol/l	0.13	2.13	1.54	26.15	2.62	4068.15
Flow 3	mmol/h	0.01	0.19	0.13	2.29	0.23	356.37

APPENDIX II. Modelling of phase 5 from cultivation 9407; Results

Data			
carrier diameter	dp	300	µm
carrier size distribution	dR	1.5	
glass density		2.20	g/ml
carrier density	ρ	1.64	g/ml
carrier porosity	ε	0.4715	
dynamic viscosity	η	0.0096	g/cm s
liquid density		1.02	g/ml
gravity	g	9.81	m/s^2
cell mass density		1.03	g/ml

Iterations			
Re(particle)	Re	6.52	
	cW	5.73	
Superficial velocity	ut	0.0205	m/s
Re(Stokes)	Re	10.1524	
Stokes velocity	u0	0.0319	m/s

APPENDIX III. Parameters determining terminal velocity in a fluidized bed

Component	MG	Ham's F-12		IMDM/F-12	
	g/mol	mg/l	mM	mg/l	mM
CaCl2	110.99	33.22	0.30	99.11	0.89
CuSO4*5aq	249.68	0.0030	0.0000	0.0015	0.0000
Fe(NO3)3*9aq	404.00				
FeSO4*7aq	278.02	0.8340	0.0030	0.4170	0.0015
KNO3	101.11			0.0380	0.0004
KCl	74.56	223.60	2.999	276.80	3.712
MgCl2	203.30	57.22	0.281	28.61	0.141
MgSO4	120.36			48.84	0.406
NaCl	58.44	7599.00	130.031	6049.50	103.516
NaHCO3	84.01	1176.00	13.998	2000.00	23.807
NaH2PO4*aq	137.99			62.50	0.453
Na2HPO4	141.96	142.04	1.001	71.02	0.500
ZnSO4*7aq	287.00	0.8630	0.0030	0.4315	0.0015
Na2SeO3*5aq	263.01			0.0085	0.0000
D-Glucose	180.16	1802.00	10.00	3150.00	17.48
Na-Pyruvate	110.00	110.00	1.00	110.00	1.00
L-Alanine	89.09	8.90	0.100	16.95	0.190
L-Arginine*HCl	210.67	211.00	1.002	147.50	0.700
L-Asparagine*aq	150.10	15.01	0.100	20.01	0.133
L-Aspartatic Acid	133.11	13.30	0.100	21.65	0.163
L-Cysteine*HCl*aq	175.60	35.12	0.200	17.56	0.100
L-Cystine*2HCl	313.20			45.62	0.146
L-Glutamic Acid	147.10	14.70	0.100	44.85	0.305
L-Glutamine	146.15	146.00	0.999	600.00	4.105
Glycine	75.07	7.50	0.100	18.75	0.250
L-Histidine*HCL*aq	209.60	20.96	0.100	31.48	0.150
L-Isoleucine	131.20	3.94	0.030	54.47	0.415
L-Leucine	131.20	13.10	0.100	59.05	0.450
L-Lysine*HCl	146.25	36.50	0.250	91.25	0.624
L-Methionine	149.20	4.48	0.030	17.24	0.116
L-Phenylalanine	165.20	4.96	0.030	35.48	0.215
L-Proline	115.13	34.50	0.300	37.25	0.324
L-Serine	105.09	10.50	0.100	26.25	0.250
L-Threonine	119.10	11.90	0.100	53.45	0.449
L-Tryptophan	204.20	2.04	0.010	9.02	0.044
L-Tyrosine*2Na	225.20	7.81	0.035	56.01	0.249
L-Valine	117.10	11.70	0.100	52.85	0.451
Biotin	244.30	0.01	0.0000	0.01	0.0000
D-Ca Pantothenate	238.30	0.50	0.0021	2.25	0.0094
Choline Chloride	139.60	13.96	0.100	8.98	0.064
Folic Acid	441.40	1.30	0.0029	2.65	0.0060
i-Inositol	180.20	18.00	0.100	12.60	0.070
Nicotinamide	122.10	0.04	0.0003	2.02	0.0165
Pyridoxal HCl	203.60	0.06	0.0003	2.03	0.0100
Riboflavin	376.40	0.04	0.0001	0.22	0.0006
Thiamine HCl	337.30	0.30	0.0009	2.15	0.0064
Vitamin B12	1355.40	1.40	0.0010	0.71	0.0005
Hypoxanthine*Na	136.10	4.77	0.035	2.39	0.018
Linoleic Acid	280.40	0.08	0.0003	0.04	0.0001
DL-68 Thioctic Acid	206.30	0.21	0.0010	0.11	0.0005
Putrescine 2HCl	161.10	0.16	0.0010	0.08	0.0005
Thymidine	242.20	0.73	0.0030	0.37	0.0015
Phenol Red	354.40	1.20	0.0034		
HEPES	238.31			2979.00	12.501
Osmolarity			316.51		312.49
log(a0/a)			0.0228		0.0217
Max DO (1bar) [µM]			946.39		948.89

APPENDIX IV. Media composition

Medium V (CHO-S-SFM II (GIBCO), Pluronic, PSN)

Component [g]	Mediumvolumen [l] 1.00	2.00	5.00	9.00	10.00
CHO-S-SFM II	18.200	36.400	91.000	163.800	182.000
Pluronic F-68, 0.1%	1.000	2.000	5.000	9.000	10.000
NaHCO3	2.450	4.900	12.250	22.050	24.500
PSN 100x [ml]	10.10	20.20	50.51	90.91	101.01

Medium IV (Ham's F-12 / IMDM (GIBCO), Pluronic, PSN, optimized)

Component [g]	Mediumvolumen [l] 1.00	2.00	5.00	9.00	10.00
IMDM	8.831	17.662	44.155	79.479	88.310
Ham's F-12	5.313	10.626	26.565	47.817	53.130
L-Asparagine, ad 2.64 mM	0.330	0.660	1.650	2.970	3.300
Pluronic F-68, 0.1%	1.000	2.000	5.000	9.000	10.000
NaHCO3	2.100	4.200	10.500	18.900	21.000
PSN 100x [ml]	10.20	20.41	51.02	91.84	102.04
FCS ad 1% [ml]	10.20	20.41	51.02	91.84	102.04

Medium IIIa (Ham's F-12 / IMDM (GIBCO), MCWB)

Component [g]	Mediumvolumen [l] 1.00	2.00	4.00	5.00	9.00
IMDM	8.831	17.662	35.324	44.155	79.479
Ham's F-12	5.313	10.626	21.252	26.565	47.817
L-Glutamine, ad 5 mM	0.366	0.732	1.463	1.829	3.292
NaHCO3	2.100	4.200	8.400	10.500	18.900
FCS ad 5% [ml]	50.51	101.01	202.02	252.53	454.55

Medium III (Ham's F-12 / IMDM (JRH Biosciences), Pluronic, PSN, optimized)

Component [g]	Mediumvolumen [l] 1.00	2.00	5.00	9.00	10.00
IMDM / F-12 (JRH), 4.1 mM Gln	14.394	28.788	71.970	129.546	143.940
L-Glutamine, ad 5 mM	0.131	0.262	0.654	1.177	1.308
Pluronic F-68, 0.1%	0.500	1.000	2.500	4.500	5.000
NaHCO3	2.000	4.000	10.000	18.000	20.000
PSN 100x [ml]	10.20	20.41	51.02	91.84	102.04
FCS ad 1% [ml]	10.20	20.41	51.02	91.84	102.04

Medium I Ham's F-12

Component [g]	Mediumvolumen [l] 1.00	2.00	4.00	5.00	10.00
Ham's F-12-Pulver	10.626	21.252	42.504	53.130	106.260
L-Glutamine	0.292	0.584	1.168	1.460	2.920
NaHCO3	1.176	2.352	4.704	5.880	11.760

APPENDIX V. Media recipe

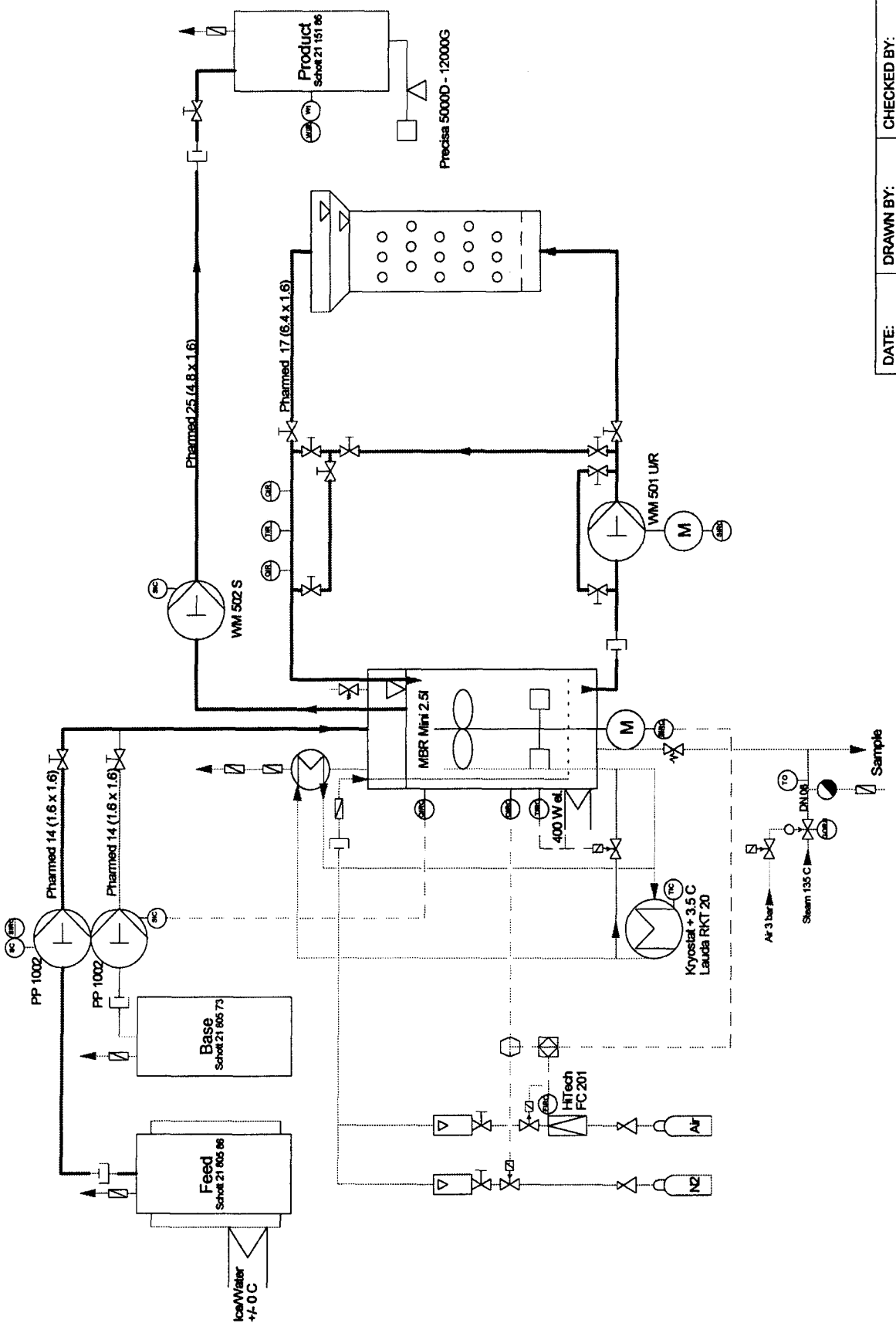
Product
Schott 21 151 86
Precisa 5000D - 12000G
Pharmed 25 (4.8 x 1.6)
Pharmed 17 (6.4 x 1.6)
WM 502 S
WM 501 UR
MBR Mini 2.5l
400 W el.
Pharmed 14 (1.6 x 1.6)
Pharmed 14 (1.6 x 1.6)
PP 1002
PP 1002
Base
Schott 21 805 73
Feed
Schott 21 805 86
Ice/Water
+/- 0 C
Kryostat + 3.5 C
Lauda RKT 20
HiTech
FC 201
Air
N2
Air 3 bar
Steam 135 C
DN 06
Sample
DATE:
05/Sep/1994
DRAWN BY:
M. R. Schuppenhauer
CHECKED BY:
REVISION:
3.0
ETH Zürich - ChemE
PROJECT:
Ares-Serono / PSI
DRAWING NO:
TITLE:
Fluidized Bed System for NMR

Leer - Vide - Empty

References

1. Alam KY, Clark DP, *Anaerobic fermentation balance of Escherichia coli as observed by in vivo NMR spectroscopy*, J Bacteriol **171** 6213-6217, 1989
2. Andersen DC, personal communication *Influence of ammonia on post-translational modification of G-CSF from CHO cells,* 1995
3. Andersen DC, Goochee CF, *Cell culture effects on the O-linked glycosylation of granulocyte colony-stimulating factor produced by CHO cells*, in: *203rd ACS National Meeting*, San Francisco, CA, April 5-10, 1992
4. Andersen DC, Goochee CF, *The effect of cell-culture conditions on the oligosaccharide structures of secreted glycoproteins*, Curr Opin Biotechnol **5** 546-549, 1994
5. Andersen DC, Goochee CF, *The effect of ammonium ion on the O-linked glycosylation of granulocyte colony-stimulating factor produced by Chinese hamster ovary cells*, Biotechnol Bioeng **47** 96-105, 1995
6. Apparailly F, Laurent-Cadoret V, Lecompte F, Chopineau M, Maurel MC, Guillou F and Combarnous Y, *Structure-function relationships and mechanism of action of pituitary and placental gonadotrophins*, Reprod Fertil Dev **6** 157-163, 1994
7. Ashwell G, Harford J, *Carbohydrate-specific receptors of the liver*, Ann Rev Biochem **51** 531-554, 1982
8. Bailey JE, Ollis DF, *Biochemical Engineering Fundamentals*, Chemical Engineering Series, McGraw-Hill, New York, NY, 1986
9. Barber J, *LabVIEW. An implementation of data flow programming in a graphical language*, in: *Advances in Instrumentation*, Research Triangle Park, NC, 1989
10. Barry JA, McGovern KA, Lien YH, Ashmore B and Gillies RJ, *Dimethyl methylphosphonate (DMMP): A ^{31}P nuclear magnetic resonance spectroscopic probe of intracellular volume in mammalian cell cultures*, Biochemistry **32** 4665-4670, 1993
11. Bedows E, Norton SE, Huth JR, Suganuma N, Boime I and Ruddon RW, *Misfolded human chorionic gonadotropin beta subunits are secreted from transfected Chinese hamster ovary cells*, J Biol Chem **269** 10574-10580, 1994
12. Berry IR, Nash RA (Ed.), *Pharmaceutical process validation*, Drugs and the Pharmaceutical Sciences Series 57, Marcel Dekker, New York, NY, 1993
13. Bielinska M, Matzuk MM, Boime I, *Site-specific processing of the N-linked oligosaccharides of the human chorionic gonadotropin alpha subunit*, J Biol Chem **264** 17113-17118, 1989

14. Biselli M, personal communication *Inokulation von Wirbelschichtreaktoren mit CHO Zellen,* 1992

15. Blackie J, Thrift J, Johnson A, Naveh D and Ozturk SS, *Process control strategies for mammalian cell culture fermentation using object oriented graphic based computer languages*, in: *209th ACS National Meeting*, Anaheim, CA, April 2-6, 1995

16. Blackie J, Thrift J, Naveh D and Ozturk SS, *Perfusion rate control based on on-line monitoring of oxygen consumption rates in mammalian cell fermentation*, in: *209th ACS National Meeting*, Anaheim, CA, April 2-6, 1995

17. Blanch HW, Clark DS, *Biochemical Engineering*, University of California, Berkeley, Berkeley, CA, 1988

18. Boime I, Keene J, Galway AB, Fares FM, Lapolt P and Hsueh AJW, *Expression of recombinant human FSH, LH, and CG in mammalian cells - a structure-function model for therapeutic drug design*, Sem Reprod Endocrinol **10** 45-50, 1992

19. Bonarius HPJ, de Gooijer CD, Tramper J and Schmid G, *Determination of the respiration quotient in mammalian cell culture in bicarbonate buffered media*, Biotechnol Bioeng **45** 524-535, 1995

20. Borys MC, Linzer DI, Papoutsakis ET, *Cell aggregation in a Chinese hamster ovary cell microcarrier culture affects the expression rate and N-linked glycosylation of recombinant mouse placental lactogen-1*, Ann N Y Acad Sci **745** 360-371, 1994

21. Bösiger P, *Visualization and quantification of the human blood flow by magnetics resonance imaging,*, J Biomechan **25** 55-67, 1992

22. Bourinbaiar AS, Nagorny R, *Effect of human chorionic gonadotropin (hCG) on reverse transcriptase activity in HIV-1 infected lymphocytes and monocytes*, FEMS Microbiolgy Letters **96** 27-30, 1992

23. Branning R, *Computerized systems validation*, in: Lubiniecki AS and Vargo SA, *Regulatory practice for biopharmaceutical production*, Wiley-Liss, New York, NY, 1994

24. Briasco CA, Karel SF, Robertson CR, *Diffusional limitations of immobilized Escherichia coli in hollow-fiber reactors. influence on ^{31}P NMR spectroscopy*, Biotechnol Bioeng **36** 887-901, 1990

25. Briasco CA, Ross DA, Robertson CR, *A hollow-fiber reactor design for NMR studies of microbial cells*, Biotechnol Bioeng **36** 879-886, 1990

26. Buchli R, Bösiger P, *Comparison of methods for the determination of absolute metabolite concentrations in human muscles by 31P MRS*, Magn Reson Med **30** 552-558, 1993

27. Burrill GS, Lee KB, *Biotech 94 - Long-term value short-term hurdles*, Thought Leadership Series 8, Ernst & Young LLP, San Fransisco, CA, 1993

28. Butler M (Ed.), *Mammalian cell biotechnology*, A Practical Approach Series Oxford University Press, New York, NY, 1991

29. Campbell-Burk SL, Shulman RG, *High-resolution NMR studies of Saccharomyces cerevisiae*, Ann Rev Microbiol **41** 1987

30. Canfield RE, *Studies of human chorionic gonadotrophin*, Rec Prog Horm Res **27** 121-164, 1971

31. Cawrse NW, de Pomerai DI, Lowe KC, *Effects of Pluronic F-68 on 2-deoxyglucose uptake and amino acid incorporation into chick embryonic fibroblasts in vitro*, Biomed Sci **2** 180-182, 1991

32. Cerdan S, Seelig J, *NMR studies of metabolism*, Annual Review of Biophysics and Biophysical Chemsitry **19** 43-67, 1990

33. Chang HN, Furusaki S, *Membrane bioreactors: present and prospects*, Adv Biochem Eng Biotechnol **44** 27-64, 1991

34. Chang HN, Moo-Young M, *Analysis of oxygen transport in immobilized whole cells*, 33-51, in: Moo-Young M, *Bioreactor, immobilized enzymes and cells: Fundamentals and applications*, Elsevier Applied Science, London, 1988

35. Chen R, Bailey JE, *Observations of aerobic, growing Escherichia coli metabolism using an on-line nuclear magnetic resonance spectroscopy system*, Biotechnol Bioeng **42** 215-221, 1993

36. Clark AS, *Computer systems validation: An investigator's view*, Pharm Technol 60-66, 1988

37. Corless CL, Bielinska M, Ramabhadran TV, Daniels-Mcqueen S, Otani T, Reitz BA, Tiemeier DC and Boime I, *Gonadotropin alpha-subunit: Differential processing of free and combined forms in human trophoblast and transfected mouse cells*, J Biol Chem **262** 14197-14203, 1987

38. Croughan MS, *Animal cell culture*, in: *AIChE Annual Meeting*, San Fransisco, CA, November 13-18, 1994

39. Cumming DA, *Physiological relevance of protein glycosylation*, Dev Biol Stand **76** 83-94, 1992

40. Curling E, Hayter P, Jenkins N, *Recombinant human IFN-gamma produced by CHO cells effects of culture environment on product quality*, in: Ladisch MR and Bose A, *Harnessing Biotechnology For The 21st Century; Ninth International Biotechnology Symposium and Exposition*, Crystal City, VA, 1992

41. Curling EM, Hayter PM, Baines AJ, Bull AT, Gull K, Strange PG and Jenkins N, *Recombinant human interferon-gamma. Differences in glycosylation and proteolytic processing lead to heterogeneity in batch culture*, Biochem J **272** 333-337, 1990

42. Curling EMA, Hayter P, Tong J, Jenkins N, Samon I and Bull AT, *Analysis of glycosylation heterogeneity in IFN-alpha produced by CHO cells during batch and continuous culture*, in: Conradt HS, *Protein Glycosylation: Cellular, Biotechnological and Analytical Aspects*, Braunschweig, Germany, June 28-30, 1990

43. Daja MM, Hiyama J, Scott GK and Renwick AGC, *The detection and isolation of protease activity associated with purified preparations of human chorionic gonadotropin*, Endocrinol **132** 1766-1773, 1993

44. Dale BE, Gillies RJ, *Nuclear magnetic resonance spectroscopy of dense cell populations for metabolic studies and bioreactor engineering: A synergistic partnership*, 107-118, in: Ho CS and Wang DIC, *Animal Cell Bioreactors*, Butterworth-Heinemann, Boston, MA, 1991

45. de Graaf AA, *Continuous-flow NMR bioreactor for in vivo studies of microbial cell suspensions with low biomass concentrations*, J Magn Reson **98** 654-659, 1992

46. Doyle A, Griffiths JB, Newell DG, *Cell & tissue culture : Laboratory procedures*, Wiley, Chichester, UK, 1993

47. Drury DD, *Analysis of hollow fiber bioreactor performance for mammalian cells by on-line NMR*, in: *Proceedings of the Annual Biochemical Engineering Symposium*, 1985

48. Dunkel L, Jia XC, Nishimori K, Boime I and Hsueh AJ, *Deglycosylated human chorionic gonadotropin (hCG) antagonizes hCG stimulation of 3',5'-cyclic adenosine monophosphate accumulation through a noncompetitive interaction with recombinant human luteinizing hormone receptors*, Endocrinol **132** 763-769, 1993

49. Dunn IJ, Heinzle E, Ingham J and Prenosil JE, *Biological Reaction Engineering*, VCH, Weinheim, Germany, 1992

50. Dunnick JK, Eustis SL, Haseman JK, *Development of kidney tumors in the male F344/N rat after treatment with dimethylmethylphosphonate*, Fund Appl Toxicol **11** 91-99, 1988

51. Egan WM, *The use of perfusion systems for nuclear magnetic resonance studies of cells*, 135-161, in: Gupta RK, *NMR spectroscopy of cells and organisms*, CRC Press, Boca Raton, FL, 1987

52. Elliott WM, Auersperg N, *Growth of normal human ovarian surface epithelial cells in reduced-serum and serum-free media*, In Vitro Cell Dev Biol **29A** 9-18, 1993

53. Erickson JC, Finch JD, Greene DC, *Direct capture of recombinant proteins from animal cell culture using a fluidized bed*, in: Spier RE, Griffiths JB and Berthold W, *12th ESACT Meeting: Animal Cell Technology: Products of today, prospects of tomorrow*, Würzburg, Germany, 1993

54. FDA, *Guide to inspection of computerized systems in drug processing*, U.S. Department of Health and Human Services, Rockville, MD, 1983

55. FDA, *Computerized drug processing*, 32a, FDA, Rockville, MD, 1987

56. FDA, *Software development activities*, U.S. Department of Health and Human services, 1987

57. Fernandez EJ, *Noninvasive studies of hybridoma metabolism by nuclear magnetic resonance*, Ph.D. Thesis, University of California at Berkeley, 1989

58. Fernandez EJ, Clark DS, *NMR spectroscopy: A non-invasive tool for studying intracellular processes*, Enzyme Microb Technol **9** 259-271, 1987

59. Fernandez EJ, Mancuso A, Clark DS, *NMR spectroscopy studies of hybridoma metabolism in a simple membrane reactor*, Biotechnol Prog **4** 173-183, 1988

60. Ferrero A, *Fluidised bed reactors for the industrial cultivation of CHO cells producing a gonadotropin*, Dr. sc. techn. Thesis, ETH Zürich, 1994

61. Fleischaker RJ, Sinskey AJ, *Oxygen demand and supply in cell culture*, Eur J Appl Microbiol Biotechnol **12** 193-197, 1981

62. Frame KK, Hu WS, *Kinetic study of hybridoma cell growth in continuous culture: I. A model for non-producing cells*, Biotechnol Bioeng **37** 55-64, 1991

63. Frame KK, Hu WS, *Kinetic study of hybridoma cell growth in continuous culture: II. Behavior of producers and comparison to nonproducers*, Biotechnol Bioeng **38** 1020-1028, 1991

64. Furuhashi M, Ando H, Bielinska M, Pixley MR, Shikone T, Hsueh AJ and Boime I, *Mutagenesis of cysteine residues in the human gonadotropin alpha subunit. Roles of individual disulfide bonds in secretion, assembly, and biologic activity*, J Biol Chem **269** 25543-25548, 1994

65. Gailliot FP, Gleason C, Wilson JJ, *Fluidized bed adsorption for whole broth extraction*, Biotechnol Prog **6** 370-375, 1990

66. Gallo RC, personal communication *Statement to the press on Nature article regarding hCG inhibiting Kaposi's sarcoma,* 1995

67. Garlick PB, Townsend RM, *NMR visibility of P_i in perfused rat hearts is affected by changes in substrate and contractility.*, Am J Physiol **263** H497-H502, 1992

68. Gillies RJ, et al., *Design and application of NMR-compatible bioreactor circuits for extended perfusion of high-density mammalian cell cultures*, NMR Biomed **6** 95-104, 1993

69. Glacken MW, *Catabolic control of mammalian cell culture*, Biotechnol **6** 1041-1050, 1988

70. Glacken MW, Adema E, Sinskey AJ, *Mathematical descriptions of hybridoma culture kinetics: I. Initial metabolic rates*, Biotechnol Bioeng **32** 491-506, 1988

71. Glacken MW, Fleischaker RJ, Sinskey AJ, *Reduction of waste product excretion via nutrient control: Possible Strategies for maximizing product and cell yields on serum in cultures of mammalian cells*, Biotechnol Bioeng **28** 1376-1389, 1986

72. Gonzalez-Mendez R, Hahn GM, Wade-Jardetzky NG and Jardetzky O, *Comparison of intracellular pH measurements by phosphorus-31 NMR and weak acid partitioning in Chinese hamster ovary fibroblasts*, Magn Reson Med **6** 373-380, 1988

73. Goochee CF, *Bioprocess factors affecting glycoprotein oligosaccharide structure*, in: *Continuous Cell Lines: An International Workshop on Current Issues*, Bethesda, MD, March 20-22, 1991, 1991

74. Goochee CF, Gramer MJ, Andersen DC, Bahr JB and Rasmussen JR, *The oligosaccharides of glycoproteins: factors affecting their synthesis and their influence on glycoprotein properties*, in: Todd PS, Sikdar K and Bier M, *Frontiers in Bioprocessing II*, Boulder, CO, June 17-21, 1990, 1990

75. Goochee CF, Monica T, *Environmental effects on protein glycosylation*, Biotechnol **8** 421-427, 1990

76. Gorfien S, Bodzjak ML, Jayme D, Weiss S and Brown P, *A new serum-free medium for growth of Chinese hamster ovary CHO cells and production of recombinant dna proteins*, in: *41st Annual Meeting of the Tissue Culture Association*, Houston, TX, June 10-13, 1990

77. Gottesman MM (Ed.), *Molecular cell genetics*, Wiley, New York, NY, 1985

78. Gottesman MM, *Chinese hamster ovary cells*, Meth Enzymol **151** 3-8, 1987

79. Gramer MJ, Goochee CF, *Glycosidase activities in Chinese hamster ovary cell lysate and cell culture supernatant*, Biotechnol Prog **9** 366-373, 1993

80. Gregory ME, Keay PJ, Dean P, Bulmer M and Thornhill NF, *A visual programming environment for bioprocess control*, J Biotechnol **33** 233-241, 1994

81. Gregory ME, Thornhill NF, *Use of a graphical programming environment for the rapid development of custom software for fermentation process control*, 231-234, in: *IFAC Symposia Series*, Pergamon Press, Tarrytown, NY, 1992

82. Griffin PD, *Immunization against hCG*, Hum Reprod **9** 267-272, 1994

83. Griffin PD, Jones WR, Stevens VC, *Anti-fertility vaccines: Current status and implications for family planning programmes*, Reprod Health Matt **3** 1994, 1994

84. Griffiths JB, *Advances in immobilization technology*, 149-166, in: Spier RE and Griffiths JB, *Animal Cell Biotechnology*, Academic Press, London, UK, 1990

85. Gupta RK, Gupta P, *Direct observation of resolved resonances from intra- and extracellular sodium-23 ions in NMR studies of intact cells and tissues using dysprosium(III)tripolyphosphates as paramagnetic shift reagent*, J Magn Reson **47** 344-350, 1982

86. Gupta RK, Gupta P, Yushok WD and Rose ZB, *Measurement of the dissociation constant of MgATP at physiological nucleotide levels by a combination of 31P NMR and optical absorbance spectroscopy*, Biochem Biophys Res Comm **117** 210-216, 1983

87. Hahn TJ, Goochee CF, *Growth-associated glycosylation of transferrin secreted by HepG2 cells*, J Biol Chem **267** 23982-23987, 1992

88. Hambach B, Biselli M, Runstadler PW and Wandrey C, *Development of a reactor-integrated aeration system for cultivation of animal cellls in fluidized beds*, in: Spier RE, Griffiths JB and MacDonald C, *Animal cell technology: Developments, processes & products*, Brighton, UK, 1991

89. Hammer BE, Heath CA, Mirer SD and Belfort G, *Quantitative flow measurements in bioreactors by NMR imaging*, Biotechnol **8** 327-330, 1990

90. Hayter PM, Curling EMA, Baines AJ, Jenkins N, Salmon I, Strange PG, Tong JM and Bull AT, *Glucose-limited chemostat culture of Chinese hamster ovary cells producing recombinant human interferon- gamma*, Biotechnol Bioeng **39** 327-335, 1992

91. Hayter PM, Curling EMA, Gould ML, Baines AJ, Jenkins N, Salmon I, Strange PG and Bull AT, *The effect of the dilution rate on CHO cell physiology and recombinant interferon-gamma production in glucose-limited chemostat culture*, Biotechnol Bioeng **42** 1077-1085, 1993

92. Heath CA, Hammer BE, Mirer SD, Pimbley JM and Belfort G, *Magnetic resonance imaging and modeling of flow in hollow-fiber bioreactors*, AIChE J **36** 547-558, 1990

93. Hedlund TE, Miller GJ, *A serum-free defined medium capable of supporting growth of four established human prostatic carcinoma cell lines*, Prostate **24** 221-228, 1994

94. Hiller GW, Clark DS, Blanch HW, *Cell retention-chemostat studies of hybridoma cells. analysis of hybridoma growth and metabolism in continuous suspension culture on serum-free medium*, Biotechnol Bioeng **42** 185-195, 1993

95. Hirsch D, Schoen FJ, Levy RJ, *Effects of metallic ions and diphosphonates on inhibition of pericardial bioprosthetic tissue calcification and associated alkaline phosphatase activity*, Biomaterials **14** 371-377, 1993

96. Hörmann R, Pörtl S, Liss I, Amir SM and Mann K, *Variation in the thyrotropic activity of human chorionic gonadotropin in Chinese hamster ovary cells arises from differential expression of the human thyrotropin receptor and microheterogeneity of the hormone*, J Clin Endocrinol Metab **80** 1605-1610, 1995

97. Hörmann R, Spöttl G, Grossmann M, Saller B and Mann K, *Molecular heterogeneity of human chorionic gonadotropin in serum and urine from patients with trophoblastic tumors*, Clinical Investigator **71** 953-960, 1993

98. Hudcova V, Machon V, Nienow AW, *Gas-liquid dispersion with dual rushton turbine impellers*, Biotechnol Bioeng **34** 617-628, 1989

99. Humphrey SM, Garlick PB, *NMR-visible ATP and intracellular phosphorus in normoxic and reperfused rat hearts: A quantitative study*, Am J Physiol **260** H6-H12, 1991

100. Hybritech, *Tandem-E HCG ImmunoEnzyMetric Assay for the quantitative & qualitative measurement of human chorionic gonadotropin in serum*, 1994

101. Jia XC, Oikawa M, Bo M, Tanaka T, Ny T, Boime I and Hsueh AJ, *Expression of human luteinizing hormone (LH) receptor: interaction with LH and chorionic gonadotropin from human but not equine, rat, and ovine species*, Mol Endocrinol **5** 759-768, 1991

102. Johnson GW, *LabVIEW Graphical Programming*, McGraw-Hill, Inc., San Francisco, CA, 1994

103. Jordan M, Sucker H, Einsele A, Widmer F and Eppenberger HM, *Interactions between animal cells and gas bubbles: the influence of serum and pluronic F-68 on the physical properties of the bubble surface*, Biotechnol Bioeng **43** 446-454, 1994

104. Kanamori K, Roberts JD, *^{15}N-NMR studies of biological systems*, Accounts of Chemical Research **16** 35-41, 1983

105. Kaplan O, van Zijl PCM, Cohen JS, *NMR studies of metabolism of cells and perfused organs*, NMR Basic Principles and Progress **28** 4-52, 1992

106. Katz LA, Swain JA, Portman MA and Balaban RS, *Intracellular pH and inorganic phosphate content of heart in vivo: A phosphorus-31 NMR study*, Am J Physiol **255** H189-H196, 1988

107. Keene JL, Matzuk MM, Boime I, *Expression of recombinant human choriogonadotropin in Chinese hamster ovary glycosylation mutants*, Mol Endocrinol **3** 2011-2017, 1989

108. Keller J, *Entwicklung und Charakterisierung eines Fliessbettreaktors für tierische Zellkulturen*, Dr. sc. techn. Thesis, ETH Zürich, 1991

109. Kirk K, Kuchel PW, *Characterization of transmembrane chemical shift differences in the ^{31}P NMR spectra of various phosphoryl compounds*, Biochemistry **27** 8795-8802, 1988

110. Kodosky J, MacCrisken J, Rymar G, *Visual programming using structured data flow*, in: *IEEE Workshop on Visual Languages*, Kobe, Japan, October 8-11, 1991, 1991

111. Kodosky J, Truchard J, MacCrisken J, *LabVIEW*, Version 3.1.1 for MacOS, Windows 3.1, SunOS, National Instruments, Inc., Austin, TX, 1995

112. Konrad M, Merz WE, *Regulation of N-glycosylation*, J Biol Chem **269** 8659-8666, 1994

113. Kornfeld R, Kornfeld S, *Assembly of asparagine-linked oligosaccharides*, Ann Rev Biochem **54** 631-664, 1985

114. Kost GJ, *pH standardization for phosphorus-31 magnetic resonance heart spectroscopy at different temperatures*, Magn Reson Med **14** 496-506, 1990

115. Kramer HW, Bailey JE, *Mass transfer characterization of an airlift probe for oxygenating and mixing cell suspensions in an NMR spectrometer*, Biotechnol Bioeng **37** 205-209, 1991

116. Kurano N, Leist C, Messi F, Kurano S and Fiechter A, *Growth behavior of Chinese hamster ovary cells in a compact loop bioreactor: 2. Effects of medium components and waste products*, J Biotechnol **15** 113-128, 1990

117. Lapthorn A, personal communication *Molecular model of hCG*, 1995

118. Lapthorn AJ, Harris DC, Littlejohn A, Lustbader JW, Canfield RE, Machin KJ, Morgan FJ and Isaacs NW, *Crystal structure of human chorionic gonadotropin*, Nature **369** 455-461, 1994

119. Leffingwell DA, *Object-oriented software development and medical devices*, Med Dev Diagn Ind **1994** 80-88, 1994

120. Lehninger AL, Nelson DL, Cox MM, *Principles of Biochemistry*, Worth Publishers, Inc., New York, NY, 1993

121. Lien YHH, Zhou HZ, Job C, Barry JA and Gillies RJ, *In vivo phosphorus-31 NMR study of early cellular responses to hyperosmotic shock in cultured glioma cells*, Biochimie (Paris) **74** 931-939, 1992

122. Lin SH, *A mathematical model for a biological fluidized bed reactor*, J Chem Technol Biotechnol **51** 473-482, 1991

123. Lindl T, Bauer J, *Zell- und Gewebekultur*, Gustav Fischer Verlag, Stuttgart, 1989

124. Link J, *The design of resonator probes with homogeneous radiofrequency fields*, 3-31, in: Rudin M, *In vivo magnetic resonance spectroscopy I: Probeheads and radiofrequncy pulses spectrum analysis*, Springer-Verlag, Heidelberg, Germany, 1992

125. Link J, personal communication *Magnetic susceptibility of microcarrier for cell culture,* 1992

126. Lippman MJ, Dager SR, *Polar migratory susceptibility (PMS): An unexpected side effect of MRI scans*, J Irrep Res **38** 15-21, 1993

127. London, Robert E., *^{13}C Labeling studies of metabolic regulation*, Progress in NMR Spectroscopy **20** 337-383, 1988

128. Looby D, Griffiths JB, *Fixed bed porous glass sphere (porosphere) bioreactors for animal cells*, Cytotechnol **1** 339-346, 1988

129. Lubiniecki AS, et al., *Effects of fermentation on product consistency*, Dev Biol Stand **76** 105-115, 1992

130. Lucas P, Müller A, Pike B, *European Biotech 95: Gathering Momentum*, Thought Leadership Series 2, Ernst & Young, Amsterdam, NL, 1995

131. Lüllau E, *Immobilisierung von Säugetierzellen auf chemisch modifizierten Sinterglasträgern*, Dr. rer. nat. Thesis, Universität Köln, 1992

132. Lüllau E, Dreisbach C, Grogg A, Biselli M and Wandrey C, *Immobilization of animal cells on chemically modified SIRAN carrier*, in: Spier RE, Griffiths JB and MacDonald C, *11th ESACT Meeting: Animal Cell Technology: Developments, Processes & Products*, Brighton, UK, 1991

133. Lunardi-Iskandar, personal communication *Future development of hCG as anti-cancer drug,* 1995

134. Lunardi-Iskandar Y, et al., *Tumorigenesis and metastasis of neoplastic Kaposi's sarcoma cell line in immunodeficient mice blocked by a human pregnancy hormone*, Nature **375** 64-68, 1995

135. Lunardi-Iskandar Y, et al., *A pregnancy hormone human chorionic gonadotropin (hCG) blocks tumorigenesis and metastasis of KS cells (KS Y-1) in immunodeficient mice*, AIDS Res Human Retrovir **10** S76, 1994

136. Lundberg P, Berners-Price SJ, Roy S and Kuchel PW, *NMR studies of erythrocytes immobilized in agarose and alginate gels*, Magn Reson Med **25** 273-288, 1992

137. MacDonald JM, Grillo MP, Tajiri DT, Schmidlin O, Kurhanewizc J, Chang LH and James TL, *A novel NMR-compatible bioreactor for MRI and multinuclear NMR spectroscopy of perfused cells: application to isolated rat hepatocytes*, Biophys J **68** A422, 1995

138. Maiorella B, Howarth B, Shauger A and Inlow D, *Optimized pH control for antibody production*, in: *198th ACS National Meeting*, Miami Beach, FL, September 10-15, 1989

139. Maiorella BL, *In vitro management of ammonia's effect on glycosylation of cell products through pH control*, U.S.P. 5,096,816, 1990

140. Mancuso A, *Nuclear magnetic resonance studies of a murine hybridoma in hollow fiber bioreactor culture*, Ph.D. Thesis, University of California at Berkeley, 1993

141. Mancuso A, Fernandez EJ, Blanch HW and Clark DS, *A nuclear magnetic resonance technique for determining hybridoma cell concentration in hollow fiber bioreactors*, Biotechnol **8** 1282-1285, 1990

142. Mancuso A, Sharfstein ST, Tucker SN, Clark DS and Blanch HW, *Examination of primary metabolic pathways in a murine hybridoma with carbon-13 nuclear magnetic resonance spectroscopy*, Biotechnol Bioeng **44** 563-585, 1994

143. Mattie DR, Hixson CJ, Gaworski CL and Thorson GR, *Toxic effects of inhaled dimethylmethylphosphonate DMMP on the testes of Fischer-344 rats*, Toxicology **47** 231-232, 1987

144. Matzuk MM, Boime I, *The role of the asparagine-linked oligosaccharides of the alpha subunit in the secretion and assembly of human chorionic gonadotrophin*, J Cell Biol **106** 1049-1059, 1988

145. Matzuk MM, Hsueh AJ, Lapolt P, Tsafriri A, Keene JL and Boime I, *The biological role of the carboxyl-terminal extension of human chorionic gonadotropin beta-subunit*, Endocrinol **126** 376-383, 1990

146. Matzuk MM, Keene JL, Boime I, *Site specificity of the chorionic gonadotropin N-linked oligosaccharides in signal transduction*, J Biol Chem **264** 2409-2414, 1989

147. Matzuk MM, Krieger M, Corless CL and Boime I, *Effects of preventing O-glycosylation on the secretion of human chorionic gonadotropin in Chinese hamster ovary cells*, Proc Nat Acad Sci USA **84** 6354-6358, 1987

148. McKeehan WL, *Glutaminolysis in animal cells*, 111-150, in: Morgan MJ, *Carbohydrate metabolism in cultured cells*, Plenum Press, New York, NY, 1986

149. McQueen A, Bailey JE, *Effect of ammonium ion and extracellular pH on hybridoma cell metabolism and antibody production*, Biotechnol Bioeng **35** 1067-1077, 1990

150. Meehan AJ, Eskey CJ, Koretsky AP and Domach MM, *Cultivator for NMR studies of suspended cell cultures*, Biotechnol Bioeng **40** 1359-1366, 1992

151. Merz WE, personal communication *Protocols for hCG detection using a Western blot*, 1994

152. Microsoft I, *Excel*, Version AV 4.0 for MacOS, Windows 3.1, Microsoft, Inc., Redmond, WA, 1992

153. Miller WM, Blanch HW, Wilke CR, *A kinetic analysis of hybridoma growth and metabolism in batch and continuous suspension culture effect of nutrient concentration dilution rate and pH*, Biotechnol Bioeng **32** 947-965, 1988

154. Miller WM, Wilke CR, Blanch HM, *Effects of dissolved oxygen concentration on hybridoma growth and metabolism in continuous culture*, J Cell Physiol **132** 524-530, 1987

155. Miller WM, Wilke CR, Blanch HW, *Transient and steady-state responses in continuous hybridoma culture*, in: *196th ACS National Meeting*, Los Angeles, CA, September 25-30, 1988

156. Miller WM, Wilke CR, Blanch HW, *The transient responses of hybridoma cells to nutrient additions in continuous culture: II. Glutamine pulse and step changes*, Biotechnol Bioeng **33** 487-499, 1989

157. Moos M, Seamon KB, *Microheterogeneity of biological products*, in: Lubiniecki AS and Vargo SA, *Regulatory practice for biopharmaceutical production*, Wiley-Liss, New York, NY, 1994

158. Murhammer DW, Goochee CF, *Sparged animal cell bioreactors: Mechanism of cell damage and Pluronic F-68 protection*, Biotechnol Prog **6** 391-397, 1990

159. Muyan M, Ryzmkiewicz DM, Boime I, *Secretion of lutropin and follitropin from transfected GH3 cells: evidence for separate secretory pathways*, Mol Endocrinol **8** 1789-1797, 1994

160. Narayan KS, Moress EA, Chatham JC and Barker PB, *^{31}P NMR of mammalian cells encapsulated in alginate gels utilizing a new phosphate-free perfusion medium*, NMR Biomed **3** 23-26, 1990

161. Neeman M, Rushkin E, Kadouri A and Degani H, *Adaptation of culture methods for NMR studies of anchorage-dependent cells*, Magn Reson Med **7** 236-242, 1988

162. Neeman M, Rushkin E, Kaye AM and Degani H, *^{31}P-NMR studies of phosphate transfer rates in T47D human breast cancer cells*, Biochim Biophys Acta **930** 179-192, 1987

163. Newsholme EA, Leech A, *Biochemistry for the medical sciences*, Wiley, New York, NY, 1983

164. Nie Z, *Fetuin: its enigmatic property of growth promotion*, Am J Physiol **263** C551-562, 1992

165. Nie Z, Jellinek D, Ham RG, *Separation of growth-promoting activity for human muscle cells from fetuin*, Biochem Biophys Res Comm **178** 959-966, 1991

166. Oh SKW, Vig P, Chua F, Teo WK and Yap MGS, *Substantial overproduction of antibodies by applying osmotic pressure and sodium butyrate*, Biotechnol Bioeng **42** 601-610, 1993

167. Ozturk SS, Palsson BO, *Chemical decomposition of glutamine in cell culture media: Effect of media type, pH, and serum concentration*, Biotechnol Prog **6** 121-128, 1990

168. Ozturk SS, Palsson BO, *Effects of ammonia and lactate on cell growth metabolism and monoclonal antibody production*, in: *200th ACS National Meeting*, Washington, D.C., August 26-31, 1990

169. Ozturk SS, Palsson BO, *Effects of dissolved oxygen on hybridoma cell growth, metabolism, and antibody production kinetics in continuous culture*, Biotechnol Prog **6** 437-446, 1990

170. Ozturk SS, Palsson BO, *Effect of medium osmolarity on hybridoma growth, metabolism, and antibody production*, Biotechnol Bioeng **37** 989-993, 1991

171. Ozturk SS, Palsson BO, *Growth, metabolic, and antibody production kinetics of hybridoma cell culture: 1. Analysis of data from controlled batch reactors*, Biotechnol Prog **7** 471-480, 1991

172. Ozturk SS, Palsson BO, *Growth, metabolic, and antibody production kinetics of hybridoma cell culture: 2. Effects of serum concentration, dissolved oxygen concentration, and medium pH in a batch reactor*, Biotechnol Prog **7** 481-494, 1991

173. Patel DJ, *Glycoprotein hormones. A clasped embrace*, Nature **369** 438-439, 1994

174. Phillips PJ, Barford JP, Harbour C and Marquis CP, *Energy considerations*, 8B:4.1-8B:4.7, in: Doyle A, Griffiths JB and Newell DG, *Cell & tissue culture : Laboratory procedures*, John Wiley, Chichester, UK, 1994

175. Pierce JG, Parsons TF, *Glycoprotein hormones: structure and function*, Ann Rev Biochem **50** 465-495, 1981

176. PMA, *Validation concepts for computer systems used in the manufature of drug products*, Pharm Technol 1986

177. Puck TT, Cieciura SJ, Robinson A, *Genetics of somatic mammalian cells III. Long-term cultivation of euploid cells from human and animal subjects*, Journal of Experimental Medicine **108** 945-955, 1958

178. Rademacher TW, Parekh RB, Dwek RA, *Glycobiology*, Ann Rev Biochem **57** 785-838, 1988

179. Reiter M, et al., *Modular integrated fluidized bed bioreactor technology*, Biotechnol **9** 1100-1102, 1991

180. Reiter M, Hoenwater O, Gaida T, Zach N, Schmatz C, Bluml G, Weigang F, Nilsson K and Katinger H, *The use of macroporous gelatin carriers for the cultivation of mammalian cells in fluidized bed reactors*, Cytotechnol **3** 271-278, 1990

181. Reitzer LJ, Wice BM, Kennell D, *Evidence that glutamine not sugar, is the majorenergy source for cultured HeLa cells*, J Biol Chem **254** 2669-2674, 1979

182. Reynolds JEF, Parfitt K, Parsons AV and Sweetman SC (Ed.), *Martindale - The Extra Pharmacopoeia*, Pharmaceutical Press, London, UK, 1993

183. Richardson JF, Zaki WN, *Sedimentation and fluidisation: Part I*, Trans Inst Chem Eng **32** 35-53, 1954

184. Roberts JKM, Jardetzky O, *Monitoring of cellular metabolism by NMR*, Biochim Biophys Acta **639** 53-76, 1981

185. Rudin M, Sauter A, *In vivo phosphorous-31 NMR: Potential and limitations*, 161-188, in: Rudin M, *In vivo magnetic resonance spectroscopy III: In vivo MR spectroscopy*, Springer-Verlag, Heidelberg, 1992

186. Rüegger-Elektronik, *IMCS Analogsystem Bedienerhandbuch*, Rüegger Elektronik AG, Wetzikon, Switzerland, 1993

187. Ryll T, Wagner R, *Intracellular ribonucleotide pools as a tool fo monitoring the physiological state of in vitro cultivated mammalian cells during production processes*, Biotechnol Bioeng **40** 934-946, 1992

188. Santos H, Fareleira P, Xavier AV, Chen L, Liu MY and LeGall J, *Aerobic metabolism of carbon reserves by the "obligate anaerobe" Desulfovibrio gigas*, Biochem Biophys Res Comm **195** 551-557, 1993

189. Schumpe A, *The estimation of gas solubilities in salt solutions*, Chem Eng Sci **48** 153-158, 1991

190. Schumpe A, Deckwer W-D, *Solubility of oxygen in electrolyte solutions*, Biotechnol Bioeng **20** 145-150, 1978

191. Schumpe A, Quicker G, Deckwer W-D, *Gas solubilities in microbial media*, Adv Biochem Eng Biotechnol **24** 1-38, 1982

192. Schuppenhauer MR, Dunn IJ, *System for non-invasive on-line investigations of fluidized bed bioreactors*, in: *207th ACS National Meeting*, San Diego, CA, March 13-17, 1994

193. Schuppenhauer MR, Dunn IJ, Kuehne G and Tiefenauer L, *Non-invasive investigations of the energy state of cells in fluidized bed bioreactors*, in: *209th ACS National Meeting*, Anaheim, CA, April 2-6, 1995

194. Seamon KB, *Genetic and biochemical factors affecting product consistency - Introduction to the issues*, in: Standardization IAoB, *Developments in Biological Standardization*, Bethesda, MD, March 20-22, 1992

195. Sharfstein ST, *Metabolic studies of mammalian cells grown in culture*, Ph.D. Thesis, University of California at Berkeley, 1993

196. Sharfstein ST, Mancuso A, Blanch HW and Clark DS, *In-vivo nuclear magnetic resonance studies of mammalian cells grown in hollow fiber bioreactors*, in: *203rd ACS National Meeting*, San Fransisco, CA, April 5-10, 1992

197. Sharfstein ST, Tucker SN, Mancuso A, Blanch HW and Clark DS, *Quantitative in vivo nuclear magnetic resonance studies of hybridoma metabolism*, Biotechnol Bioeng **43** 1059-1074, 1994

198. Shedd SF, Spicer LD, *Characterization of a microcarrier cell culture system for ^{23}Na MR spectroscopy studies*, NMR Biomed **4** 246-253, 1991

199. Shulman RG, *NMR spectroscopy of living cells*, Scientific American **248** 76-83, 1983

200. Smala AM, *Einfluss der Kultivierungsparameter eines Bioreaktors auf die Produktbildung einer rekombinanten CHO-Zellinie*, Dipl.-Ing. Thesis, TFH Berlin, 1994

201. Sobrinho D, Tanner H-R, personal communication *IEF and Western blot of hCG*, 1993

202. Sonderhoff SA, Kilburn DG, Piret JM, *Analysis of mammalian cviable cell biomass based on cellular ATP*, Biotechnol Bioeng **39** 859-864, 1992

203. Sonnleitner B, Locher G, Fiechter A, *Automatic bioprocess control 1. A general concept*, J Biotechnol **19** 1-18, 1991

204. Sonntag K, Schwinde J, De Graaf AA and Sahm H, *Determination of carbon fluxes in the amino acid producing Corynebacterium glutamicum by NMR spectroscopy*, Biol Chem HS **374** 691, 1993

205. Spier RE, *Gradients in fluidized beds*, in: Spier RE, *Gradients in fluidized beds*, Amsterdam, NL, 1994

206. Sri-Pathmanathan RM, Braddock P, Brindle KM, *^{31}P-NMR studies of glucose and glutamine metabolism in cultured mammalian cells*, Biochim Biophys Acta **1051** 131-137, 1990

207. Stanley P, *Chinese hamster ovary cell mutants with multiple glycosylation defects for production of glycoproteins with minimal carbohydrate heterogeneity*, Mol Cell Biol **9** 377-383, 1989

208. Storring PL, Gaines-Das RE, Bangham DR, *International reference preparations of human chorionic gonadotrophin for immunoassay*, J Endocrinol **84** 295, 1980

209. Strohhäcker J, de Graaf AA, Schoberth SM, Wittig RM and Sahm H, *Phosphorus-31 nuclear magnetic resonance studies of ethanol inhibition in Zymomonas mobilis*, Arch Microbiol **159** 484-490, 1993

210. Stults NL, Cummings RD, *O-linked fucose in glycoproteins from chinese hamster ovary cells*, Glycobiol **3** 589-596, 1993

211. Sucker HG, *Entwicklung des Blasenbettreaktors zum Vermeiden der Zellschädigung bei der Begasung serumfrei kultivierter tierischer Zellen*, Dr. sc. techn. Thesis, ETH Zürich, 1992

212. Szkudlinski MW, Thotakura NR, Bucci I, Joshi LR, Tsai A, East-Palmer J, Shiloach J and Weintraub BD, *Purification and characterization of recombinant human thyrotropin (TSH) isoforms produced by Chinese hamster ovary cells: the role of sialylation and sulfation in TSH bioactivity*, Endocrinol **133** 1490-1503, 1993

213. Takeuchi Y, Sakakibara R, Ishiguro M, *Synthesis and secretion of human chorionic gonadotropin and its subunits in choriocarcinoma cells: a comparative study with normal placental cells*, Mol Cell Endocrinol **69** 145-156, 1990

214. Thömmes J, Halfar M, Lenz S and Kula MR, *Purification of monoclonal antibodies from whole hybridoma fermentation broth by fluidized bed adsorption*, Biotechnol Bioeng **45** 205-211, 1995

215. Thotakura NR, Szkudlinski MW, Weintraub BD, *Structure-function studies of oligosaccharides of recombinant human thyrotrophin by sequential deglycosylation and resialylation*, Glycobiol **4** 525-533, 1994

216. Tilkins ML, Judd D, Weiss S, Boime I, Pixley M and Gorfien SF, *Serum-free medium options for Chinese hamster ovary cell culture*, in: *32nd Annual Meeting of The American Society For Cell Biology*, Denver, CO, November 15-19, 1992, 1992

217. Truchard JJ, *Graphical environmental provides next generation test solutions*, in: *ELECTRO '87*, New York, NY, 7-9 April 1987, 1987

218. Turner C, Gregory ME, Thornhill NF, *Closed-loop control of fed-batch cultures of recombinant Escherichia coli using on-line HPLC*, Biotechnol Bioeng **44** 819-829, 1994

219. Ugurbil K, Guernsey DL, Brown TR, Glynn P, Tobkes N and Edelman IS, *^{31}P NMR studies of intact anchorage-dependent mouse embryo fibroblasts*, Proc Nat Acad Sci USA **78** 4843-4847, 1981

220. Ulloa-Aguirre A, Mendez JP, Cravioto A, Grotjan E, Damian-Matsumura P and Espinoza R, *Studies on the microheterogeneity of chorionic gonadotrophin secreted by the human cytotrophoblast in culture*, Hum Reprod **5** 661-669, 1990

221. van der Pol LA, Bonarius D, van de Wouw G and Tramper J, *Effect of silicone antifoam on shear sensitivity of hybridoma cells in sparged cultures*, Biotechnol Prog **9** 504-509, 1993

222. van der Veen JWC, de Beer R, Luyten PR and van Ormondt D, *Accurate quantification of in vivo phosphorus-31 NMR signals using the variable projection method and prior knowledge*, Magn Reson Med **6** 92-98, 1988

223. van Wezel AL, *Growth of cell-strains and primary cells on micro-carriers in homogeneous culture*, Nature **216** 64-65, 1967

224. Wang S, Haslam SZ, *Serum-free primary culture of normal mouse mammary epithelial and stromal cells*, **30A** 859-866, 1994

225. Warner B, Papes R, Heile M, Spitz D and Wispe J, *Expression of human Mn SOD in Chinese hamster ovary cells confers protection from oxidant injury*, Am J Physiol **264** L598-605, 1993

226. Watson E, Shah B, Leiderman L, Hsu Y-R, Karkare S, Lu HS and Lin F-K, *Comparison of N-linked oligosaccharides of recombinant human tissue kallikrein produced by Chinese hamster ovary cells on microcarrier beads and in serum-free suspension culture*, Biotechnol Prog **10** 39-44, 1994

227. Wehrli SL, Palmieri MJ, Berry GT and Kirkman HN, *Phosphorus-31 analysis of red blood cell UDP glucose and UDP Galactose: Comparison with HPLC and enzymatic methods*, Anal Biochem **202** 105-110, 1992

228. Wehrli SL, Palmieri MJ, Reynolds RA and Segal S, *Phosphorus NMR spectra of intact red blood cells: Quantitation of UDPGlucose and UDPGalactose*, Magn Reson Med **30** 494-497, 1993

229. Weide H, Páca J, Knorre WA (Ed.), *Biotechnologie*, VEB Gustav Fischer, Jena, Germany, 1987

230. Werner RG, Bassarab S, Hoffmann H and Schlueter M, *Quality aspects of fibrinolytic agents based on biochemical characterization*, Arzneim-Forsch **41** 1196-1200, 1991

231. Werner RG, Langlouis-Gau H, *Meeting the regulatory requirements for pharmaceutical production of recombinant dna derived products*, Arzneim-Forsch **39** 108-111, 1989

232. Werner RG, Langlouis-Gau H, Walz F, Allgaier H and Hoffman H, *Validation of biotechnological production processes*, Arzneim-Forsch **38** 855-862, 1988

233. Werner RG, Noe W, *Mammalian cell cultures. Part II: Genetic engineering, protein glycosylation, fermentation and process control*, Arzneim-Forsch **43** 1242-1249, 1993

234. Westermeier R, *Elektrophorese-Praktikum*, VCH Verlagsgesellschaft, Weinheim, Germany, 1990

235. Zang M, Trautmann H, Gandor C, Messi F, Asselbergs F, Leist C, Fiechter A and Reiser J, *Production of recomdinant proteins in Chinese hamster ovary cells using a protein-free cell culture medium*, Biotechnol **13** 389-392, 1995

236. Zielke HR, Zielke CL, Ozand PT, *Glutamine: a major energy source for cultured mammalian cells*, Fed Proc **43** 121-125, 1984

237. Zirvi KA, *Development of serum-free media for the growth of human gastrointestinal adenocarcinoma xenografts as primary tissue cultures*, **117** 515-518, 1991

238. Zupke C, Foy B, *Nuclear magnetic resonance analysis of cell metabolism*, Curr Opin Biotechnol **6** 192-197, 1995

Michael Rainer Schuppenhauer

1992 - 1995	**Ph.D., Chemical Engineering, ETH Zürich** Department of Chemical Engineering (LTC), Zürich, Switzerland Graduate student with PD Dr. Irving J. Dunn *Metabolic Studies of Mammalian Cells in a Fluidized Bed* Research assistant; supervised two students (M.Sc. level); Initiated and organized academic and industry seminars;
1988 - 1992	**Dipl.-Ing., Chemical Engineering, TU Hamburg-Harburg** Hamburg, Germany, Chemical Engineering, M.Sc. level Research assistant in process development and control; Fermentation and analytic chemistry; Thesis with Prof. Garabed Antranikian based on work done
1991	**Visiting Researcher, University of California at Berkeley** Department of Chemical Engineering, Berkeley, CA Research with Prof. Douglas S. Clark on *Pressure-Temperature Relationships of Thermophiles*
1989	**Internship, Ciba-Geigy AG, Basel, Switzerland** 3 months; downstream-processing of recombinant proteins
1985 - 1988	**Vordiplom, Friedrich-Alexander Universität Erlangen** Erlangen-Nürnberg, Germany, Chemical Engineering, B.Sc. level
1976 - 1985	**Abitur, Sankt-Ansgar-Schule** Hamburg, Germany
Born	November 16, 1966 in Hamburg, Germany
Affiliations	AIChE, ACS, ISPE ESACT, EFB-Working Parties VDI-GVC, DECHEMA